
Article:
Sarrigiannis, P.G., Zhao, Y., He, F. et al. (8 more authors) (2018) The cortical focus in childhood absence epilepsy; evidence from nonlinear analysis of scalp EEG recordings. Clinical Neurophysiology, 129 (3). pp. 602-617. ISSN 1388-2457

https://doi.org/10.1016/j.clinph.2017.11.029

The cortical focus in childhood absence epilepsy; evidence from nonlinear analysis of scalp EEG recordings

Ptolemaios G Sarrigiannis,[1] Yifan Zhao,[2] Fei He,[3] Stephen A Billings,[3] Kathleen Baster,[4] Chris Rittey,[5] John Yianni,[6] Panagiotis Zis,[1] Hualiang Wei,[3] Marios Hadjivassiliou,[7] Richard Grünewald[7]

1 Department of Clinical Neurophysiology, Sheffield Teaching Hospitals, NHS Foundation Trust, Royal Hallamshire Hospital, Sheffield S10 2JF, UK

2 Through-life Engineering Services, Cranfield University, MK43 0AL, UK

3 Department of Automatic Control and Systems Engineering, University of Sheffield, S1 3JD, UK

4 School of Mathematics and Statistics, University of Sheffield, Hicks Building, Hounsfield Road, Sheffield, S3 7RH, UK

5 Department of Paediatric Neurology, Sheffield Children's Hospital, NHS Foundation Trust, Western Bank, Sheffield, S10 2TH, UK

6. Department of Neurosurgery, Sheffield Teaching Hospitals NHS Foundation Trust, Royal Hallamshire Hospital, Sheffield S10 2JF, UK

7 Department of Neurology, Sheffield Teaching Hospitals NHS Foundation Trust, Royal Hallamshire Hospital, Sheffield S10 2JF, UK

Correspondence to:

Ptolemaios G Sarrigiannis

Department of Clinical Neurophysiology (N floor), Sheffield Teaching Hospitals, NHS Foundation Trust, Royal Hallamshire Hospital, Sheffield S10 2JF, UK

E-mail: p.sarrigiannis@sheffield.ac.uk

Abstract

Objective: To determine the origin and dynamic characteristics of the generalised hyper-synchronous spike and wave (SW) discharges in childhood absence epilepsy (CAE).

Methods: We applied nonlinear methods, the error reduction ratio (ERR) causality test and cross-frequency analysis, with a nonlinear autoregressive exogenous (NARX) model, to electroencephalograms (EEGs) from CAE, selected with stringent electro-clinical criteria (17 cases, 42 absences). We analysed the pre-ictal and ictal strength of association between homologous and heterologous EEG derivations and estimated the direction of synchronisation and corresponding time lags.

Results: A frontal/fronto-central onset of the absences is detected in 13 of the 17 cases with the highest ictal strength of association between homologous frontal followed by centro-temporal and fronto-central areas. Delays consistently in excess of 4 ms occur at the very onset between these regions, swiftly followed by the emergence of "isochronous" (0-2ms) synchronisation but dynamic time lag changes occur during SW discharges.

Conclusions: In absences an initial cortico-cortical spread leads to dynamic lag changes to include periods of isochronous interhemispheric synchronisation, which we hypothesize is mediated by the thalamus.

Significance: Absences from CAE show ictal epileptic network dynamics remarkably similar to those observed in WAG/Rij rats which guided the formulation of the cortical focus theory.

Highlights

- The transition into the absences is dominated by a frontocentral rise in nonlinear synchronisation.
- A dynamic rapidly engaging bilaterally distributed epileptic network highlights typical absences.
- Trails leading to the thalamus relaying homotopic areas to isochronous synchronisation during absences.

Keywords: absence; Zero-Lag; nonlinear; cortical focus theory; thalamus; ERR causality test.

Abbreviations: CAE=childhood absence epilepsy; EEG = electroencephalogram; ERR=error reduction ratio; GTCS = generalized tonic clonic seizure; ILAE = International League against Epilepsy; OIRDA = occipital intermittent rhythmical delta activity; TV-GFRF= time-varying generalised frequency response function; TV-NARX= ~~time varying~~time-varying nonlinear autoregressive exogenous model

1. Introduction

Gibbs, in his pioneering work on the newly developed electroencephalogram, described in 1935 the characteristic 3Hz spike and wave (SW) discharge of "petit mal" (Gibbs FA, 1935). In 1941 Jasper and Kershman on EEGs of patients with "petit mal" seizures reported the abrupt onset and offset of bilateral highly synchronous SW discharges, and postulated a subcortical origin as the generator of the attacks (Jasper et al., 1941). A midline placed pacemaker projecting to both hemispheres could explain both the bilateral synchrony and the generalised onset and termination of the absences. Since then, the electro-clinical characteristics of absence seizures have been the subject of debate (Meeren et al., 2005, Avoli, 2012).

The electro-encephalogram (EEG) of a typical absence seizure is characterised by almost identical SW discharges over distant homologous brain areas. In 1954 Pendfield proposed the centrencephalic theory based on the concept of a "centrencephalic integrating system" in the diencephalon and brainstem supposed to control consciousness (Penfield, 1952, Penfield et al., 1954). Buzsaki (Buzsaki, 1991) refined this concept into the "thalamic clock" hypothesis where a thalamic pacemaker drives the cortical SW discharges. In contrast, Gibbs and Gibbs (Gibbs et al., 1952) proposed the cortex as the region of the generation of the SW discharges and suggested this activity depended on diffuse cortical processes. Injection of pro-convulsive agents into the carotid (supplying the cerebral cortex) has been demonstrated to produce generalised SW discharges. In contrast, such discharges were not reported from injections into the vertebral artery, supplying the brainstem and diencephalon either in patients or cats (Bennett, 1953, Gloor, 1968, Gloor et al., 1974). The experiments favoured the cortical theory and provided the basis for Gloor's concept of the cortico-reticular epilepsies (Gloor, 1968), where thalamus/reticular formation and cortex were all important constituents of the epileptic network generating SW discharges.

More recently, the dynamic network mechanisms that generate the SW complexes and the anatomical pathways through which the widespread synchronisation during absence seizures occurs has been studied in WAG/Rij rats (Meeren et al., 2002, Meeren et al., 2004, Meeren et al., 2005). The requirement for a functionally intact cortex as a prerequisite for SW generation and that the intrathalamic circuitry in isolation is not sufficient for the cortico-thalamic oscillations to occur resulted in the formulation of the cortical focus theory (Meeren et al., 2005). Employing high spatial and temporal resolution, the dynamic spatiotemporal characteristics of the epileptic network during absences, particularly at the transition into an attack were revealed. Cortico-cortical, cortico-thalamic and intrathalamic functional coupling of relevant local field potentials, with a non-parametric

nonlinear association method, the "h^2", have been demonstrated. Time lags between the anatomical regions were described, shedding light on the causality, i.e. driver-response interactions, of the various epileptic network constituents in typical absences. Meeren ~~e~~at al emphasised the significance of nonlinear analysis particularly in detecting cortico-thalamic coupling in absences. They demonstrated that the h^2 nonlinear association coefficient can be significantly higher in comparison to the linear correlation coefficient r^2 and that hence, corticothalamic coupling can have a significant nonlinear component. Noticeably, the two methods could also produce a different direction of the time delay. ~~–~~This consistent direction of the coupling at the beginning of the seizures, the cortex leading the thalamus, would have been missed should a linear association methodology have been implemented (Meeren et al., 2002). The ERR causality test we use in this study has the ability to detect dynamic linear and nonlinear interactions over time, automatically identify the strongest of the two and then estimate synchronisation strength and corresponding time lags between pairs of EEG electrodes. Already at cellular level neurons exhibit dynamic behaviours governed by phenomena of threshold, integration and saturation (Lehnertz, 2008). These physiological facts indicate that nonlinear behaviour is introduced already at a cellular level and is valid to expect that huge neuronal networks also behave in a nonlinear way (Lehnertz, 2008). Epileptic seizures are highly nonlinear phenomena and analysis of ictal and pre-ictal EEG recordings help to better define the spatial and temporal characteristics of an epileptic networks in humans (Lehnertz, 1999, Elger et al., 2000, Lehnertz et al., 2001, Lehnertz, 2008). Other previous work has also shown that nonlinear phenomena can occur during a seizure (Lopes da Silva et al., 1989) and no assumptions can be made as to the type of interactions (linear vs nonlinear) between different constituents of an epileptic network. Particularly for the generalised epilepsies, the propagation of SW discharges occurs between cortical and thalamic constituents of the epileptic network within milliseconds and only special nonlinear analytical methods were able to determine the initial sequence of events, the cortex leading the thalamus (Stefan et al., 2013). We have also shown in previous work the importance of nonlinear interactions both in focal (Sarrigiannis et al., 2014) and in generalised epilepsies (Zhao et al., 2012, He et al., 2013, Zhao et al., 2013a, Zhao et al., 2013b, Sarrigiannis et al., 2014). All these observations make the case for the fundamental role nonlinear complex signal analysis methods have to play in decoding the dynamic spatiotemporal characteristics of epileptic networks.

In this work we reveal on scalp EEG recordings from children with childhood absence epilepsy (CAE) the most functionally coupled brain areas during absences and show the dynamic fluctuations that take place during the attacks. We measure time lags between homologous and heterologous brain areas, including contiguous EEG recording positions, and discuss the interpretation of dynamic

Formatted: Superscript

Formatted: Superscript

time lags estimates to infer the anatomical pathways involved. Synchronous neuronal activity is the hallmark of absences and we show how a very short-lived rise in nonlinear synchronisation, exclusively seen during the transition period into the absences, can identify the source of SW discharges. We compare our findings to the observations made in the genetic rat model of absence epilepsy that led to the formulation of the cortical focus theory (Meeren et al., 2002) confirmed later by other authors in other rat models of absence epilepsy (Polack et al., 2009, Depaulis et al., 2016).

2. Methods

In this study the terms causality, synchronisation and strength of association are used interchangeably and refer to the degree of phase coupling estimated between various bipolar EEG channel pairs.

2.1. Case selection for analysis

We selected patients with CAE fulfilling the current International League against Epilepsy (ILAE) diagnostic criteria (2016), but additionally excluding patients with photosensitivity. Our case selection was based on the following electro-clinical criteria: normal development, drug naïve, no previous history of generalised tonic clonic seizures (GTCS) and/or myoclonic jerks, age 4-10 years, no clinical or EEG evidence of photosensitivity, a normal background EEG, no consistent focal EEG abnormalities, regular 2.5-4Hz generalised ictal SW discharges without fragmentations. Fragments of less than 2-second duration of generalised or focal SW abnormalities were allowed in the interictal record. To avoid hyperventilation-induced high amplitude generalised synchronous slow wave activity that could interfere with quantitative EEG (QEEG) analysis, only patients with at least one spontaneous epileptic absence occurring before or 3 or more minutes after the completion of hyperventilation were selected. EEGs recorded at a sampling rate of 500Hz (i.e. time resolution of 2ms) were selected.

We searched our EEG database for the term “Childhood Absence Epilepsy” and identified 231 standard EEGs recordings between January 2005 and July 2014. Of those only 17 fulfilled the stringent selection criteria.

A Paediatric Neurologist and a Clinical Neurophysiologist reviewed the EEGs and the clinical information of these 17 cases and the syndromic classification of CAE was confirmed. For all 42 absences included in this work none of the children were responsive when repeatedly, verbally prompted during their attacks. They all immediately recovered following the cessation of the ictal

SW discharges. Ethics approval for use of patients' EEGs for the development of these new qEEG methods was obtained both from the University of Sheffield and the NHS ethics committees (SMBRER207 and 11/YH/0414).

2.2. EEG acquisition

All EEGs were recorded between 2005 and 2014 with a Natus Headbox (Optima Medical Ltd) at a sampling rate of 500 Hz (analogue bandwidth 0.1–200 Hz). Standard international 10-20 system of electrode placement positions were used for the recordings in all patients.

2.3. EEG data selection

A total of 42 absences from 17 patients, were exported in spike 2 software (version 7, CED Ltd). With a referential montage (all 10-20 international system of electrode placement positions were displayed) the following epochs were isolated:

- Ictal periods to include the very onset and offset of all 42 absences (e.g. Fig. 1 A).
- Transition period into the absence, to include an epoch of 4 seconds for each absence, 3 seconds before and 1 second after the first generalised SW discharge (e.g. Supplementary Figure S1).

All EEG data was then exported in text file format and analysed with the ERR causality test. For few of the cases a custom-built ~~time varying~~time-varying nonlinear autoregressive exogenous (~~TVNARX~~TV-NARX) model was constructed.

2.4. Quantitative EEG analysis

2.4.1. General

The following bipolar electrode derivations (to reduce volume conduction effects from a common reference) were used: F8F4, F7F3, F4C4, F3C3, T4C4, T3C3, FzCz, CzPz, T4T6, T3T5, T6O2, T5O1, P4O2, P3O1. We have then created all potential combinations between these bipolar channels in pairs of two (91 pairs, 182 for partial directed synchronisation). For each of the 91 pairs of channels, bi-directional average strength and percentage of zero-lag synchronisation (-2 to 2ms for our EEG sampling at 500Hz) were computed with the ERR causality test.

2.4.2. Time domain analysis, the error reduction ratio (ERR) causality test

A description of this method previously developed by us, can be found in Appendix A and in previous work (Zhao et al., 2012, Zhao et al., 2013a, Zhao et al., 2013b, Sarrigiannis et al., 2014).

2.4.3. Nonlinear analysis with ERR causality test

While developing the nonlinear methodology we have identified a consistent sharp rise in nonlinear synchronisation at or just before the onset of the SW discharges frequently involving the frontal and frontocentral areas. We have shown this effect in previous papers (Zhao et al., 2012, He et al., 2013, Zhao et al., 2013a, Zhao et al., 2013b, Sarrigiannis et al., 2014).

To study the transition period into the absences a nonlinear analysis was performed with a custom built function within the ERR causality software with a window size h=500 data points (for the sampling frequency of 500Hz used for the EEG recordings this corresponds to 1s). A sliding window (t-h, t) was applied and hence, for any point in time t, synchronisation estimates were exclusively based on past EEG data. Therefore, a rise in nonlinear synchronisation before the appearance on EEG of a spike or a SW discharge implies a rise in phase coupling, i.e. association between two areas. In the case of nonlinear synchronisation, the ERR causality strength was estimated for both directions (e.g. F8F4-F7F3 and F7F3-F8F4 were computed separately). A change in the order of the bipolar derivation of a channel pair could produce very different results and this is why the partial directed nonlinear synchronisation was estimated to determine the source of the earliest rise in synchronisation for each absence. For example, a high rise in synchronisation from F8F4 to P4O2, implies an anteroposterior direction on the coupling between these 2 recording positions. This is important information to define the temporal sequence of engagement of the various constituents of a widely distributed epileptic network that characterises absence seizures. The standard 14 bipolar derivations used in this work produce a total of 182 one-direction nonlinear synchronisation combinations of pairs. For each absence we have identified which of the 182 pairs of channels showed the earliest rise in nonlinear synchronisation. For this purpose we have constructed a window, defined by the highest value of nonlinear synchronisation observed in each of the 42 absences for all 182-channel pairs minus 25%, so only the pairs with the most substantial rise in synchronisation were selected for each seizure.

2.4.5. Quantitative EEG surrogate marker statistical approach

To determine the statistical significance of the causal influence between two signals, a ~~time-varying~~time-varying threshold was constructed, representing the level of causality above which values had less than a 5% probability of occurring by chance (Zhao et al., 2013b). The widely used amplitude adjusted Fourier transform (AAFT) surrogate was employed in this study (Theiler et al., 1992). This procedure was repeated 100 times and then the 95% quantile was determined as the

threshold for each time point. This routine has been applied for all EEG data analysis (including when a nonlinear algorithm is used in isolation).

2.4.6. Frequency domain EEG analysis

The ~~TVNARX~~TV-NARX model implemented in this study is described in Appendix B and in great detail in previous work (He et al., 2013, Zhao et al., 2013b, He et al., 2014a, He et al., 2014b, He et al., 2015, He et al., 2016)

3. Results and statistical analysis

3.1. Ictal EEG analysis with the ERR causality test

A total of 42 absences from 17 patients were analysed to include the onset and offset of each seizure (e.g. Fig. 1). Bespoke software implementing the ERR causality test was used to estimate the average level of synchronisation and the proportion of zero-lag encountered for each of the 91 channel sets that reflect all potential combinations of electrode pairs between 14 bipolar derivations covering frontal, central, temporal, parietal and occipital areas. Essential demographic and other information including age of onset, seizure duration, presence or absence of occipital intermittent rhythmical delta activity (OIRDA) and the channel pairs with the highest scores of average strength and percentage of zero-lag synchronisation are shown in Table 1. The results from the 91 channel pairs for each absence were then ranked to show in decreasing order the channels with the highest level of synchronisation and percentage of zero-lag (Table 2). A total of 14 channels were placed at least twice in the top 5 for average strength of synchronisation in all 42 absence seizures and when only the first absence of each of the 17 cases was included (Table 2 and 3). Fourteen channels were also found to be ranked more than once in the top 5 for percentage of zero-lag synchronisation for all 42 absences (Table 2).

To demonstrate similarities in the lengthy 91-channel pair-ranking list between all 17 cases (total of 42 absences), the binomial exact confidence interval (CI) was estimated for the frequency of a specific combination of channels to be ranked in the top 5. The highest point estimate of the probability of a set of channels to appear in the top five in all 42 absences was found between F8F4-F7F3 at 95% (95%CI, 84-99%), the second amongst T4C4-T3C3 at 83% (95%CI, 69-93%) and the third amid F4C4-F3C3 at 60% (95%CI, 43-74%). Probabilities for all 42 absences and then 17

individual cases (i.e. 1 absence/case) are shown in Table 2 and Table 3. Case 17, a patient that had a total of 7 absences, was used to estimate the probability that a specific pair of channels would rank in the top 5, for a single case (Table 2). This produced for the top ranked two channels; F8F4-F7F3 and T4C4-T3C3 point estimates of 100% (CI 59-100%).

Taking the subset of (14) channel pairs, that ranked in top 5 for highest synchronisation level more than once in the 42 absences, the contribution of age, sex, seizure duration, presence or absence of OIRDA and percentage of zero-lag synchronisation on the mean strength of synchronisation was explored in a mixed model regression. Case (or patient) was included as a random factor.

For most of the models, none of the explanatory factors had a significant effect (alpha set at 0.001 to accommodate multiple testing). However, for the channel pairs P3O1-P4O2, P3O1-T6O2 and T5O1-T6O2 the percentage of time with zero-lag synchronisation was a significant predictor ($p<0.0001$, $p=0.0003$ and $p<0.0001$ respectively).

Based on the latter findings, and for the channel pair P3O1-P4O2, further analysis was performed. After having adjusted for percentage of zero-lag synchronisation there is a significant difference in the average strength of synchronisation during the absences depending on whether the person is OIRDA positive or negative, with the latter group showing a counterintuitive higher average strength of ictal synchronisation at 0.73 versus the former at 0.53 (average difference 0.2; 95%CI: 0.07-0.33; $p=0.005$). On the other hand, after having adjusted for average strength of synchronisation, there is a significant difference in the percentage of zero-lag synchronisation between OIRDA positive and negative groups with higher average percentage of zero-lag synchronisation in the positive group at 0.22, versus the negative group, at 0.12 (mean difference 0.096; 95%CI: 0.004-0.189; $p=0.043$).

After selecting the absence showing the highest average score of synchronisation for each case, the 17 absences chosen were used to plot the top 9 channel pairs, ranked for strength of synchronisation, to include the top ranked homologous, heterologous contiguous and heterologous bi-hemispheric bipolar derivations (Fig. 2). A one way ANOVA multiple comparison test (Dunnett's multiple comparisons test) with the top ranked F8F4-F7F3 pair as a control column reveals no significant differences with the remaining homologous channels but differences with the heterologous contiguous channel pairs ($p=0.0022$ with channel pair FzCz-F3C3, $p= 0.0068$ with channel pair FzCz-F4C4, $p= 0.0038$ with T4C4-F8F4, $p= 0.0031$ with T3C3-F7F3) and differences with the heterologous bi-hemispheric channel pairs ($p= 0.0004$ with channel pair T3C3-F8F4 and $p= 0.0003$ with T4C4-F7F3).

Finally, a comparison was made between the mean time lags measured during the absences, between the top three homologous channel pairs ranked for average synchronisation strength (the channel with the highest percentage of zero-lag synchronisation was selected from those three) and the frontocentral midline versus the parasagittal right or left frontal derivation (Fig. 3 and Table 4). This demonstrates a very significant difference in time lags in the interactions between those 2 recording positions (mean difference 3.7ms +/-2.7 standard deviation (SD) (95%CI: 2.28-5.13ms, $p<0.0001$). Additionally, the prevailing direction of synchronisation is from the lateral to the medial frontal/frontocentral areas and very rarely in the opposite direction (mean difference for these opposite directions is at 74%+/-25%SD and 95%CI: 61%-87%, $p<0.0001$). This can be appreciated in Figure 3 and Table 4.

3.2. Results from Nonlinear Synchronisation analysis

When the ERR nonlinear causality is estimated in isolation for the 4 second epochs leading into the generalised SW discharges, for all absences there is a sharp short-lived rise in nonlinear synchronisation at or just before the onset of the epileptic activity (Supplementary PowerPoint 1). The absence seizure with the highest nonlinear synchronisation rise for the transition period into the attacks was selected for each case and then explored for the earliest nonlinear rise (source) using a window constructed for each absence by the highest value of nonlinear synchronisation minus 25%. For the majority of the cases (13/17) the source was found in the frontal and frontocentral regions (Fig. 4 and 5). Noticeably, this sharp rise involves only some of the EEG channel pairs (range 3-47 out of 182 possible pairs, median 16) for each absence seizure (Supplementary XL). This sharp rise starts in one pair of electrodes and spreads then to involve other areas with variable area involvement for each absence, even in absences from the same patient (spreading occurs within 650ms for 16 of the cases and within 1200ms for one). Noticeably in none of the analysed absences did the source of nonlinear rise involve the temporal, centro-temporal and temporo-occipital areas (Supplementary PDF).

The nonlinear frequency domain analysis with a ~~NARX~~TV-NARX model was also produced for 3 of the cases for the channel pair showing the earliest rise in nonlinear synchronisation on the ERR test analysis and the linear and nonlinear time-varying generalised frequency response functions (TV-GFRF) were produced (Fig. 6 and 7).

4. Discussion

Absence seizures are a ~~the best~~ paradigm of widely distributed ictal neuronal synchronisation. In this study we explore the validity of the cortical focus theory in absences recorded from human subjects with childhood absence epilepsy. By applying stringent electro-clinical criteria we selected a cohort with a pure form of CAE (17 cases) and we isolated 42 spontaneous occurring absences characterised by regular generalised SW discharges. By applying nonlinear quantitative EEG methodologies we explored the validity of the cortical focus theory in these seizures. The importance of nonlinear methods in studying absences is in keeping with previous observations in rats (Meeren et al., 2002, Depaulis et al., 2016).

We analysed the ictal and pre-ictal epileptic network dynamics, starting with the transition period into the absence seizures. We have identified the source of the epileptic network by applying a nonlinear signal analysis methodology to the 4-second epochs selected using as reference the earliest generalised epileptiform discharge. We applied a time domain non-linear method, the ERR causality test, which out-performs other commonly used techniques (Zhao et al., 2012, Sarrigiannis et al., 2014) to detect the earliest rise in nonlinear synchronisation in the transition period into the absences. This shows that only some of the 182 EEG (bidirectional) channel pairs covering frontal, central, parietal, temporal and occipital regions display a transitory and short-lived (< 300ms) rise in nonlinear synchronisation, above the surrogate level of statistical significance (Supplementary XL and Supplementary PowerPoint 1). Additionally, the channel pairs engaging in a sharp rise in nonlinear synchronisation in the pre-ictal and/or early ictal period do not show a simultaneous rise in synchronisation but on the contrary, this rise spreads from one channel pair into the other in an unpredictable way, within 600ms in 16 of the 17 cases and for one within 1200ms (Supplementary XL). Analysis of the absence with the highest nonlinear rise in synchronisation, for each patient, reveals a source, localising in 13 (76%) of the cases in the frontal and frontocentral areas (Fig. 4 and 5 and Supplementary PDF) consistent with previous EEG studies (van Luijtelaar et al., 2006) and with findings on MEG recordings where nonlinear association techniques were used (Amor et al., 2009, Westmijse et al., 2009, Tenney et al., 2013).

From the remaining cases, three show a source in the parieto-occipital areas and one in the centro-parietal region; three of these four cases, showing a posterior onset, are OIRDA positive (Fig. 5). Noticeably, this latter EEG pattern is characterised by high levels of interictal EEG synchronisation in the posterior quadrant regions and may correlate with a better clinical outcome (Guilhoto et al., 2006, Watemberg et al., 2007). From those patients where a frontal/frontocentral source was identified (four left, four right and five in the frontocentral midline region), 38% (5/13) were OIRDA positive while for those with posterior onset, 75% (3/4) were OIRDA positive. Furthermore, in our

statistical analysis between the parieto-occipital homologous areas (after having adjusted for average strength of synchronisation) we found a significant difference in the percentage of zero-lag synchronisation between OIRDA positive and negative groups (p=0.043). Apart from these findings the epileptic network dynamics and characteristics do not differ between OIRDA positive and negative patients.

In three of the cases and in the same channel pairs where the initial sharp rise in nonlinear synchronisation was documented with the ERR method (Fig. 4 and 5), a frequency domain ~~TVNARX~~TV-NARX based model, also developed by our team, was applied (He et al., 2013, He et al., 2014a, He et al., 2014b). We found very similar results with this approach (Fig. 6), with the advantage of additional detail of frequency content from which we can infer something of the complexity of the cross-frequency nonlinear interactions that take place in the transition phase into the absences. Just before the onset of the SW discharges there is a rise of nonlinear interactions >20Hz followed by paucity of these phenomena when the absences initiate, while a simultaneous increase in linear synchronisation dominates the epileptic network dynamics during the seizures (Fig. 6 and 7). Neuronal synchronization between brain structures constitutes in normal circumstances a flexible mechanism to coordinate information flow in the cerebral cortex across several spatiotemporal scales and may be essential for conscious perception and cognition (Buzsáki et al., 2004, Helfrich et al., 2014). Our findings reaffirm the concept that a balanced and temporally precise pattern of synchronisation and desynchronisation is pertinent to cognitive function (Schnitzler et al., 2005). In absence seizures, bilaterally distributed networks "lock" into a state of high linear synchronisation while cross-frequency interactions fall precipitously after onset and stay low for a range of frequencies during the time when cognitive function is impaired throughout the SW discharges (e.g. case 1 in Fig. 7 and cases 1, 3, 17 in Supplementary PowerPoint 1).

In the time domain, ERR estimates demonstrated that time lags consistently exceed 4 ms at the beginning of each absence, followed by the appearance within two seconds (for 14 of the cases within the first second and for the remaining 3 within the first 2 seconds), of a tight, practically isochronous synchronisation at or under 2ms (Fig. 3 and Supplementary PowerPoint 2). Although the strength of association remains consistently high during the absences, the percentage of zero-lag synchronisation ($0 \leq$zero-lag< 2ms), in the homotopic channels with the highest percentage of zero-lag, varies (28-67%, Table 1). In addition, time shift estimates change dynamically and unpredictably during each absence with a tendency for the longer delays to be seen at the beginning and the end of the seizures (Supplementary PowerPoint 2).

Delays in excess of 4ms between distant homotopic brain areas, suggest cortico-cortical spreading in the very early ictal/pre-ictal phase, through a fast transcallosal path. Three milliseconds is the shortest interhemispheric lag estimate reported between homotopic areas a value considered to be an underestimate (Brown et al., 1991, Nowicka et al., 2011). This is also our experience based on interhemispheric delay measurements in rare cases of cortical myoclonus where transcallosal spread occurs (Sarrigiannis et al., 2014). The children included in this work are between the ages of 5-10 and callosal delays are expected to be, if anything, longer in this age group due to incomplete myelination (Salamy, 1978). The delays shown (Fig. 3 and for the majority of the cases in Supplementary PowerPoint 2) at or just before the onset of the SW discharges are close to 10ms, in keeping with transcallosal spread for children of the age group included in our study.

In WAG/Rij rats during absences there is a difference in the ictal strength of association between inter-hemispheric homologous and intra-hemispheric cortical recording sites (for the same inter-electrode distance) favoring the former (Meeren et al., 2002). Additionally, the propagation velocity was found in these experiments to be 3 times higher for the inter-hemispheric homotopic versus the intra-hemispheric cortico-cortical ictal relationships, indicating that the relevant inter-hemispheric transcallosal connectivity is faster. This is also reflected in our work, where the homotopic areas show the highest average strength of ictal association for all 42 absences. Furthermore, we found a shorter average time delay between homologous areas versus the equivalent midline frontocentral and the parasagittal right and left frontal/frontocentral derivations. This is anatomically consistent with connectivity in humans provided by the major interhemispheric commissure, the corpus callosum that connects mostly homotopic and to a lesser extent heterotopic areas (Jarbo et al., 2012). In both animal models and humans with generalised seizures from onset, the bilateral synchrony of SW discharges is disrupted by transection of the corpus callosum (Marcus et al., 1966, 1968, Vergnes et al., 1989, Spencer et al., 1993). This topography of the direct anatomical connections is also reflected in our findings (Fig. 2) as the denser homologous projections produce much higher ictal strength of association between relevant areas, in comparison to the heterotopic equivalent regions and the corresponding intra-hemispheric recording sites.

Following the initial relatively prolonged lags (at or above 4ms) found in all absences studied in this work, sustained periods of zero-lag synchronisation occur between distant homotopic areas during the seizures. These zero-lag estimates are due to a genuine network zero-lag as the time delays measured are not fixed and change dynamically over time during an absence (e.g. Fig. 3 and Supplementary PowerPoint 2). Specifically, the ictal zero-lag periods we found between distant

anterior homotopic areas occur intermittently in-between intervals with time lags at or above 2ms that cannot be explained through volume conduction. Most importantly, the average ictal time delays between the bi-hemispheric equivalent frontal, frontocentral and centrotemporal areas are much shorter in comparison ($p<0.0001$) to those found between the right and left parasagittal frontal and frontocentral derivations and the frontocentral midline channel (Fig. 3 and Table 4). Synchronisation analysis between one of these homotopic areas, right or left (e.g. F4C4 or F3C3) and a recording point between these two homologous regions, (e.g. FzCz) typically shows time lags much above 2ms, when at the same time periods with zero-lag are detected between the more distant homologous areas (e.g. Fig. 3, case 7). Therefore, our zero-lag estimates between distant homotopic areas are highly likely the result of a network zero phase-lag, independent of volume conduction (Thatcher, 2012).

Near-zero lag synchronisation between distinct brain regions is thought to be the mechanism through which perceptual binding and feature integration occurs during normal brain function (Singer et al., 1995, Munk et al., 1996, Roelfsema et al., 1997, Slotnick et al., 2002, Witham et al., 2007, Rajagovindan et al., 2008). Close to zero phase-lag synchronisation is also reported in the lack of a stimulus input (Roelfsema et al., 1997, von Stein et al., 2000). We have similarly documented in previous work, with the ERR causality test, isochronous synchronisation between homotopic areas in stage II sleep and during absence seizures (Zhao et al., 2013a, Zhao et al., 2013b, Sarrigiannis et al., 2014) and also shown that average methods for estimating synchronisation like cross-correlation and coherence, commonly used in this field of research, can produce spurious results. Understanding of the mechanisms through which this tight synchronisation of large-scale networks occurs has been elusive but over the last decade significant progress has been made. Fisher et al first demonstrated in coupled laser semiconductors, with long inter element delays that two of these delay-coupled oscillators can achieve isochronous synchronisation by relaying their dynamics via a third mediating element that lags behind the synchronised outer elements (Fischer et al., 2006, Vicente et al., 2008a). Neurons are also oscillators characterised by pulse-like interactions that transmit from one element to its partners (Ernst et al., 1995). With this analogy in mind it is easy to understand how two neuronal populations can achieve zero-phase lag synchrony when they interact through a relay oscillator (Viriyopase et al., 2012). A study of the zero-lag synchrony phenomenon when inhomogeneities (i.e. difference in firing rate) were present in two delayed coupled pools of neurons, connected through a relay population of cells found that the relay cells require a temporally equidistant location from the two group of neurons for the pools to be synchronised; this symmetry of the system was the single

most important factor for isochronous synchronisation to take place (Ghasemi Esfahani et al., 2014). Earlier Vicente et al also reproduced with simulated neural network topologies the findings from the laser semiconductor experiments and shown that two populations of neurons can achieve zero-lag synchronisation if reciprocally coupled to a third population and that this holds true even for axonal delays between the three populations of neurons reaching tens of milliseconds (Vicente et al., 2008b). The authors refer to the anatomical position of the thalamus and the cortico-thalamo-cortical loops; the dense connectivity between the thalamus and the different cortical areas renders the former an ideal candidate for being the relaying nucleus through which isochronous dynamics can occur in remote cortical regions. There is also indication that the thalamus maintains an equal time distance from different brain areas through changes in the degree of myelination of the interconnecting axons (Salami et al., 2003, Wang et al., 2008). This idea of the thalamus being the relay nucleus to generate zero-lag synchronisation between distant cortical areas was further explored with a simulation approach; it revealed that this relay was feasible, occurs at a fast time scale and depends only on the identical conduction delays of two cortical areas from the thalamus (Gollo et al., 2010).

However, if the thalamus is the deep relay nucleus that also facilitates the zero-lag interhemispheric synchronisation, the question then arises as to what would be the anatomical pathway of such a connection. Each hemi-thalamus would have to be either connected to its counterpart and/or to contralateral cortical regions. Evidence of crosstalk between the two sides of the thalamus through the reticular nucleus, via the intrathalamic commissure, has been previously documented in rats (Raos et al., 1993, Battaglia et al., 1994, Luijtelear et al., 2000). To our knowledge there is no evidence of a direct thalamic midline functional connection in humans (Jones, 2007, Zhang et al., 2008). However, there is evidence from animal experiments, in rats, cats and primates of bilateral efferent motor cortical projections directed to the thalamus (Molinari et al., 1985, Preuss et al., 1987, Carretta et al., 1996). More recently, tractography diffusion weighted imaging in humans has demonstrated *in vivo* both ipsilateral (Behrens et al., 2003) and corpus callosal contralateral (Jarbo et al., 2012) connections between cortex and thalamus. In a single patient undergoing deep brain stimulation (DBS) for refractory tremor there was evidence of a crossed corticothalamic pathway, with short latency cortical evoked responses by stimulating the Vim thalamus through the DBS leads. This produced bilateral frontocentral evoked responses with interhemispheric lags of less than 0.37ms implying that the homologous frontocentral areas were practically equidistant from the stimulated thalamic position (Sarrigiannis et al., 2015).

Additional indirect evidence for a crossed corticothalamic connection comes from the transient zero-lag synchronisation we have shown in previous EEG work in sleep spindles recorded from

centrotemporal homologous areas in bipolar derivations (Sarrigiannis et al., 2014). Sleep spindles require reticular thalamic cells for their generation and occur in the thalamus of decorticated cats although they seem to be modulated by cortical feedback and hence cortex and thalamus constitute a unified oscillatory structure (Steriade et al., 1985, Timofeev et al., 1996). Zero-lag estimates in sleep spindles shown before, accompanied by very high levels of interhemispheric synchronisation, are consistent with our current findings and may occur through the nucleus reticularis thalami (RT) and corticothalamic (CT) relay cell involvement (Timofeev et al., 1996, Manning et al., 2003, Hughes, 2009a, Chen et al., 2014, Depaulis et al., 2016). These lines of evidence suggest that the thalamus relays distant cortical neuronal networks into a tight zero lag synchronicity during typical absences.

Thalamic involvement in humans during typical absences has been previously clearly documented; firstly in the fifties, intracranial recordings in patients with absences revealed SW discharges in the thalamus during the attacks (Spiegel et al., 1950, Spiegel et al., 1951, Williams, 1953) and more recently with fMRI studies (Aghakhani et al., 2004, Gotman et al., 2005, Hamandi et al., 2006, David et al., 2008, Moeller et al., 2008a, Moeller et al., 2008b, Hughes, 2009b, Li et al., 2009, Stefan et al., 2013). However, these latter observations lack the time resolution required to characterise the sequence of dynamic interactions between the various constituents of the epileptic network during absences that as shown in our work occur within a time scale of milliseconds. Despite the indisputable evidence of thalamic involvement during typical absences, little is reported about the remarkable periods of isochronous interhemispheric synchronisation that we hypothesise and provide evidence for being generated by the thalamus. With regards to the dynamic changes in the time lag estimates during the absences, in the nervous system firing rates are not constant and synaptic efficacies change due to short and long term plasticities (Ghasemi Esfahani et al., 2014). Neuronal and synaptic changes over short time scales could explain the transient appearance of zero-time lags and the dynamic switch between long and short delays that we demonstrate extensively in this work.

A limitation of this study is the two-dimensional scalp EEG recordings; the earliest epileptic focus could be hidden from view. Despite this, our nonlinear approach reveals a rapidly engaging widely distributed epileptic network in the transition phase into the absences with an anterior source in the majority of our patients and not a simultaneous rise in synchronisation over many channels, as the centrencephalic and the thalamic clock theories would suggest. In our analysis we made no empirical assumptions and the epileptic network in absences was characterised through estimates of synchronisation with the corresponding lags between bipolar EEG recordings while all our estimates were above the level of statistical significance. The nonlinear ~~TVNARX~~TV-NARX parametric analysis in few of the cases also corroborates with an entirely different approach the findings with

the time domain ERR causality test and reveals a sharp rise in cross frequency nonlinear interactions at the transition into the absences. We display in one example (Fig. 7 and Supplementary PowerPoint 1) the loss of nonlinear phenomena for the entire period of the absence while strong linear interactions dominate the ictal phase. This relationship reverses dramatically at the very end of the absences and coincides with the reinstatement of normal cognitive function. This observation merits further consideration and it is worth considering if cross-frequency nonlinear phenomena between constituents of widely distributed cortical networks are a prerequisite for higher cognitive functioning.

5. Conclusion

Despite no single consistent ictal focus being found in this work, we demonstrate, for the first time on ictal scalp EEG recordings of CAE, that the epileptic network dynamics and underlying anatomical pathways are remarkably similar to those observed in the WAG/Rij rat experiments that guided the development of the cortical focus theory to explain the generation of typical absence seizures. An early rise in nonlinear synchronisation reveals a frontocentral source in the transition phase into the absences in 76% of the cases with time lags around the same period exceeding 4ms, suggesting cortico-cortical spreading. A frequency domain parametric ~~TVNARX~~TV-NARX model analysis confirms independently the early nonlinear rise in synchronisation that involves frequencies above 20Hz. Within two seconds from onset, discrete periods of zero-lag synchronisation emerge and predominate between homotopic areas. This is not fixed for the ictal period but dynamically interchanges with longer delays in an unpredictable way. Our findings would be in favour of the thalamus being the relay nucleus that allows distant homologous cortical areas to achieve isochronous synchronisation and we postulate this to be the electrophysiological signature of thalamic involvement, a similar finding having been identified with sleep spindles. Additionally, we document a prevailing ictal frontocentral lateral to medial direction of spreading in 16 of the 17 cases similar to that of WAG/Rij rats in which the perioral focus spreads towards the hind paw during the seizures. The absence epileptic network in rats and humans is based on homologous underlying anatomical pathways with the corpus callosum homotopic connections producing the highest degree of synchronisation between distant homologous areas and offering the means for bilaterally distributed networks to engage rapidly in high levels of bi-hemispheric synchronisation from onset.

Conflict of interest

None of the authors have potential conflicts of interest to be disclosed.

Funding

The Ryder Briggs trust fund provided us with a small grant to develop the nonlinear software used for the analysis of the data on this work. Part of the work was funded by an EPSRC Platform Grant. No other funding was received.

Acknowledgements

We thank Ryder Briggs Neuroscience Research charitable trust fund for financially supporting the development of the error reduction ratio causality software. We would also like to thank Dr Peter Baxter for his invaluable guidance in preparing and editing this manuscript. This is research carried out at the National Institute for Health Research (NIHR) Sheffield Biomedical Research Centre (Translational Neuroscience) / NIHR Sheffield Clinical Research Facility.

References

Aghakhani Y, Bagshaw AP, Benar CG, Hawco C, Andermann F, Dubeau F, et al. fMRI activation during spike and wave discharges in idiopathic generalized epilepsy. Brain. 2004;127:1127-44.

Amor F, Baillet S, Navarro V, Adam C, Martinerie J, Quyen MeV. Cortical local and long-range synchronization interplay in human absence seizure initiation. Neuroimage. 2009;45:950-62.

Avoli M. A brief history on the oscillating roles of thalamus and cortex in absence seizures. Epilepsia. 2012;53:779-89.

Battaglia G, Lizier C, Colacitti C, Princivalle A, Spreafico R. A reticuloreticular commissural pathway in the rat thalamus. J Comp Neurol. 1994;347:127-38.

Behrens TE, Johansen-Berg H, Woolrich MW, Smith SM, Wheeler-Kingshott CA, Boulby PA, et al. Non-invasive mapping of connections between human thalamus and cortex using diffusion imaging. Nat Neurosci. 2003;6:750-7.

Bennett FE. Intracarotid and intravertebral metrazol in petit mal epilepsy. Neurology. 1953;3:668-73.

Billings SA, Chen S, Korenberg MJ. Identification of Mimo Non-Linear Systems Using a Forward-Regression Orthogonal Estimator. Int J Control. 1989;49:2157-89.

Brown P, Day BL, Rothwell JC, Thompson PD, Marsden CD. Intrahemispheric and interhemispheric spread of cerebral cortical myoclonic activity and its relevance to epilepsy. Brain. 1991;114 (Pt 5):2333-51.

Buzsaki G. The thalamic clock: emergent network properties. Neuroscience. 1991;41:351-64.

Buzsáki G, Draguhn A. Neuronal oscillations in cortical networks. Science. 2004;304:1926-9.

Carretta D, Sbriccoli A, Santarelli M, Pinto F, Granato A, Minciacchi D. Crossed thalamo-cortical and cortico-thalamic projections in adult mice. Neurosci. Lett. 1996;204:69-72.

Chen S, Billings SA, Luo W. Orthogonal least squares methods and their application to nonlinear system identification. Int J Control. 1989;50:1873-96.

Chen Y, Parker WD, Wang K. The role of T-type calcium channel genes in absence seizures. Front Neurol. 2014;5:45.

David O, Guillemain I, Saillet S, Reyt S, Deransart C, Segebarth C, et al. Identifying neural drivers with functional MRI: an electrophysiological validation. PLoS Biol. 2008;6:2683-97.

Depaulis A, David O, Charpier S. The genetic absence epilepsy rat from Strasbourg as a model to decipher the neuronal and network mechanisms of generalized idiopathic epilepsies. J Neurosci Methods. 2016;260:159-74.

Elger CE, Widman G, Andrzejak R, Arnhold J, David P, Lehnertz K. Nonlinear EEG analysis and its potential role in epileptology. Epilepsia. 2000;41 Suppl 3:S34-8.

Ernst U, Pawelzik K, Geisel T. Synchronization Induced by Temporal Delays in Pulse-Coupled Oscillators. *Phys. Rev. Lett.* 1995;74:1570-3.

Fischer I, Vicente R, Buldu JM, Peil M, Mirasso CR, Torrent MC, et al. Zero-lag long-range synchronization via dynamical relaying. *Phys. Rev. Lett.* 2006;97:123902.

Ghasemi Esfahani Z, Valizadeh A. Zero-lag synchronization despite inhomogeneities in a relay system. PLoS One. 2014;9:e112688.

Gibbs FA DH, Lennox WG. The EEG in epilepsy and in conditions of impaired consciousness Arch Neurol Psychiatr 1935;34:1133–48.

Gibbs FA, Gibbs EL. Atlas of electroencephalography, by F.A.Gibbs and E.L.Gibbs: Cambridge, Mass: Addison-Wesley; 1952.

Gloor P. Generalized cortico-reticular epilepsies. Some considerations on the pathophysiology of generalized bilaterally synchronous spike and wave discharge. Epilepsia. 1968;9:249-63.

Gloor P, Testa G. Generalized penicillin epilepsy in the cat: Effects of intracarotid and intravertebral pentylenetetrazol and amobarbital injections. Electroencephalogr Clin Neurophysiol. 1974;36:499-515.

Gollo LL, Mirasso C, Villa AE. Dynamic control for synchronization of separated cortical areas through thalamic relay. Neuroimage. 2010;52:947-55.

Gotman J, Grova C, Bagshaw A, Kobayashi E, Aghakhani Y, Dubeau F. Generalized epileptic discharges show thalamocortical activation and suspension of the default state of the brain. P Natl Acad Sci USA. 2005;102:15236-40.

Granger CWJ. Investigating Causal Relations by Econometric Models and Cross-spectral Methods. Econometrica. 1969;37:424-38.

Guilhoto LM, Manreza ML, Yacubian EM. Occipital intermittent rhythmic delta activity in absence epilepsy. Arq Neuropsiquiatr. 2006;64:193-7.

Hamandi K, Salek-Haddadi A, Laufs H, Liston A, Friston K, Fish DR, et al. EEG-fMRI of idiopathic and secondarily generalized epilepsies. Neuroimage. 2006;31:1700-10.

He F, Billings SA, Wei HL, Sarrigiannis PG, Zhao Y. Spectral analysis for nonstationary and nonlinear systems: a discrete-time-model-based approach. IEEE Trans Biomed Eng. 2013;60:2233-41.

He F, Billings SA, Wei HL, Sarrigiannis PG. A nonlinear causality measure in the frequency domain: Nonlinear partial directed coherence with applications to EEG. J Neurosci Methods. 2014a;225:71-80.

He F, Wei HL, Billings SA, Sarrigiannis PG. A nonlinear generalization of spectral Granger causality. IEEE Trans Biomed Eng. 2014b;61:1693-701.

He F, Wei H-L, Billings SA. Identification and frequency domain analysis of non-stationary and nonlinear systems using time-varying NARMAX models. Int J Syst Sci. 2015;46:2087-100.

He F, Sarrigiannis PG, Billings SA, Wei H, Rowe J, Romanowski C, et al. Nonlinear interactions in the thalamocortical loop in essential tremor: A model-based frequency domain analysis. Neuroscience. 2016;324:377-89.

Helfrich RF, Knepper H, Nolte G, Struber D, Rach S, Herrmann CS, et al. Selective modulation of interhemispheric functional connectivity by HD-tACS shapes perception. PLoS Biol. 2014;12:e1002031.

Hughes JR. Absence seizures: a review of recent reports with new concepts. Epilepsy Behav. 2009a;15:404-12.

Jarbo K, Verstynen T, Schneider W. In vivo quantification of global connectivity in the human corpus callosum. Neuroimage. 2012;59:1988-96.

Jasper H, Kershman J. Electroencephalographic classification of the epilepsies. Arch Neurol Psychiatry. 1941;45:903-43.

Jones EG. The Thalamus. Cambridge, UK: Cambridge Univ. Press; 2007.

Lehnertz K. Non-linear time series analysis of intracranial EEG recordings in patients with epilepsy--an overview. Int J Psychophysiol. 1999;34:45-52.

Lehnertz K, Andrzejak RG, Arnhold J, Kreuz T, Mormann F, Rieke C, et al. Nonlinear EEG analysis in epilepsy: its possible use for interictal focus localization, seizure anticipation, and prevention. J Clin Neurophysiol. 2001;18:209-22

Lehnertz K. Epilepsy and nonlinear dynamics. J Biol Phys. 2008;34:253-66Li QF, Luo C, Yang TH, Yao ZP, He L, Liu L, et al. EEG-fMRI study on the interictal and ictal generalized spike-wave discharges in patients with childhood absence epilepsy. Epilepsy Res. 2009;87:160-8.

Lopes da Silva F, Pijn JP, Boeijinga P. Interdependence of EEG signals: linear vs. nonlinear associations and the significance of time delays and phase shifts. Brain Topogr. 1989;2:9-18.

Luijtelear GV, Welting J, Quiroga QR. The reticular thalamic nucleus is involved in interhemispheric synchronization of the EEG. Sleep-wake Res Netherlands. 2000;11:86-95.

Manning JP, Richards DA, Bowery NG. Pharmacology of absence epilepsy. Trends Pharmacol Sci. 2003;24:542-9.

Marcus EM, Watson CW. Bilateral synchronous spike wave electrographic patterns in the cat. Interaction of bilateral cortical foci in the intact, the bilateral cortical-callosal, and adiencephalic preparation. Arch Neurol. 1966;14:601-10.

Marcus EM, Watson CW. Symmetrical epileptogenic foci in monkey cerebral cortex. Mechanisms of interaction and regional variations in capacity for synchronous discharges. Arch Neurol. 1968;19:99-116.

Meeren H, van Luijtelaar G, Lopes da Silva F, Coenen A. Evolving concepts on the pathophysiology of absence seizures: the cortical focus theory. Arch Neurol. 2005;62:371-6.

Meeren HK, Pijn JP, Van Luijtelaar EL, Coenen AM, Lopes da Silva FH. Cortical focus drives widespread corticothalamic networks during spontaneous absence seizures in rats. J Neurosci. 2002;22:1480-95.

Meeren HK, van Luijtelaar EL, Lopes da Silva FH, Berdiev RK, Chepurnova NE, Chepurnov SA, et al. [The cortico-thalamic theory for generalised spike-wave discharges]. Usp Fiziol Nauk. 2004;35:3-19.

Moeller F, Siebner HR, Wolff S, Muhle H, Boor R, Granert O, et al. Changes in activity of striato-thalamo-cortical network precede generalized spike wave discharges. Neuroimage. 2008a;39:1839-49.

Moeller F, Siebner HR, Wolff S, Muhle H, Granert O, Jansen O, et al. Simultaneous EEG-fMRI in drug-naive children with newly diagnosed absence epilepsy. Epilepsia. 2008b;49:1510-9.

Molinari M, Minciacchi D, Bentivoglio M, Macchi G. Efferent fibers from the motor cortex terminate bilaterally in the thalamus of rats and cats. Exp Brain Res. 1985;57:305-12.

Munk MH, Roelfsema PR, Konig P, Engel AK, Singer W. Role of reticular activation in the modulation of intracortical synchronization. Science. 1996;272:271-4.

Nowicka A, Tacikowski P. Transcallosal transfer of information and functional asymmetry of the human brain. Laterality. 2011;16:35-74.

Penfield W. Epileptic automatism and the centrencephalic integrating system. Res Publ Assoc Res Nerv Ment Dis. 1952;30:513-28.

Penfield W, Jasper HH. Epilepsy and the functional anatomy of the human brain. Boston: Little, Brown; 1954.

Polack PO, Mahon S, Chavez M, Charpier S. Inactivation of the somatosensory cortex prevents paroxysmal oscillations in cortical and related thalamic neurons in a genetic model of absence epilepsy. Cereb Cortex. 2009;19:2078-91.

Preuss TM, Goldman-Rakic PS. Crossed corticothalamic and thalamocortical connections of macaque prefrontal cortex. J. Comp. Neurol. 1987;257:269-81.

Rajagovindan R, Ding M. Decomposing neural synchrony: toward an explanation for near-zero phase-lag in cortical oscillatory networks. PLoS One. 2008;3:e3649.

Raos V, Bentivoglio M. Crosstalk between the two sides of the thalamus through the reticular nucleus: a retrograde and anterograde tracing study in the rat. J Comp Neurol. 1993;332:145-54.

Roelfsema PR, Engel AK, König P, Singer W. Visuomotor integration is associated with zero time-lag synchronization among cortical areas. Nature. 1997;385:157-61.

Salami M, Itami C, Tsumoto T, Kimura F. Change of conduction velocity by regional myelination yields constant latency irrespective of distance between thalamus and cortex. Proc Natl Acad Sci U S A. 2003;100:6174-9.

Salamy A. Commissural transmission: maturational changes in humans. Science. 1978;200:1409-11.

Sarrigiannis PG, Zhao Y, Wei HL, Billings SA, Fotheringham J, Hadjivassiliou M. Quantitative EEG analysis using error reduction ratio-causality test; validation on simulated and real EEG data. Clin Neurophysiol. 2014;125:32-46.

Sarrigiannis PG, Zhao Y, He F, Wei H, Billings SA, Lawrence S, et al. Direct Functional Connectivity between the Thalamus (Vim) and the Contralateral Motor Cortex: Just a Single Case Observation or a Common Pathway in the Human Brain? Brain Stimul. 2015;8:1230-3.Schnitzler A, Gross J. Normal and pathological oscillatory communication in the brain. Nat Rev Neurosci. 2005;6:285-96.

Singer W, Gray CM. Visual feature integration and the temporal correlation hypothesis. Annu Rev Neurosci. 1995;18:555-86.

Slotnick SD, Moo LR, Kraut MA, Lesser RP, Hart J, Jr. Interactions between thalamic and cortical rhythms during semantic memory recall in human. Proc Natl Acad Sci U S A. 2002;99:6440-3.

Spencer SS, Katz A, Ebersole J, Novotny E, Mattson R. Ictal EEG changes with corpus callosum section. Epilepsia. 1993;34:568-73.

Spiegel EA, Wycis HT. Thalamic recordings in man with special reference to seizure discharges. Electroencephalogr Clin Neurophysiol. 1950;2:23-7.

Spiegel EA, Wycis HT, Reyes V. Diencephalic mechanisms in petit mal epilepsy. Electroencephalogr Clin Neurophysiol. 1951;3:473-5.

Stefan H, Lopes da Silva FH. Epileptic neuronal networks: methods of identification and clinical relevance. Front Neurol. 2013;4:8.

Steriade M, Deschênes M, Domich L, Mulle C. Abolition of spindle oscillations in thalamic neurons disconnected from nucleus reticularis thalami. J Neurophysiol. 1985;54:1473-97.

Tenney JR, Fujiwara H, Horn PS, Jacobson SE, Glauser TA, Rose DF. Focal corticothalamic sources during generalized absence seizures: a MEG study. Epilepsy Res. 2013;106:113-22.

Thatcher RW. Coherence, Phase Differences, Phase Shift, and Phase Lock in EEG/ERP Analyses. Dev Neuropsychol. 2012;37:476-96.

Theiler J, Eubank S, Longtin A, Galdrikian B, Doyne Farmer J. Testing for nonlinearity in time series: the method of surrogate data. Physica D. 1992;58:77-94.

Timofeev I, Steriade M. Low-frequency rhythms in the thalamus of intact-cortex and decorticated cats. J Neurophysiol. 1996;76:4152-68.

V~~v~~an Luijtelaar G, Sitnikova E. Global and focal aspects of absence epilepsy: the contribution of genetic models. Neurosci Biobehav Rev. 2006;30:983-1003.

Vergnes M, Marescaux C, Lannes B, Depaulis A, Micheletti G, Warter JM. Interhemispheric desynchronization of spontaneous spike-wave discharges by corpus callosum transection in rats with petit mal-like epilepsy. Epilepsy Res. 1989;4:8-13.

Vicente R, Fischer I, Mirasso CR. Synchronization properties of three delay-coupled semiconductor lasers. Phys Rev E Stat Nonlin Soft Matter Phys. 2008a;78:066202.

Vicente R, Gollo LL, Mirasso CR, Fischer I, Pipa G. Dynamical relaying can yield zero time lag neuronal synchrony despite long conduction delays. Proc. Natl. Acad. Sci. 2008b;105:17157-62.

Viriyopase A, Bojak I, Zeitler M, Gielen S. When Long-Range Zero-Lag Synchronization is Feasible in Cortical Networks. Front Comput Neurosci. 2012;6:49.

von Stein A, Sarnthein J. Different frequencies for different scales of cortical integration: from local gamma to long range alpha/theta synchronization. Int J Psychophysiol. 2000;38:301-13.

Wang SSH, Shultz JR, Burish MJ, Harrison KH, Hof PR, Towns LC, et al. Functional trade-offs in white matter axonal scaling. J. Neurosci. 2008;28:4047-56.

Watemberg N, Linder I, Dabby R, Blumkin L, Lerman-Sagie T. Clinical correlates of occipital intermittent rhythmic delta activity (OIRDA) in children. Epilepsia. 2007;48:330-4.

Westmijse I, Ossenblok P, Gunning B, van Luijtelaar G. Onset and propagation of spike and slow wave discharges in human absence epilepsy: A MEG study. Epilepsia. 2009;50:2538-48.

Williams D. A study of thalamic and cortical rhythms in petit mal. Brain. 1953;76:50-69.

Witham CL, Wang M, Baker SN. Cells in somatosensory areas show synchrony with beta oscillations in monkey motor cortex. Eur J Neurosci. 2007;26:2677-86.

Zhang D, Snyder AZ, Fox MD, Sansbury MW, Shimony JS, Raichle ME. Intrinsic Functional Relations Between Human Cerebral Cortex and Thalamus. J. Neurophysiol. 2008;100:1740-8.

Zhao Y, Billings SA, Wei H, Sarrigiannis PG. Tracking time-varying causality and directionality of information flow using an error reduction ratio test with applications to electroencephalography data. Phys Rev E Stat Nonlin Soft Matter Phys. 2012;86:051919.

Zhao Y, Billings SA, Wei H, He F, Sarrigiannis PG. A new NARX-based Granger linear and nonlinear casual influence detection method with applications to EEG data. J Neurosci Methods. 2013a;212:79-86.

Zhao Y, Billings SA, Wei HL, Sarrigiannis PG. A parametric method to measure time-varying linear and nonlinear causality with applications to EEG data. IEEE Trans Biomed Eng. 2013b;60:3141-8.

Appendix A

The error reduction ratio (ERR) causality test

This is a test that we have previously introduced which overcomes most of the disadvantages of existing methods. (Zhao et al., 2012, Zhao et al., 2013b, Sarrigiannis et al., 2014) The aim of this approach is to characterise the causal interaction over time between two signals, denoted by X and Y. At a specific time the following possibilities can occur, signal X causes Y, Y causes X, X and Y are coincident, there is no interaction, or bidirectional interactions occur between them. Both X and Y may have been caused by an input u but here u is unknown and un-measurable. For a complex system, the causality is often ~~time varying~~time-varying and the interactions are often dynamic and nonlinear.

Initially, construct a candidate term set which is typically constructed by past information of Y, for example y(t -1),y(t – 2), . . . and past information of X, for example x(t-1),x(t-2),. . .with a specific model order d. Apply the adaptive-forward-OLS algorithm (See Appendix B) which has been derived from the orthogonal least squares (OLS) algorithm (Billings et al., 1988) and compute ERR and the penalized error-to-signal ratio PESR) (Billings and Wei, 2008) value for each candidate term. ERR indicates how much of the variance change in the system response is caused by the considered term, in a percentage form. If the significant terms selected by this algorithm based on values of ERR include any term from the past information of X, this indicates that signal X leads Y during the considered time duration (t-h, t) where h denotes the sampling window size - this was selected at 500~~12~~ data points (corresponding to 1s) for this work. The ERR-causality from X to Y at time t, expressed as $F_{x\rightarrow y}(t)$ is then defined as 1. If no component from the past information of X is included in the selected significant terms, this indicates that X has no interaction with Y during [t-h, t] and $F_{x\rightarrow y}(t)$ is defined to be 0. The strength of $F_{x\rightarrow y}(t)$ can be estimated using the summed ERR values of all the selected terms from past information of X, the maximum strength being 1. The time shift of $X\rightarrow Y$ is defined as the time lag of X in the first term ranked by the values of ERR. The key advantage of this test is that it can be applied to both linear and nonlinear dynamic systems. Unlike the well-established Granger-based tests (Granger, 1969) to quantify the causality between two signals, ERR-Causality method does not depend on the full knowledge or the estimation of a complete and unbiased system model. By exploiting an important property of the ERR-Causality test, part of the orthogonal least squares algorithm, it is shown that the causal flow can be detected even when the model is incomplete. This is a significant advantage when the underlying system is nonlinear and dynamic and the measurements may be noisy, because a complete and full model

including a nonlinear noise model, which would normally be required to yield unbiased model estimates, is not required and indeed not even the full parameter estimates are used in the test. These advantages mean that the test is relatively easy to apply and can be used to track fast transitions between causal effects to detect the direction of linear or nonlinear causal interactions, determine the strength of these interactions, and provide an estimate of the time lag shift between two EEG signals in this instance. The ERR causality, when significant, depends on the phase relationship of the signals and not from their amplitudes as shown with the surrogate marker (i.e. the time-varying threshold above which the causal influence between two signals is statistically significant). The surrogate level is estimated by randomising the phases of the signals while preserving amplitudes. The ERR method also has a very good performance against noise (Zhao et al., 2012). Furthermore, linear and nonlinear interactions can be separated and analysed independently with this method. As shown by Meeren et al ~~.~~ in rat experiments the nonlinear estimates can be of paramount importance for the detection of correct time lags and direction of synchronisation, particularly for the very brief transition period into the absence.

Formatted: Font: 12 pt

Appendix B

Time-varying nonlinear parametric modeling

To analyse the nonlinear interactions between EEG recording derivations, a robust and high-resolution nonlinear frequency domain approach was additionally implemented in three of the cases to show the frequency content of cross frequency interactions. With this approach we were also able to independently assess the reproducibility of the ERR findings with an entirely different algorithm. Firstly, a recent proposed time-varying NARX (~~TVNARX~~TV-NARX) model is applied in the time domain to identify both the linear and nonlinear interactions between key EEG channels. It will later be mapped to the frequency domain to reveal important frequency related features and interactions between signals. The ~~TVNARX~~TV-NARX model is a nonlinear polynomial regression model with the following form:

$$y(t)=\sum_{n=1}^{M} y_n(t)+e(t)$$
$$y_n(t)=\sum_{p=0}^{n}\sum_{k_1,k_{p+q}=1}^{K} c_{p,q}(k_1,\ldots,k_{p+q},t)\times\prod_{i=1}^{p} y(t-k_i)\prod_{i=p+1}^{p+q} u(t-k_i) \qquad \text{(B.1)}$$

where $y_n(t)$ is the n[th]-order output of the system and M is the maximum order of the nonlinearity, with $p+q=n$, $k_i=1,\ldots,K$, $\sum_{k_1,k_{p+q}=1}^{K} \equiv \sum_{k_1=1}^{K}\cdots\sum_{k_{p+q}=1}^{K}$. The time-varying parameters $c_{p,q}(k_1,\ldots,k_{p+q},t)$ are then expanded using multi-wavelet basis functions (He *et al*., 2015), and the time-varying model is transformed into an expanded time invariant regression model. Detecting the correct model structure and reducing the number of terms in the expanded model is crucial. The forward regression with orthogonal least squares (FROLS) method (Billings et al., 1989, Chen et al., 1989) can be used to select the expanded model structure and estimated relevant coefficients, and the original TV parameters can then be recovered. The model selection procedure can be validated using the generalized cross-validation criterion (Golub, Heath, and Wahba 1979) or Akaike information criterion (Akaike 1974). The former validation routine is applied to the examples shown in this paper.

Frequency domain mapping and analysis

Spectral analysis for linear systems is a well-established and widely used tool in signal processing. It is well known that the output frequency response of a stable linear time invariant system can be expressed as $Y(f)=H(f)\cdot X(f)$, where $X(f)$ and $Y(f)$ are the Fourier transforms of the system input and output time series, $x(t)$ and $y(t)$, respectively. The frequency response function (FRF) $H(f)$ describes the frequency domain characteristics of a linear systems. For example, the 'peaks' in the FRF, known as the 'resonance frequencies', describe at which frequencies the output response will be amplified. However, a linear system would never generate extra new frequency components in the output spectrum. To study the cross-frequency interactions in the brain (He et al., 2016), nonlinear model based frequency domain analysis has to be used.

The frequency domain analysis of a nonlinear system is much more complicated. The input-output relationship of a nonlinear time-varying system can be described by a time-varying output frequency response function (TV-OFRF):

$$Y(f,t)=\sum_{n=1}^{M}\left(\frac{1}{\sqrt{n}}\int_{f_1+\cdots+f_n=f} H_n(f_1,\ldots,f_n,t)\prod_{i=1}^{n}X(f,t)df\right) \quad \text{(B.2)}$$

The n[th]-order time-varying generalized frequency response function (TV-GFRF), $H_n(f_1,\ldots,f_n,t)$, extends the linear FRF to higher orders and includes an extra time dimension (t). It can be expressed directly from the identified time domain ~~TVNARX~~TV-NARX model, and integrated over the n-dimensional hyper-plane $f_1+\ldots+f_n=f$ with the input spectrum to provide the nth-order TV-OFRFs.

The first-order GFRF describes the linear frequency response (similar to the FRF in a linear system) and only corresponds to the linear part of the nonlinear time-domain model. The gains of a second or a higher order GFRF would be in a high dimensional space and their maxima are the 'ridges' rather than 'peaks'. The

locations of the 'ridges' indicate the transfer of energy from input spectral components to the output spectra at their summation, to produce nonlinear effects such as harmonics or intermodulation .

We have shown in previous work by implementing a NARX model how pivotal nonlinear interactions are in detecting state specific cortico-thalamic coupling within the central tremorogenic network in essential tremor (He et al., 2016). We are hereto applying a ~~time varying~~time-varying but otherwise similar approach on EEG recordings from absence seizures.

The contributions of the pure input, output and cross-product non-linearities in (2) are given as

$$
\begin{aligned}
H_{n_u}(f_1,\ldots,f_n) &= \sum_{k_1,k_n=1}^{K} c_{0,n}(k_1,\ldots,k_n)e^{-j2\pi(f_1k_1+\cdots+f_nk_n)/f_s} \\
H_{n_{uy}}(f_1,\ldots,f_n) &= \sum_{q=1}^{n-1}\sum_{p=1}^{n-q}\sum_{k_1,k_{p+q}=1}^{K} c_{p,q}(k_1,\ldots,k_{p+q}) \\
&\quad \times H_{n-q,p}(f_1,\ldots,f_{n-q})e^{-j2\pi(f_{n-q+1}k_{n-q+1}+\cdots+f_nk_{p+q})/f_s} \\
H_{n_y}(f_1,\ldots,f_n) &= \sum_{p=2}^{n}\sum_{k_1,k_n=1}^{K} c_{0,n}(k_1,\ldots,k_n)H_{n,p}(f_1,\ldots,f_n)
\end{aligned}
\qquad \text{(B.3)}
$$

The contribution of the pth-order non-linearity in $y(t)$ to the nth-order GFRF, $H_{n,p}(\cdot)$, can be recursively computed according to (Peyton Jones and Billings 1989) as

$$
H_{n,p}(\cdot) = \sum_{i=1}^{n-p+1} H_i(f_1,\ldots,f_i)H_{n-i,p-i}(f_{i+1},\ldots,f_n)e^{-j2\pi(f_1+\ldots+f_i)k_p/f_s} \qquad \text{(B.4)}
$$

The above recursion finishes with p=1, where the $H_{n,1}(f_1,\ldots,f_n)$ is defined as

$$
H_{n,1}(f_1,\ldots,f_n) = H_n(f_1,\ldots,f_n)e^{-j2\pi(f_1+\ldots+f_i)k_1/f_s} \qquad \text{(B.5)}
$$

Table 1

Case	Gender	Age	Absences ✣	Duration ✦	OIRDA ✧	Av. Synch ✻	%0Lag ✺
1	F	5	3	26-40s	+	F8F4-F7F3[1] 0.91	F8F4-F7F3[2] 39%
2	F	6	1	20s	+	T5O1-T6O2 0.94	P3O1-T6O2 27%
3	M	9	2	5-6s	-	F8F4-F7F3[1] 0.93	T4C4-T3C3[2] 61%
4	M	8	2	9-12s	-	F8F4-F7F3[2] 0.89	T4C4-T3C3 44%
5	M	8	2	8-11s	-	F8F4-F7F3[1] 0.92	F8F4-F7F3[1] 67%
6	M	7	3	6-10s	-	T3C3-F7F3[1] 0.9	T3C3-F7F3[1] 45%
7	F	5	2	13s	-	F4C4-F3C3[2] 0.86	F4C4-F3C3[2] 47%
8	F	7	2	4-6s	+	FzCz-F4C4[2] 0.82	T3T5-F7F3[1] 51%
9	F	6	2	7-8s	+	T3C3-F7F3[2] 0.86	CzPz-P3O1[2] 39%
10	M	10	1	16s	-	F8F4-F7F3 0.85	F4C4-F3C3 28%
11	F	9	2	17-22s	-	FzCz-F4C4[2] 0.9	FzCz-F4C4[2] 66%
12	F	6	3	9-19s	-	F8F4-F7F3[1] 0.89	T4C4-T3C3[3] 34%
13	F	7	4	14-23s	+	F8F4-F7F3[2] 0.91	F8F4-F7F3[1] 42%
14	F	9	2	5-6s	+	F8F4-F7F3[1] 0.83	T3T5-T4T6[2] 44%
15	M	10	3	4-5s	+	F8F4-F7F3[1] 0.93	F8F4-F7F3[3] 61%
16	F	6	1	30s	-	T4C4-T3C3 0.92	T4C4-T3C3 44%
17	M	10	7	5-14s	+	F8F4-F7F3[1] 0.92	T4C4-T3C3[2] 53%
All ☒	10F/7M	5-10y	1-7	4-40s	9-/8+	T5O1-T6O2[case2] 0.94	F8F4-F7F3[case 5] 67%

✣Absences, total number of spontaneous absences, excluding those from hyperventilation

✦Duration, range of duration estimated from the very onset to the offset of each absence/patient

✧OIRDA, occipital intermittent rhythmical delta activity

✻Av. Synch, highest average strength of synchronisation including onset and offset of each absence (highest score/patient)

✺% Zero-lag, highest % of 0-lag synchronisation including onset and offset of each absence (highest score/patient)

☒ALL, range for age, number of absences and duration for the individual cases, in last two columns the set of channels with the highest value are shown (superscript refers to the case with highest score)

The superscript in the last two columns indicates the number of absence in chronological order that the highest value was observed

Table 2

Ranking Order for average strength and % of 0-Lag synchronisation

Av. Synch ✻ All 42 abs		**%0-Lag** ✺ All 42 abs		**Probability top 5** ✧ All 42 abs - Av. Synch		**Probability top 5** ✧ Case 17, 7 abs - Av. Synch	
Channel pair	**Freq.**	**Channel pair**	**Freq.**	**Channel pair**	**Prob. & CI**	**Channel pair**	**Prob. & CI**
F8F4-F7F3	*40*	**F4C4-F3C3**	**19**	**F8F4-F7F3**	95% CI (84-99)	**F8F4-F7F3**	100% CI (59-100)
T4C4-T3C3	*35*	**F8F4-F7F3**	**18**	**T4C4-T3C3**	83% CI (69-93)	**T4C4-T3C3**	100% CI (59-100)
F4C4-F3C3	*25*	**T4C4-T3C3**	**17**	**F4C4-F3C3**	60% CI (43-74)	**T3T5-T4T6**	0.86 CI (42-100)
FZCZ-F3C3	*22*	**P3O1-P4O2**	**11**	**FZCZ-F3C3**	52% CI (36-68)	**FZCZ-F3C3**	71% CI (29-96)
FZCZ-F4C4	*20*	**FZCZ-F3C3**	**9**	**FZCZ-F4C4**	48% CI (32-64)	**T4C4-F8F4**	71% CI (29-96)
T4C4-F8F4	*16*	T5O1-T6O2	9	T4C4-F8F4	38% CI (24-54)	F4C4-F3C3	71% CI (29-96)
T3C3-F7F3	*10*	FZCZ-F4C4	4	T3C3-F7F3	24% CI (12-39)	F4C4-F3C3	29% CI (4-71)
T5O1-T6O2	*10*	T3T5-F8F4	4	T5O1-T6O2	24% CI (12-39)	T3C3-F8F4	29% CI (4-71)
P3O1-P4O2	*9*	F3C3-F8F4	3	P3O1-P4O2	21% CI (10-37)	FZCZ-F4C4	14% CI (0-58)
T3T5-T4T6	*9*	T3T5-T4T6	3	T3T5-T4T6	21% CI (10-37)	T5O1-T3C3	14% CI (0-58)
T3C3-F8F4	*7*	T6O2-T4C4	3	T3C3-F8F4	17% CI (7-31)		
T4C4-F7F3	*6*	T3C3-F7F3	2	T4C4-F7F3	14% CI (5-29)		
F3C3-F8F4	*5*	T3T5-F7F3	2	F3C3-F8F4	12% CI (4-26)		
P3O1-T6O2	*2*	T6O2-T3C3	2	P3O1-T6O2	5% CI (1-16)		

✻Av Synch, highest average strength of synchronisation including onset and offset of each absence (first absence/patient)
✺% Zero-lag, highest % of 0-lag synchronisation including onset and offset of each absence (first absence/patient)
✧Probability top 5, probability of being ranked in top 5 channel pairs for highest average level of synchronisation

Freq= Frequency for pairs of channels ranked in top 5, for highest levels of Av. Synch and %0-lag
CI= 95% confidence intervals
Prob= probability

Table 3

Ranking Order for average strength of synchronisation

Av. Synch* All 17 cases- 1abs/case		**Probability top 5** ✧ All 17 cases - Av. Synch	
Channel pair	**Freq.**	**Channel pair**	**Prob & CI**
F8F4-F7F3	15	**F8F4-F7F3**	88% CI(64-99)
T4C4-T3C3	14	**T4C4-T3C3**	82% CI(57-96)
F4C4-F3C3	9	**F4C4-F3C3**	53% CI(28-77)
FZCZ-F4C4	9	**FZCZ-F4C4**	53% CI(28-77)
FZCZ-F3C3	8	**FZCZ-F3C3**	47% CI(23-72)
P3O1-P4O2	6	**P3O1-P4O2**	35% CI(14-62)
T4C4-F8F4	6	**T4C4-F8F4**	35% CI(14-62)
T3C3-F7F3	4	**T3C3-F7F3**	24% CI(7-50)
T5O1-T6O2	4	**T5O1-T6O2**	24% CI(7-50)
T3C3-F8F4	3	**T3C3-F8F4**	18% CI(4-43)
T4C4-F7F3	3	**T4C4-F7F3**	18% CI(4-43)
F3C3-F8F4	2	**F3C3-F8F4**	12% CI(1-36)
P3O1-T6O2	2	**P3O1-T6O2**	12% CI(1-36)
T3T5-T4T6	2	**T3T5-T4T6**	12% CI(1-36)

*Av Synch, highest average strength of synchronisation including onset and offset of each absence (first absence/patient)

✧ Probability top 5, probability of being ranked in top 5 channel pairs for highest average level of synchronisation

Freq= Frequency for pairs of channels ranked in top 5 for Av. Synch level
CI= 95% confidence intervals
Prob= probability

Table 4

Case & Absence ☒	FzCz to F4C4 or F3C3 Ranking order for Av. Syn. Strength n°/91 ◆	Direction of synchronisation between FzCz(M), F4C4(R) and F3C3(L)					FzCz to F4C4 or F3C3 Time lags	EEG homologous pair ranked in top 3 for Av. Syn. Strength with highest % of 0-Lag synchronisation				
		R➢M	M➢R	L➢M	M➢L	R/L=M	Mean lags +/- SD	Channel pair	Mean lags +/- SD	R➢L	L➢R	R=L
1, abs 3	2	-	-	93%	5%	2%	8.1 (3.7)	F8F4-F7F3	2.64 (3.4)	61%	7%	32%
2, abs 1	8	-	-	90%	5%	5%	4.98 (4.36)	F8F4-F7F3	1.89 (3.9)	62%	17%	21%
3, abs 1	4	-	-	97%	0%	3%	7.89 (3)	F4C4-F3C3	2.6 (3.8)	3%	35%	62%
4, abs 1	3	83%	6%	-	-	11%	6.23 (4.5)	F8F4-F7F3	2.4 (3.8)	15%	52%	33%
5, abs 1	5	89%	-	-	-	11%	3.32 (2.24)	F8F4-F7F3	0.47 (1.1)	4%	29%	67%
6, abs 3	9	68%	10%	-	-	22%	4.2 (4.3)	T4C4-T3C3	0.05 (5.3)	34%	44%	22%
7, abs 2	3	97%	-	-	-	3%	6.6 (2.9)	F4C4-F3C3	0.75 (2.6)	40%	17%	44%
8, abs 2	**1**	**72%**	**6%**	-	-	**23%**	**2.19 (2.88)**	**T4C4-T3C3**	**0.19 (3.9)**	**48%**	**28%**	**23%**
9, abs 1	19	-	-	95%	3%	2%	8.24 (3.97)	F8F4-F7F3	2 (3.75)	64%	12%	24%
10, abs 1	3	-	-	93%	-	6%	8 (2.39)	F4C4-F3C3	3 (2.66)	2%	70%	28%
11, abs 1	**1**	**41%**	**7%**	-	-	**52%**	**1.2 (2.2)**	**F4C4-F3C3**	**0.71 (3.23)**	**22%**	**44%**	**34%**
12, abs 1	5	89%	7%	-	-	4%	7.38 (4.35)	T4C4-T3C3	0.25 (3.19)	35%	39%	26%
13, abs 1	3	-	-	97%	1%	2%	8.11 (2.4)	F8F4-F7F3	0.03 (3.5)	36%	23%	41%
14, abs 2	3	-	-	72%	14%	14%	3.2 (5.5)	F4C4-F3C3	1 (3.23)	44%	24%	32%
15, abs 3	4	90%	10%	-	-	0%	4.2 (2.0)	F8F4-F7F3	0.85 (2.92)	15%	21%	64%
16, abs 1	3	68%	6%	-	-	26%	1.92 (2.27)	T4C4-T3C3	0.43 (2.3)	20%	37%	44%
17, abs 5	**1**	-	-	**39%**	**35%**	**27%**	**0.41 (2.6)**	**F4C4-F3C3**	**3.9 (6.1)**	**60%**	**22%**	**18%**

☒For each of the 17 cases the absence with the highest average synchronisation strength, between midline and parasagittal frontocentral derivations, was selected.

◆Ranking order within 91 channel pair estimates for ictal average synchronisation strength.

There are only 3 cases where the parasagittal versus midline channel pairs score a higher level of synchronisation in comparison to the top ranked homologous derivations (highlighted in bold).
Av. Syn.= average synchronisation

Figure legends

Figure 1.

Estimates of synchronisation with ERR causality, time lags and spectra.

(A-E) The absence with the highest percentage of ictal zero-Lag synchronisation is shown (case 5) and the estimates of ictal Error Reduction Ratio Causality for the frontal EEG homologous projections are produced. (A) Normalised right and left frontal EEG recordings. (B) Color-coded time lags (blue and red indicate the direction of synchronisation, from right to left and vice versa, respectively). These are estimates of time lags between the two EEG time series shown in A, which are equivalent to phase lags. (C) Normalised levels of synchronisation, with blue and red colours indication the direction of causality, as above, while green colour refers to time lags close to isochronous synchronisation (≤2ms). (D) In blue the contour of the strength of synchronisation and in red the surrogate estimates, indicating that all synchronisation values are statistically very significant (much above the surrogate 95% confidence interval). The surrogate time-varying threshold, shown in red, defines the level of causality above which values have less than 5% probability of occurring by chance. -(E) Sliding FFT window (500 data blocks with half a window overlap) illustrating a~~the~~ drop in high frequencies, towards the completion of the absence.

Figure 2.

Ictal strength of synchronisation for Homotopic versus Heterotopic areas.

Mean and 95% confidence intervals (CI) of ictal average synchronisation strength for each channel pair shown (one absence for each of the 17 cases, the one with the highest average ictal synchronisation strength is included). The channel pairs shown are within the top 5/91 ranked for average synchronisation strength. There are statistically significant differences when comparing the mean value from F8F4-F7F3 to the heterologous contiguous and the heterologous bi-hemispheric channel pairs, reflecting the underlying anatomical direct structural connectivity between these regions. The findings are remarkably similar to those observed in the WAG/Rij rat model of absence epilepsy (Meeren et al 2002), where cortico-cortical versus transcallosal connectivity produces much higher synchronisation levels for the latter.

Figure 3.

Homologous versus midline interactions.

Five examples of ERR synchronisation strength estimates with their respective time lags to include the onset of each absence are shown. The upper half of the figure shows the estimates between the top ranked (for synchronisation strength) homologous frontal or frontocentral derivations. The lower half, of the figure displays the time locked values between the top ranked right or left parasagittal frontocentral derivation,

versus the frontocentral midline channel. Noticeably time shifts between homologous anterior areas show at the very beginning of each absence lags ≥ 4ms. Then, within a second from onset, causality lags drop ≤2ms; they are colour coded in green to discern the occurrence of tight, practically isochronous synchronisation.

Figure 4.

Source of nonlinear synchronisation (ERR causality test) for the transition into the absences.

(A-D) Eight examples (from different cases) showing the earliest rise in nonlinear synchronisation for the pre-ictal and/or early ictal period. For each of the absence shown the upper part shows the normalised EEG recordings and the lower, highlighted in yellow, the estimates of nonlinear synchronisation (the surrogate level is shown in blue). The vertical purple cursors shows an attempt to mark the subjective onset of the first reasonably formed SW discharge on the EEG data and the objective rise in nonlinear synchronisation, above the surrogate level, for each of the nonlinear sharp rises in synchronisation. Nonlinear synchronisation strength in C (i) versus combined linear and nonlinear (ii) estimates for the same epoch from case 14. Nonlinear D (i) versus linear D (ii) estimates of synchronisation for case 17.

Distinctively, in all examples shown the short-lived rise in nonlinear synchronisation occurs at or just before the onset of the electrographic changes. Please note that this analysis is exclusively in the time domain, and information for the frequency content of the interactions can be found in figures 6 and 7.

Figure 5.

Source of nonlinear synchronisation rise for the transition into the absences.

(A) Diagram showing the earliest rise of nonlinear synchronisation for the absence with the highest nonlinear rise in synchronisation for each of the 17 patients. (B) The same diagram for each of the seven and four absences captured from case 17 and 13, respectively.

For the 17 absences shown in A the source localises in the frontal and frontocentral areas in 13/17 (76%). In B multiple absences from 2 OIRDA patients (cases 17 and 13) show variability on the localisation of the earliest nonlinear synchronisation rise. Note that again none of the absences from the latter 2 patients show an onset from the temporal or temporo-occipital recording sites. Five out of 7 absences in case 17 and 2 out of 4 in case 13, in total 7/11 (64%) show an anterior source despite showing an OIRDA EEG phenotype on their interictal records.

The strength of synchronisation is expressed by the proportionally sized dotted lines.

Figure 6.

Nonlinear ~~time varying~~time-varying generalised frequency response functions (TV-GFRFs).

The directional TV-GFRFs are produced to include the pre-ictal and initial ictal period of three absences (case1, case 3 and case17). The channel pair shown here for each of the three cases was revealed as the source of the nonlinear ERR causality rise during the transition into the same absences (Fig. 4 and 5).

(A and B) Linear and nonlinear TV- GFRFs. The black dotted arrows denote the onset of the generalised SW discharges on the EEG. There is a rise in the nonlinear interactions involving high frequencies >20Hz at or before the onset of each of the absence seizures while there is a significant rise in linear synchronisation and a drop in the nonlinear effects during the seizures.

Figure 7.

~~Time varying~~Time-varying generalised frequency response functions (TV-GFRFs) to include pre-ictal, ictal and post-ictal period.

(A-B) Dynamic changes in the spectra of the TV-GFRFs of a single absence (case 1). The black dotted arrows denote the onset of the generalised SW discharges on the EEG. In the initial and brief pre-ictal period of the seizure, a short-lived rise in nonlinear associations B (i) is followed by a precipitous drop that coincides with a very significant rise in linear interactions A (i). This persists during the absence A and B (ii). Nonlinear effects, to include higher frequencies (>15Hz), rise again towards the final part of the attack whilst at the same time the linear synchronisation drops significantly, A and B (iii).

Legends for the Supplementary Material

Supplementary Figure S1.

Referential channels in Spike 2 software.

Selection of the transition period into an absence seizure. A four second epoch was selected for each absence with a referential montage. The same sweep speed was used for all data selection. Each four-second epoch included three seconds before the onset of the first generalised spike and one second after, as shown in this example.

Supplementary PowerPoint 1.

The earliest rise in nonlinear synchronisation for all 17 cases for the absence with the highest nonlinear value for each case are shown. For each 4-second epoch, the nonlinear partial directed synchronisation was estimated for all possible 182 combinations of channels pairs. Subsequently the pairs with the highest synchronisation strength were selected (a window defined by the highest level minus 25% was constructed for each absence). With a custom build software function, constructed for the purpose, the channel pair with the earliest rise in nonlinear synchronisation, selected with the aforementioned synchronisation strength criterion, was detected. With this approach the source of the strongest nonlinear synchronisation emergence is found. EER estimates of nonlinear synchronisation throughout the absences are also shown for case 1, 3 and case 17, for the same derivations shown in Fig. 4 and Fig. 6 for consistency.

Supplementary PowerPoint 2.

Ictal synchronisation estimates with the ERR causality test for the first absence for each of the 17 cases. The top ranked (for average strength of ictal bidirectional synchronisation) homotopic channel pair, included in the top 5/91 for each absence is shown. Noticeably a tight synchronisation lag $\leq$2ms is reached 1 second after the commencement of each absence for 15 of the cases and within 2 seconds for the remaining 2 (cases 6 and 17). For all cases, time lags $\geq$4ms are seen at or just before the emergence of spikes and spike and wave discharges.

Supplementary XL.

For each absence we have identified which of the 182 pairs of channels showed the earliest rise in nonlinear synchronisation. For this purpose we have constructed a window, defined by the highest value of nonlinear synchronisation observed in each of the 42 absences for all 182-channel pairs minus 25%, so only the pairs with the most substantial rise in synchronisation were selected for each seizure. The channel pairs and the

time sequence reaching this threshold are shown. All results are statistically significant (i.e. above surrogate level of nonlinear synchronisation).

Supplementary PDF.

Nonlinear Synchronisation source pdf.

Source of nonlinear synchronisation rise for all 17 cases (the absence with highest nonlinear rise in synchronisation for each case was selected). All seizures show a dramatic rise in nonlinear synchronisation, above the surrogate level of statistical significance, at or just before the onset of the ictal EEG perturbations.

Figure 1

Click here to download high resolution image

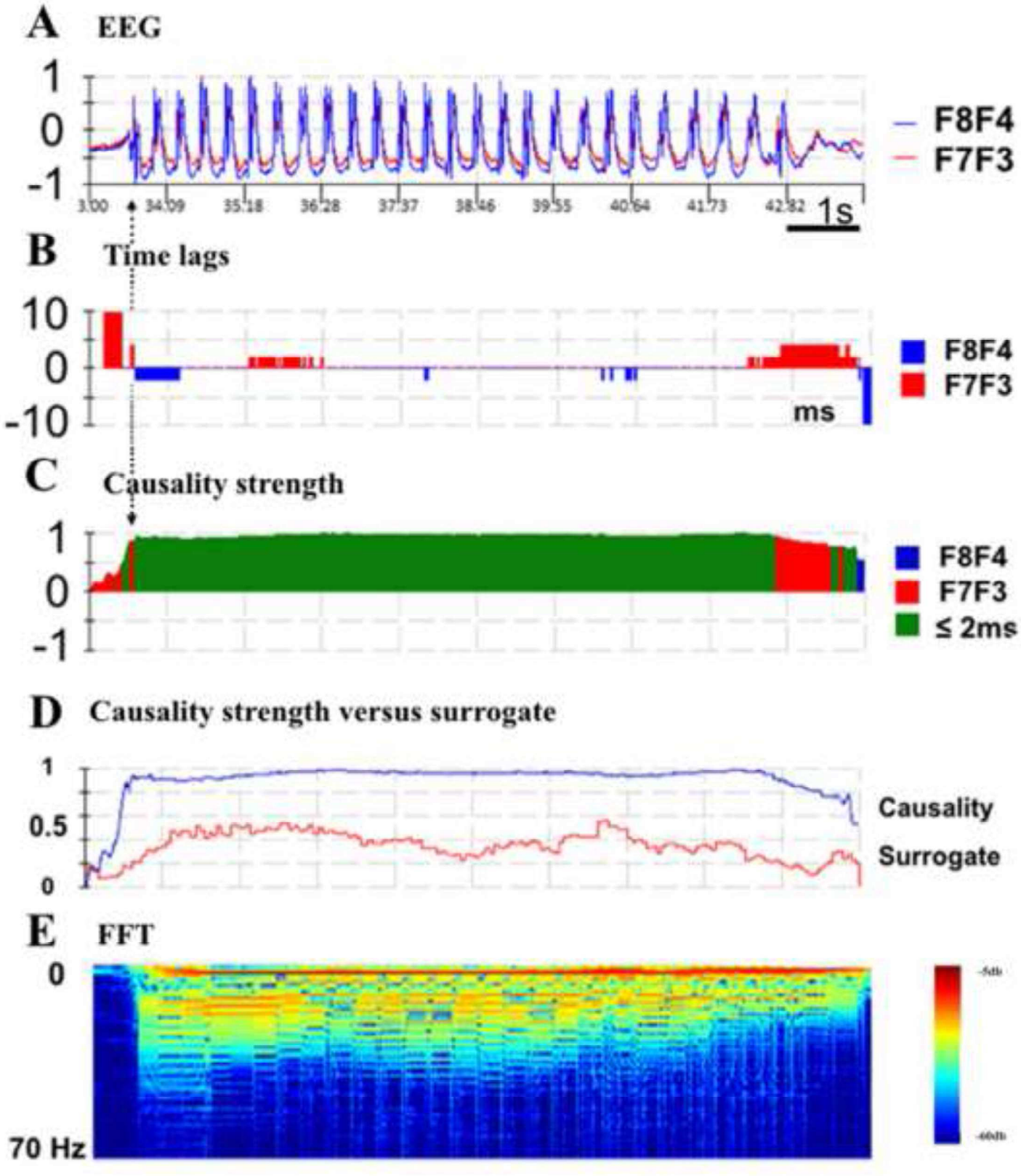

Figure 2
Click here to download high resolution image

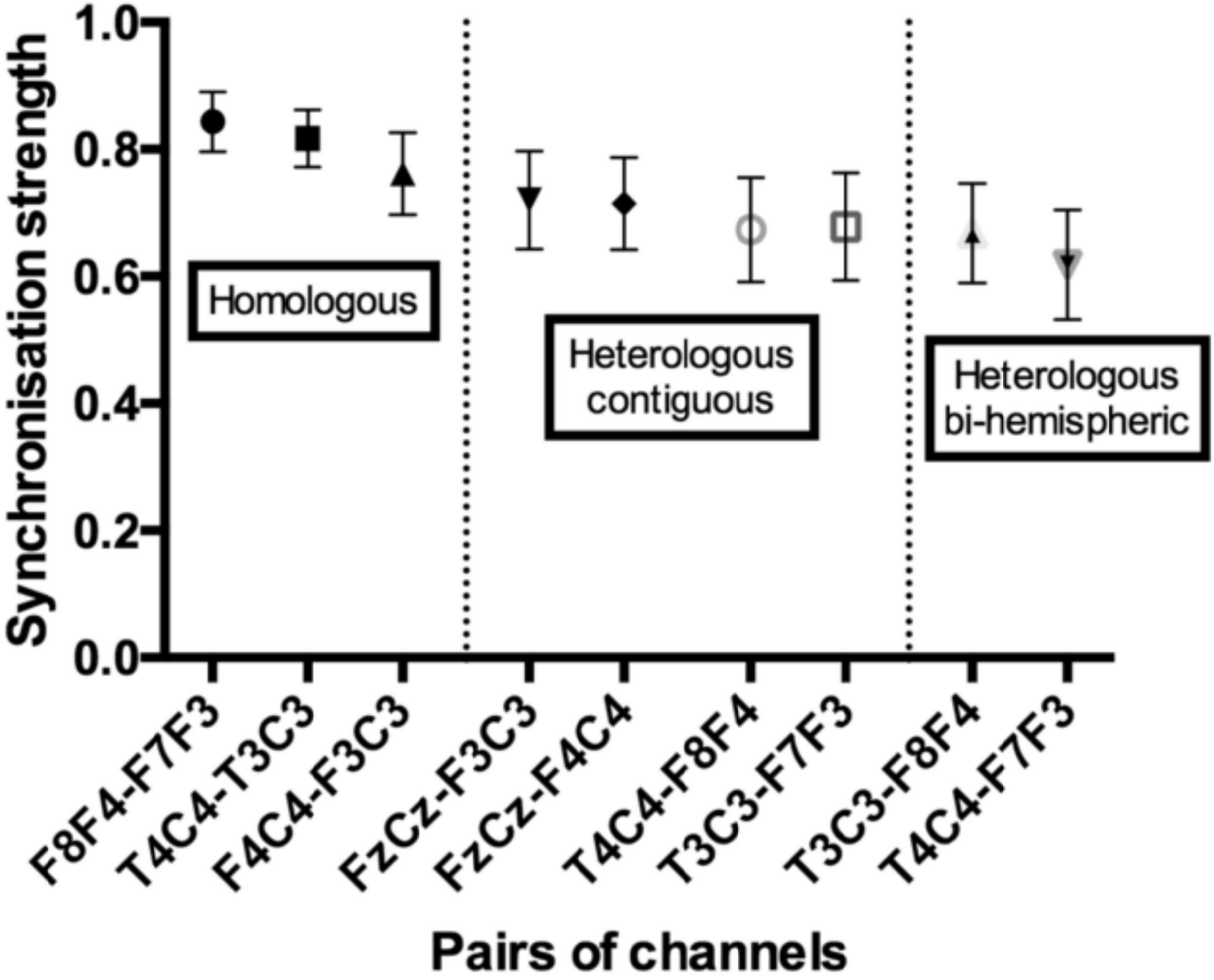

Figure 3

Click here to download high resolution image

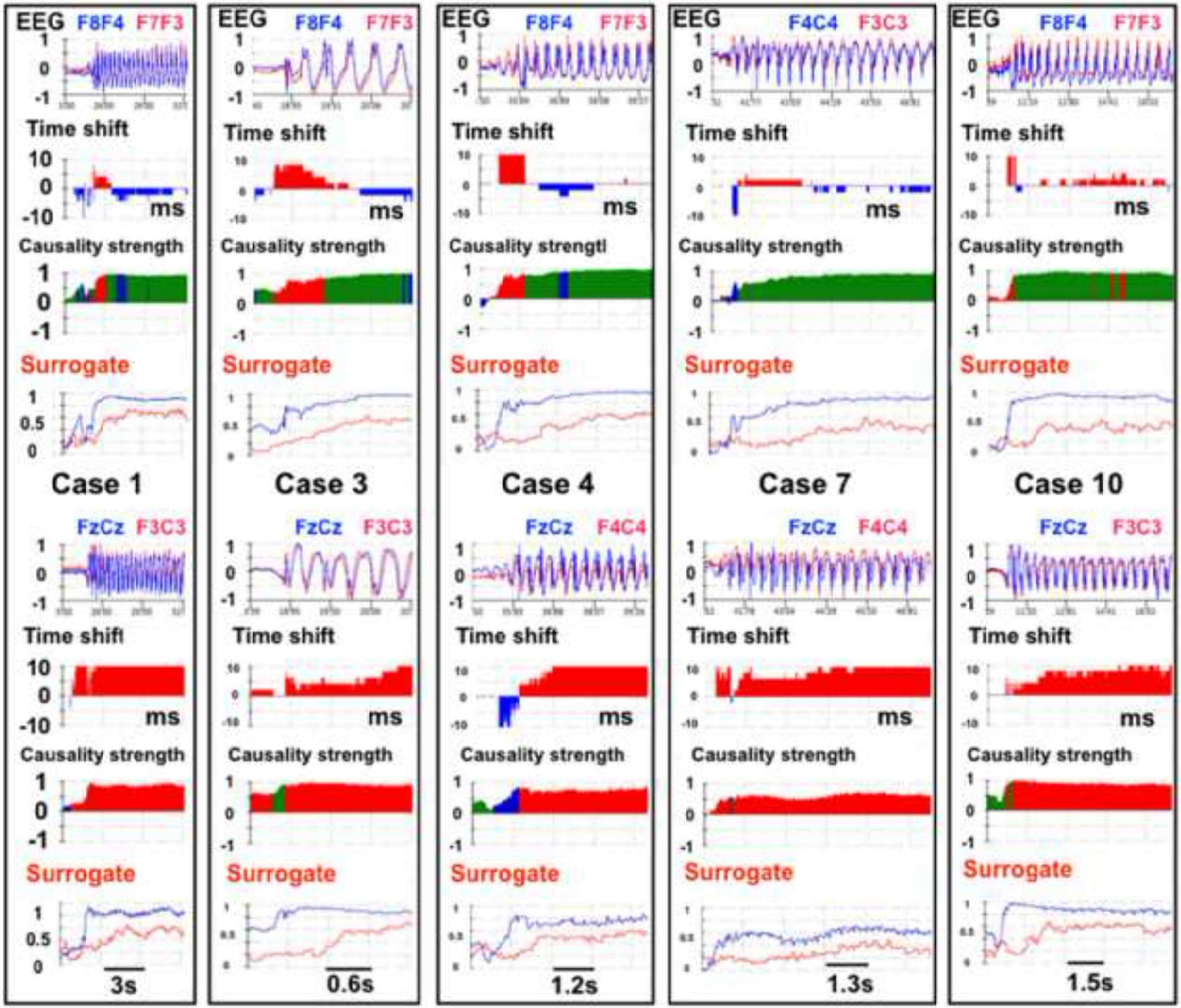

Figure 4

Click here to download high resolution image

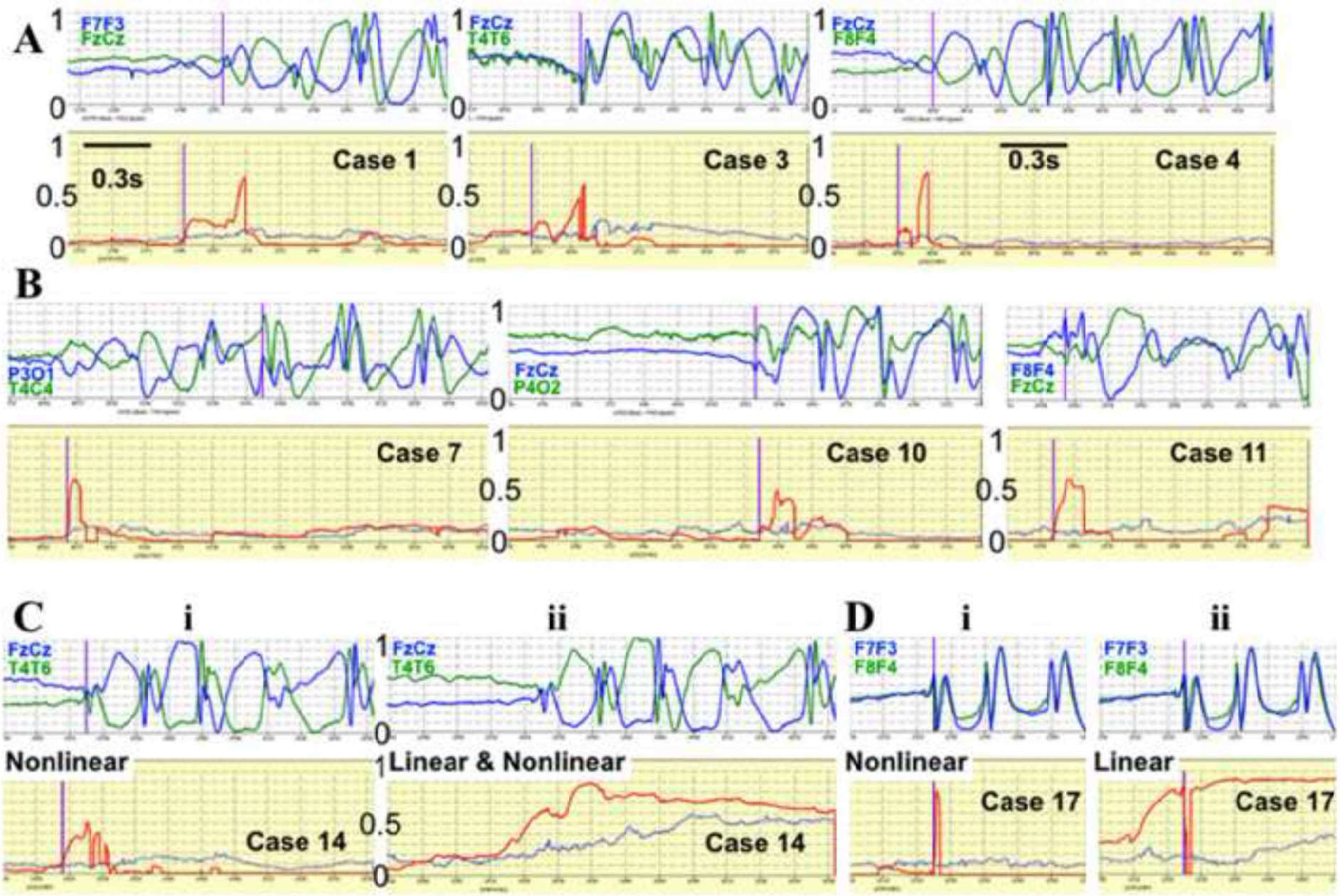

Figure 5

Click here to download high resolution image

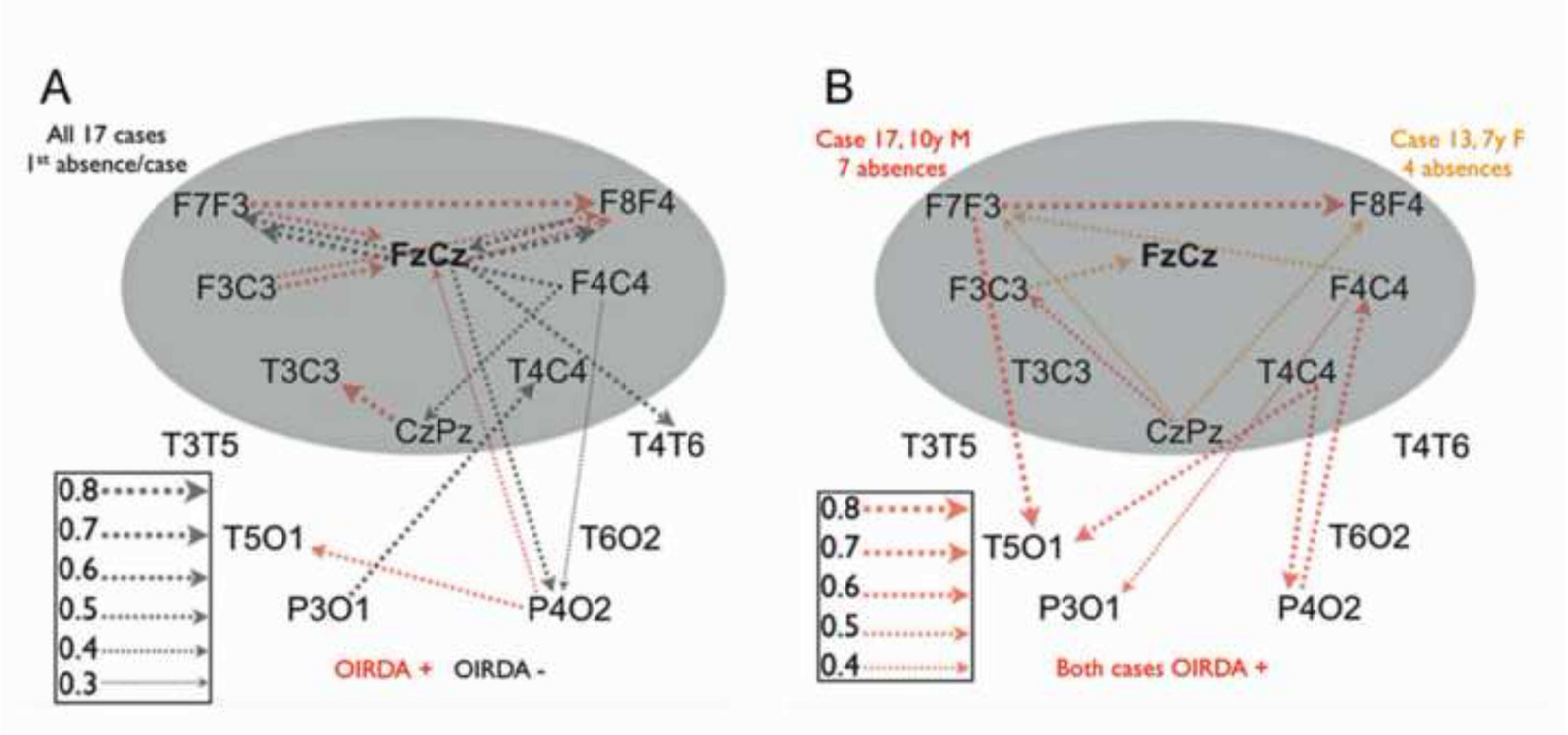

Figure 6

Click here to download high resolution image

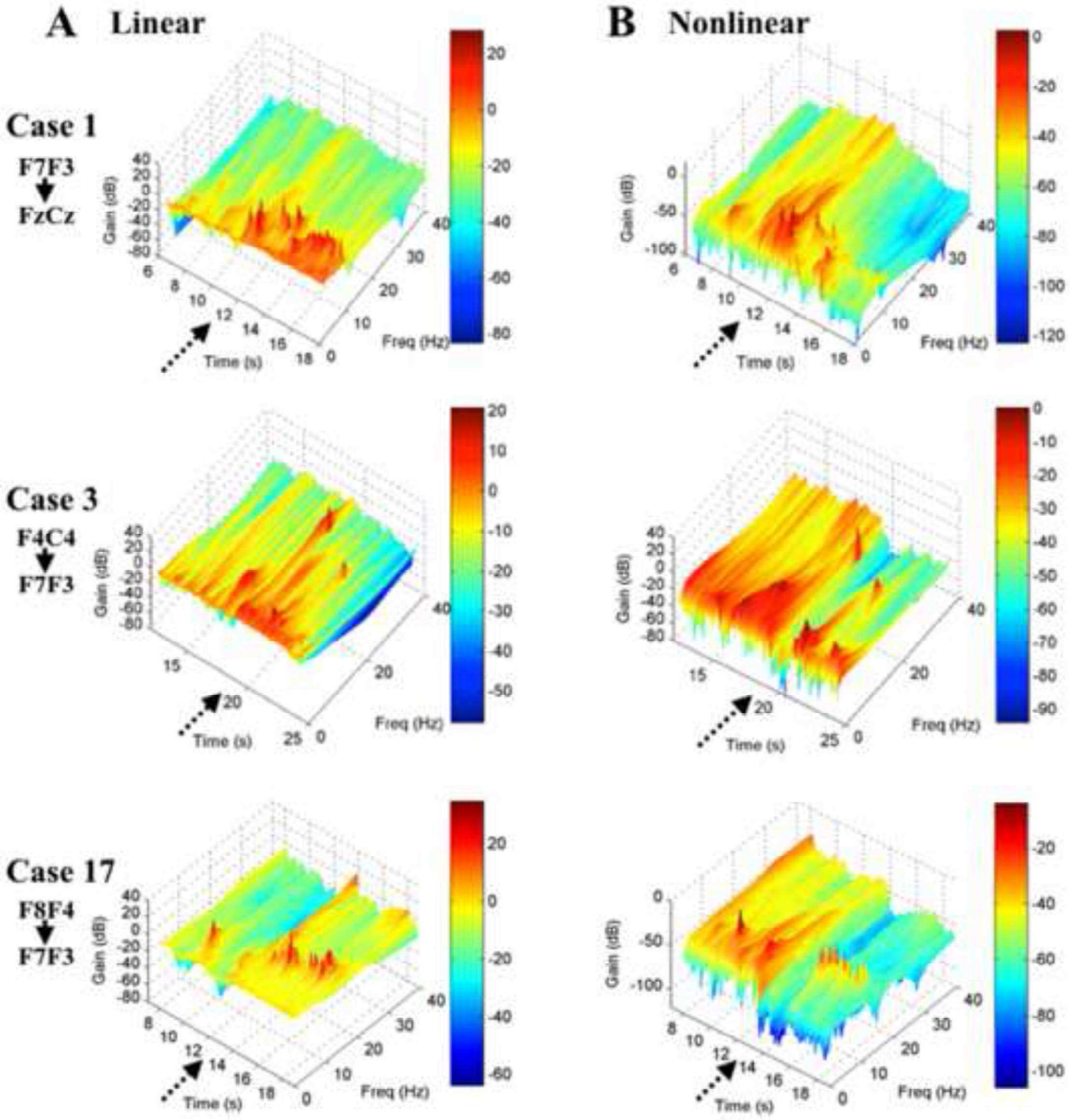

Figure 7

Click here to download high resolution image

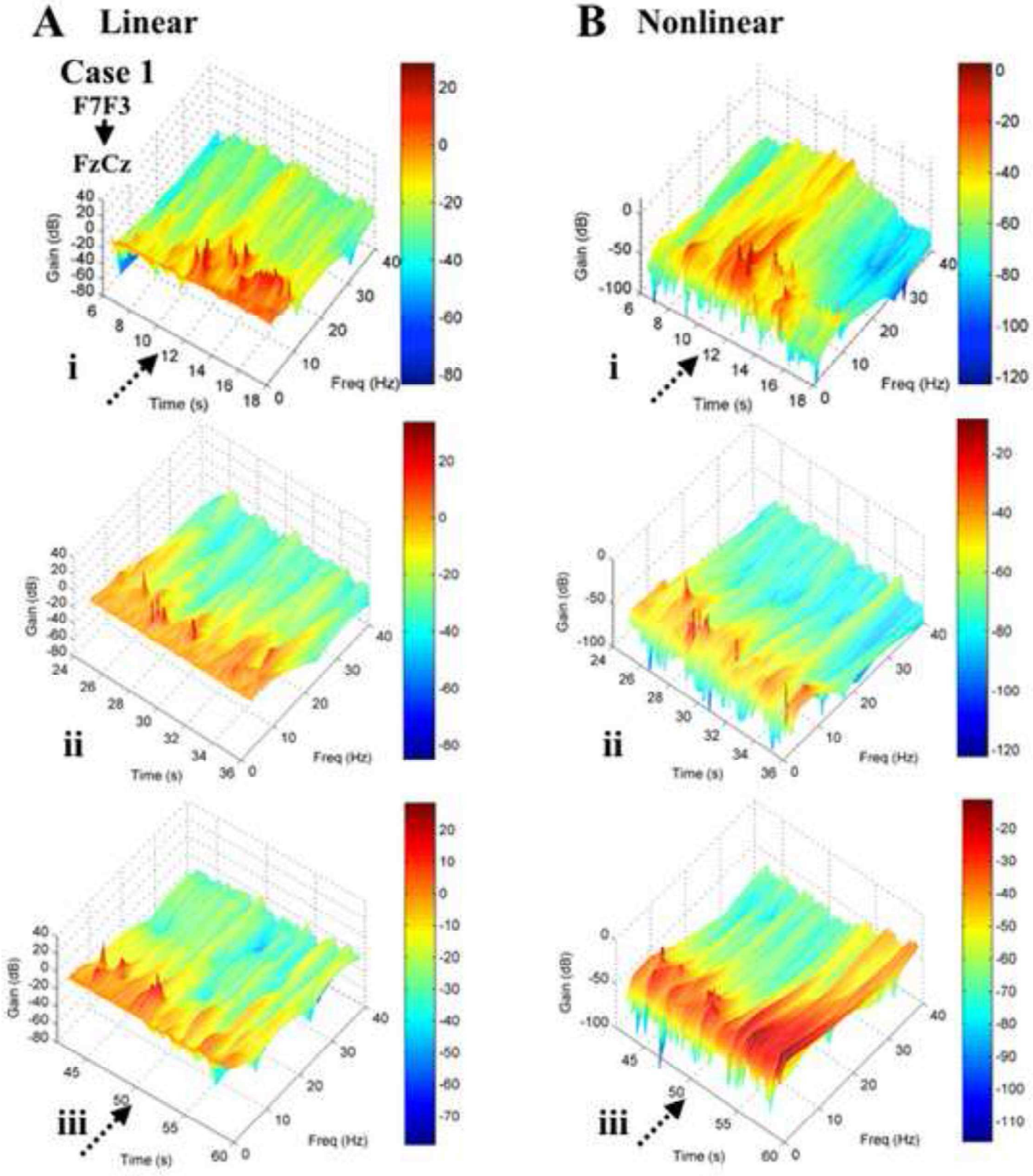

Supplementary Figure S1

Click here to download high resolution image

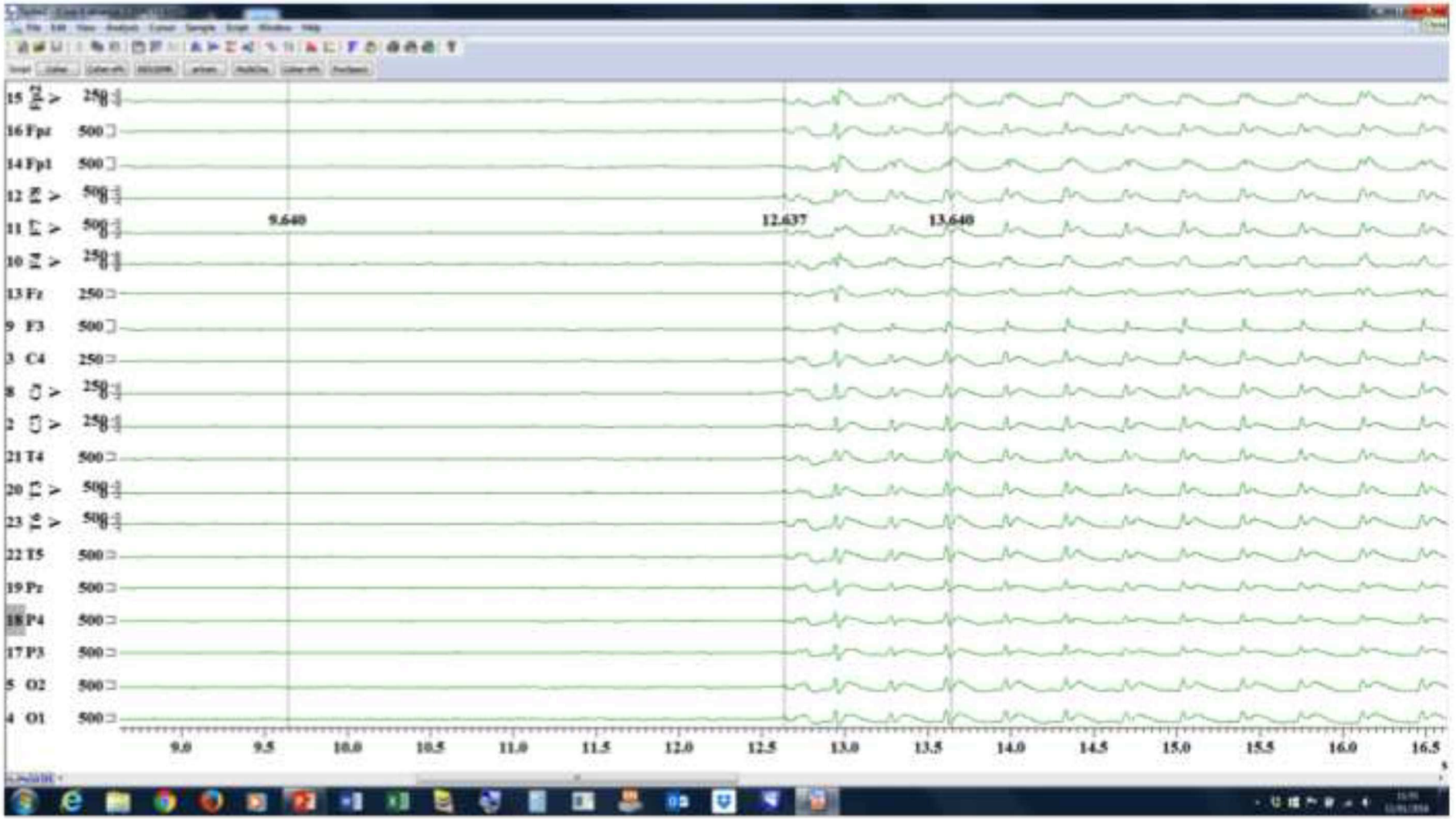

Supplementary PowerPoint 1

Earliest rise (i.e. source) of nonlinear synchronisation

- Top row shows the normalised, color coded, EEG data for each channel pair shown
- Second row shows in red the time locked to the EEG nonlinear synchronisation strength and the surrogate level of statistical significance in blue
- Third row the estimated lags
- Please note that unless specified otherwise for each slide the partial directed nonlinear causality strength is shown
- The surrogate marker, marking the level above which the results are statistically significant is shown in blue

Case 1 abs 3
Nonlinear rise 170ms before first SW

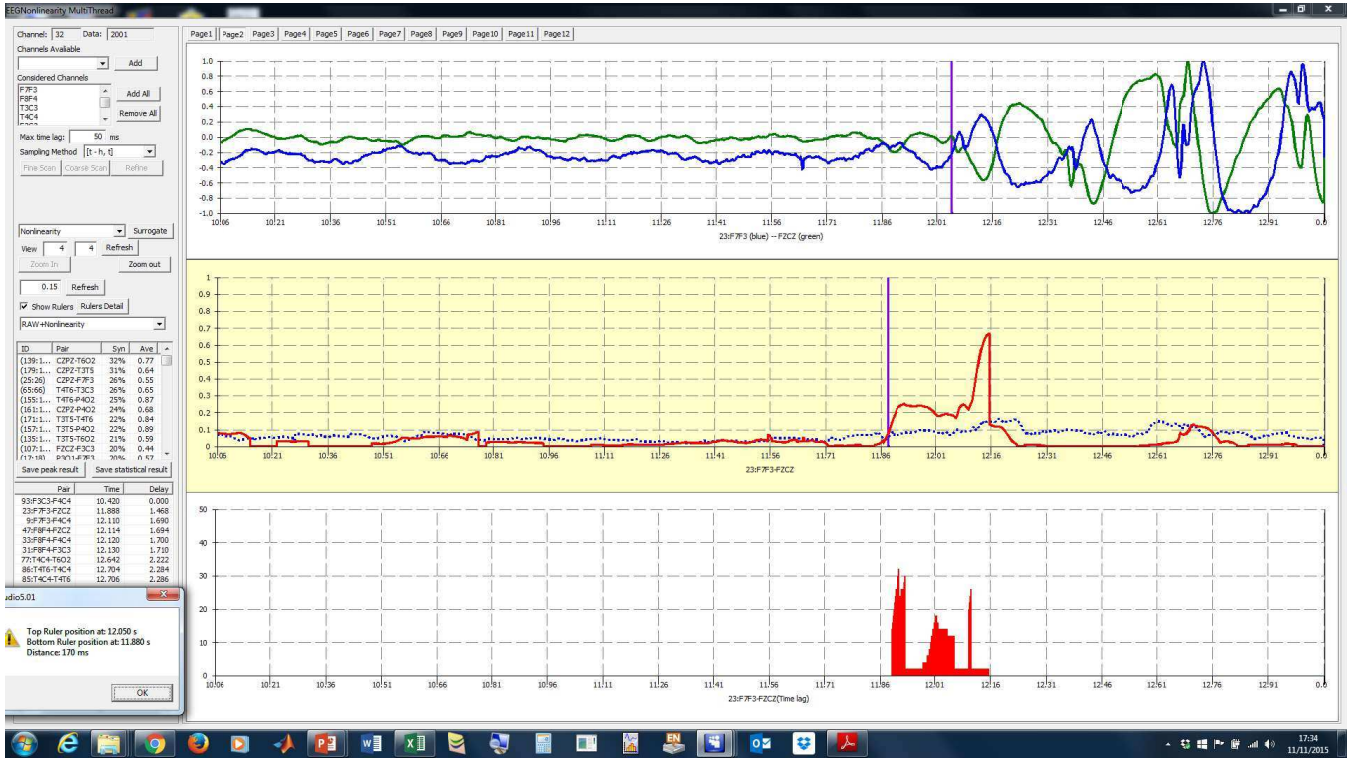

Case 2 absence 1
OIRDA case
Earliest rise of nonlinear synchronisation

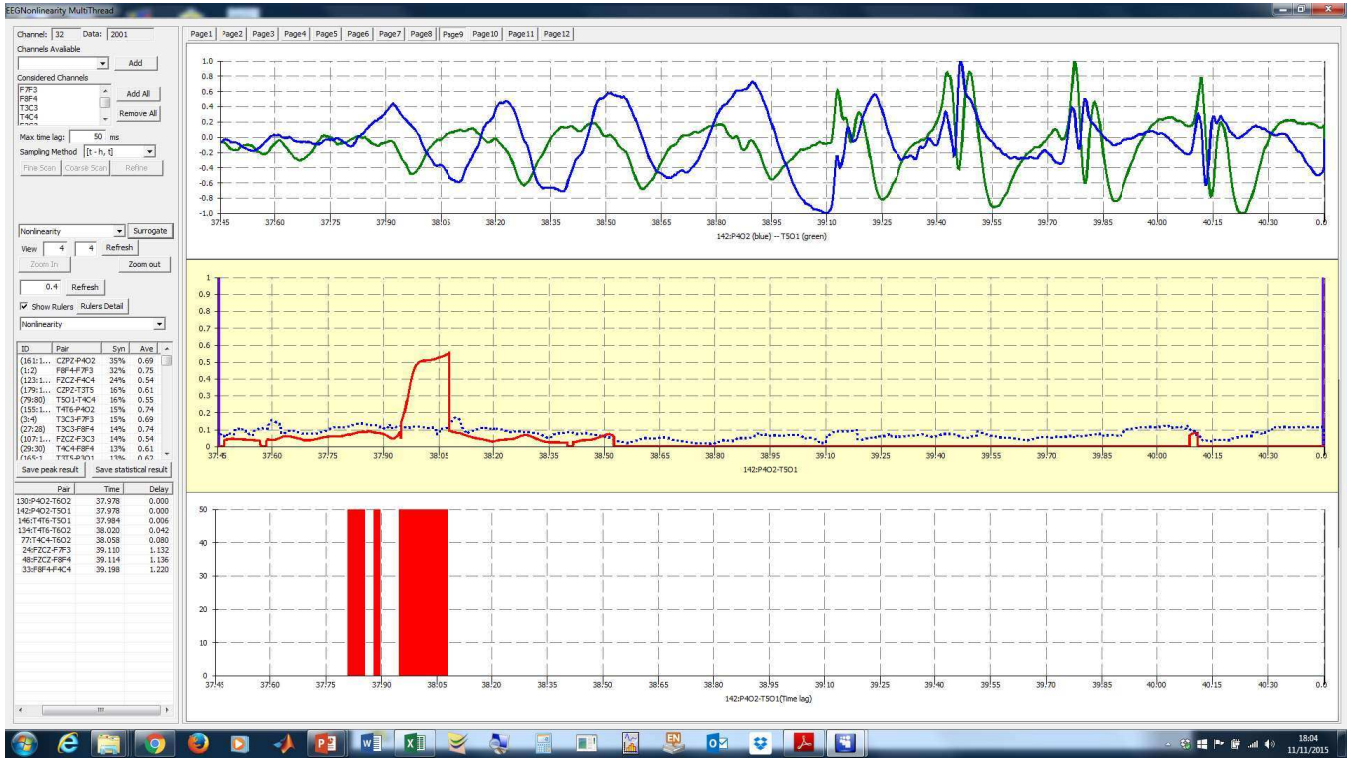

Case 2 absence 1
OIRDA positive case
Anterior channel pair with earliest rise in nonlinear synchronisation

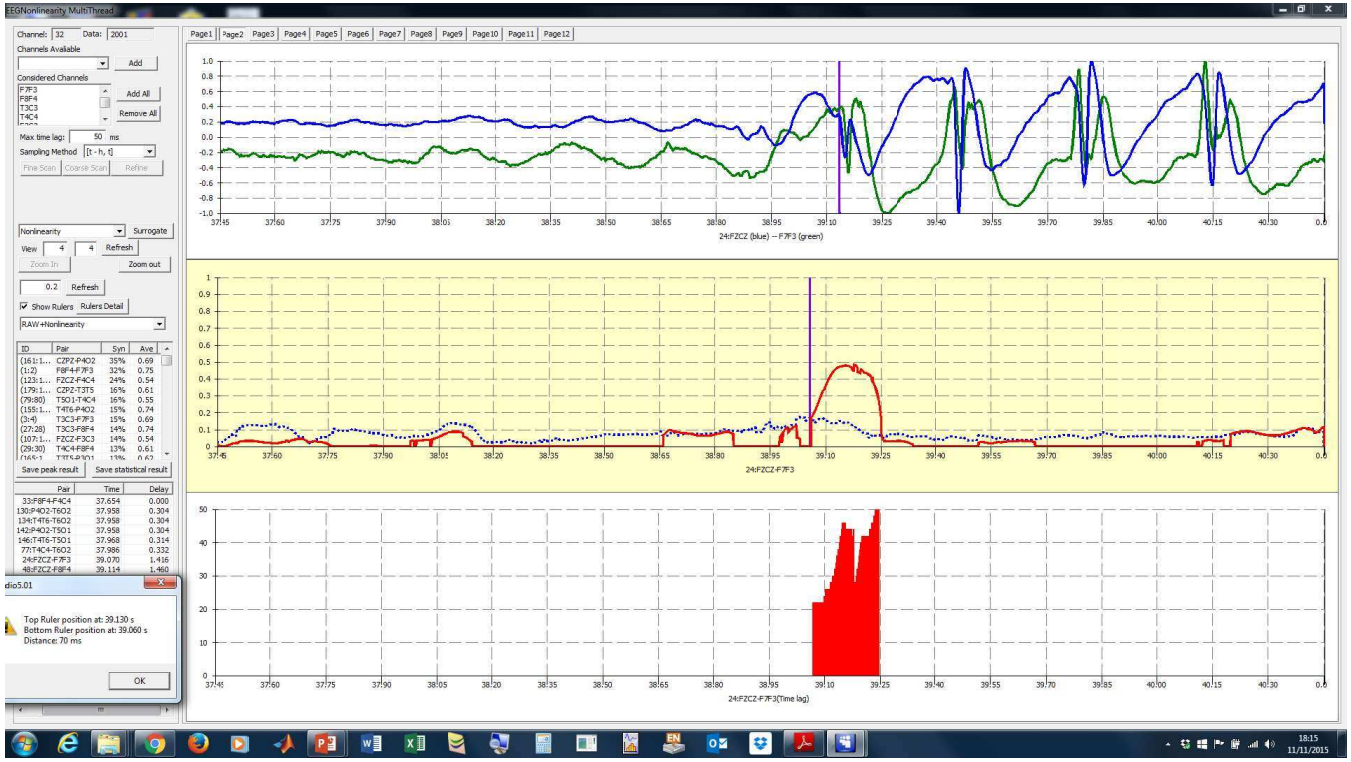

Case 3 absence 1

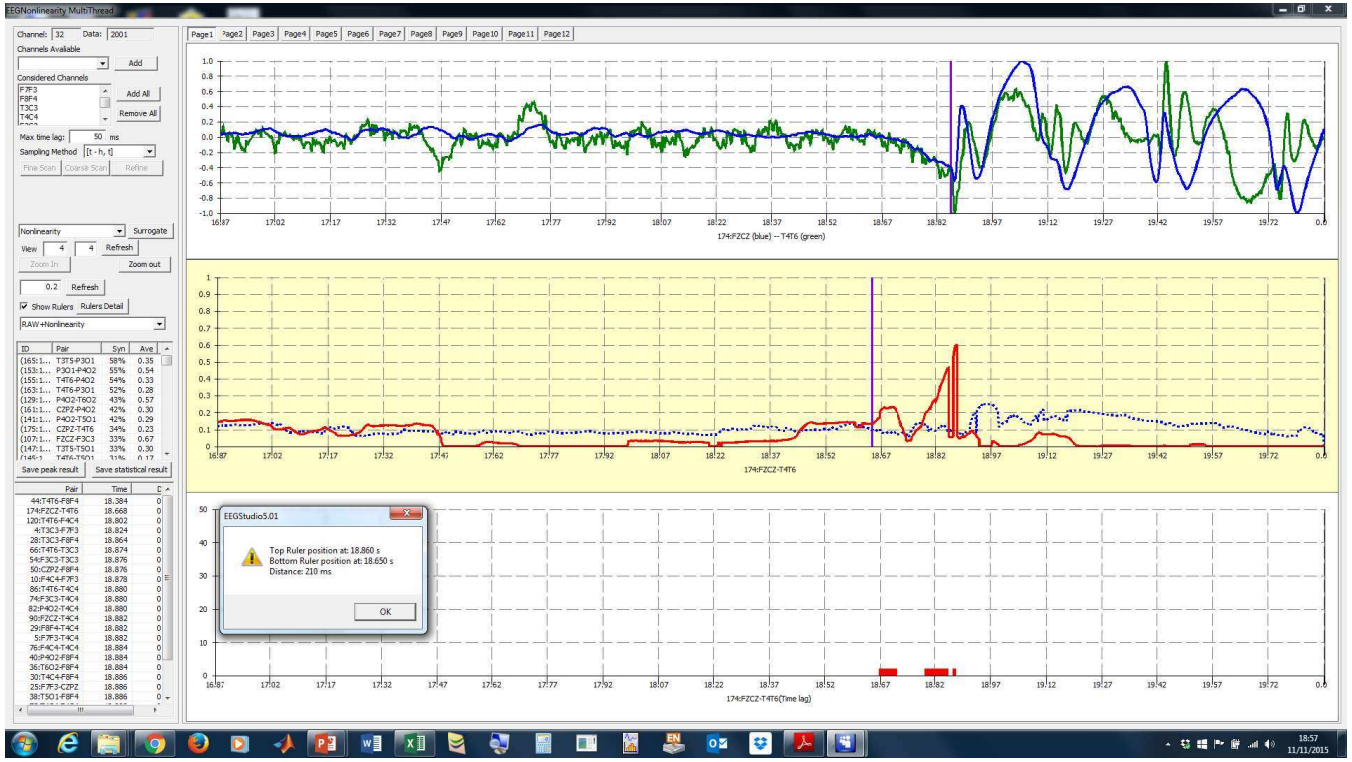

Case 4 absence 2 highest level 0.7

Case 5 absence 2 level 0.8

Case 6 absence 2

Case 7 absence 1

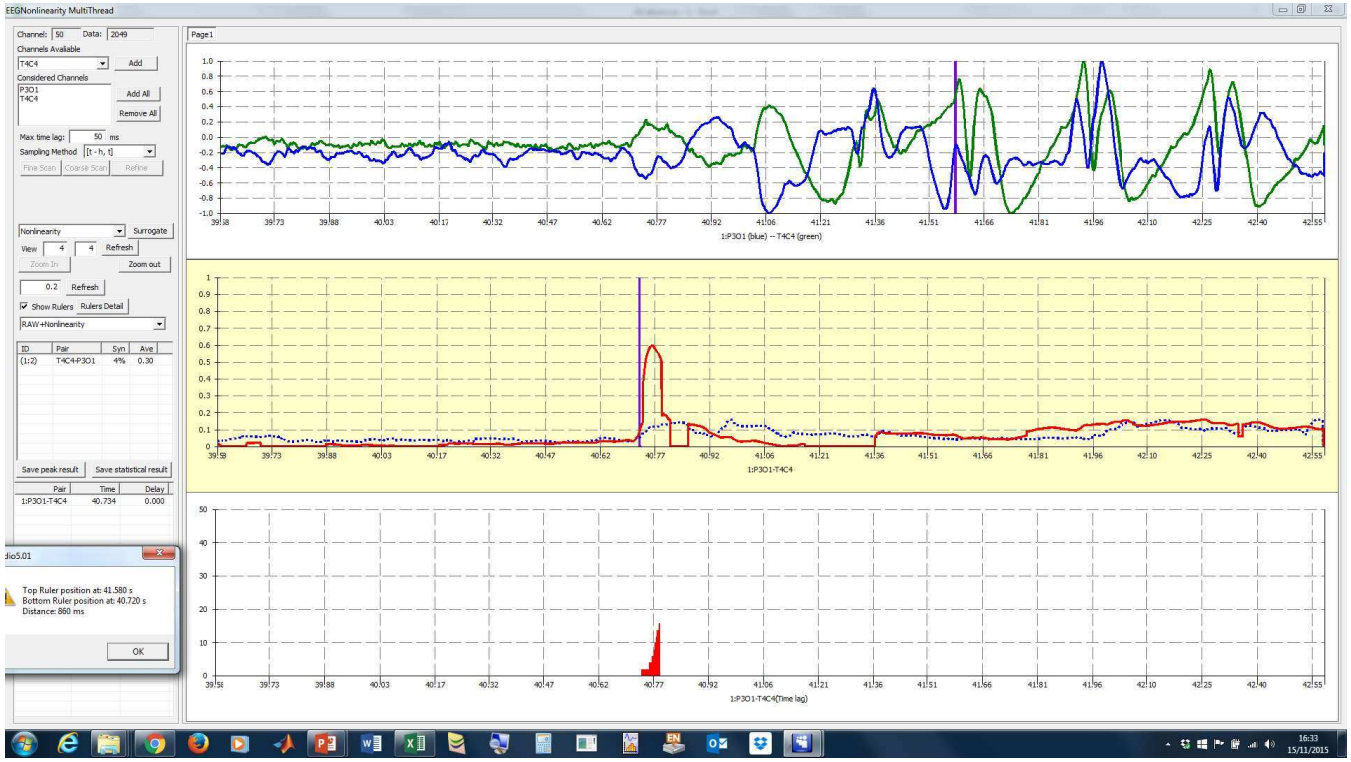

Case 8 abs 1

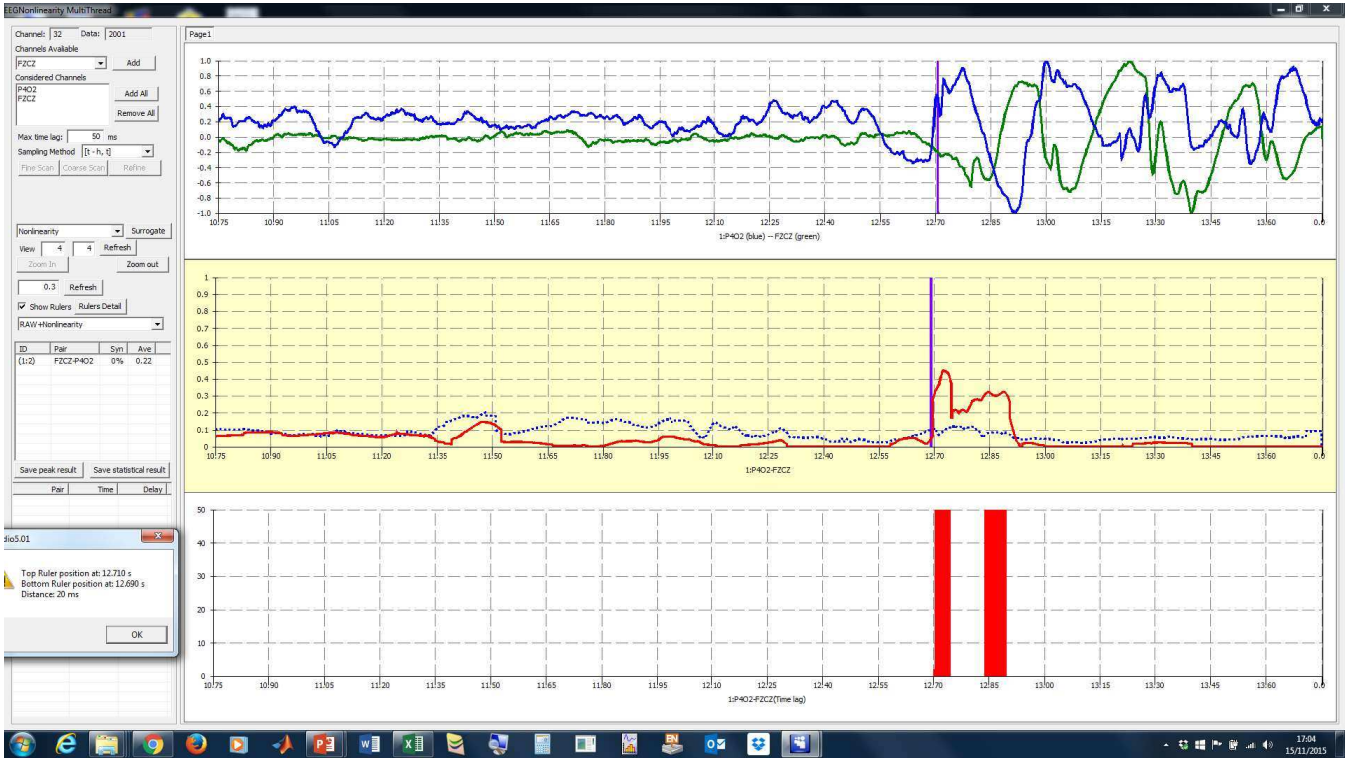
EEGNonlinearity MultiThread
Channel: 32
Data: 2001
Channels Available
FZCZ
Add
Considered Channels
P4O2
FZCZ
Add All
Remove All
Max time lag: 50 ms
Sampling Method [t - h, t]
Fine Scan
Coarse Scan
Refine
Nonlinearity
Surrogate
View 4 4 Refresh
Zoom In
Zoom out
0.3 Refresh
Show Rulers
Rulers Detail
RAW +Nonlinearity
ID Pair Syn Ave
(1:2) FZCZ-P4O2 0% 0.22
Save peak result
Save statistical result
Pair Time Delay
Page1
1:P4O2 (blue) -- FZCZ (green)
1:P4O2-FZCZ
1:P4O2-FZCZ(Time lag)
Top Ruler position at: 12.710 s
Bottom Ruler position at: 12.690 s
Distance: 20 ms
OK
17:04
15/11/2015

Case 9 absence 1

Case 9 absence 1 linear

Case 10 absence 1

Case 11 absence 1

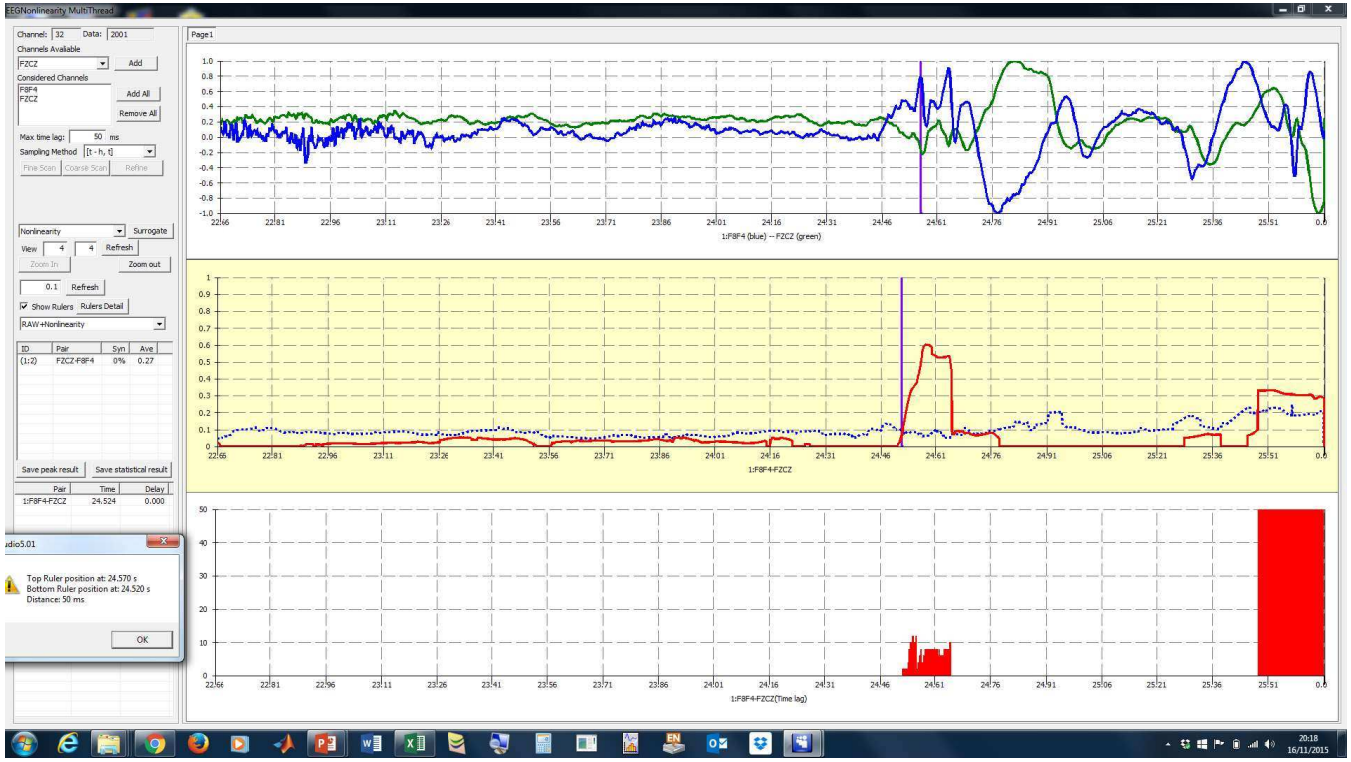

Case 12 absence 2

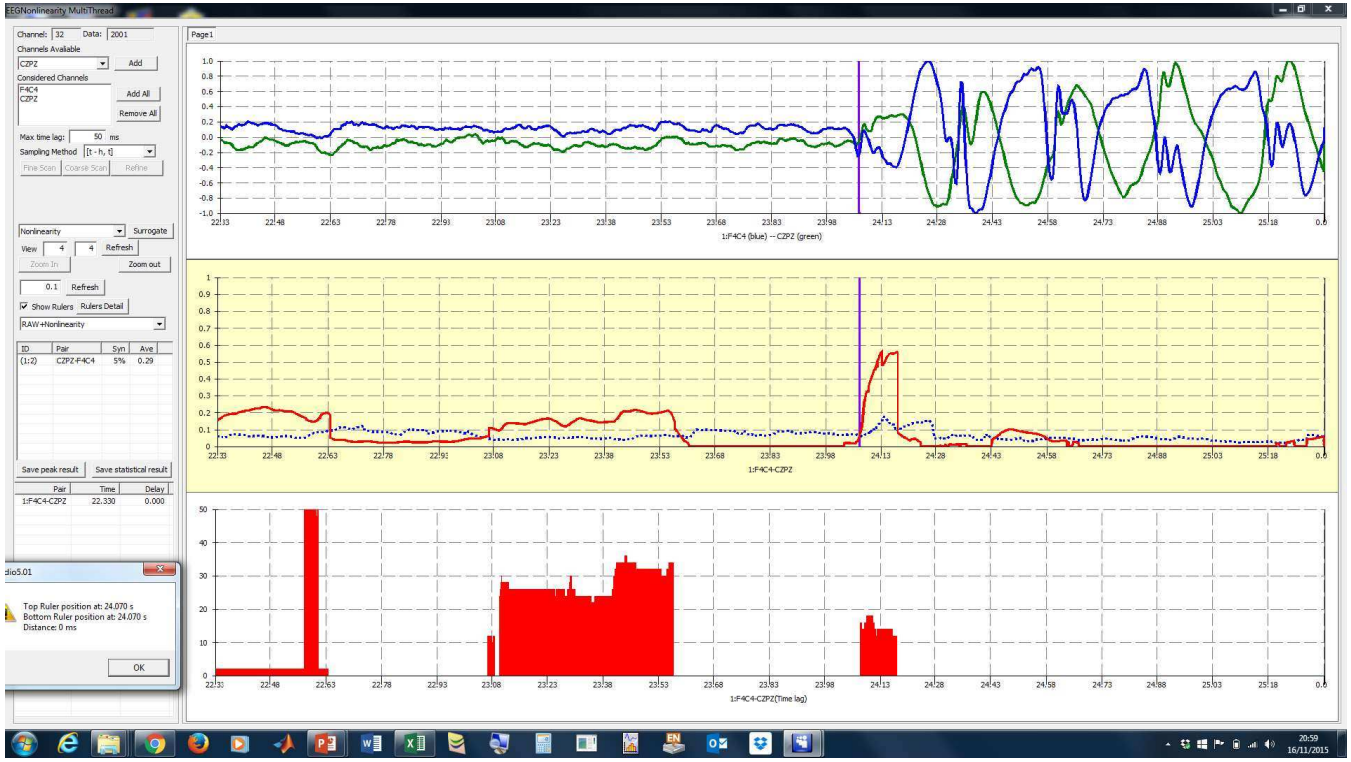

Case 13 absence 3

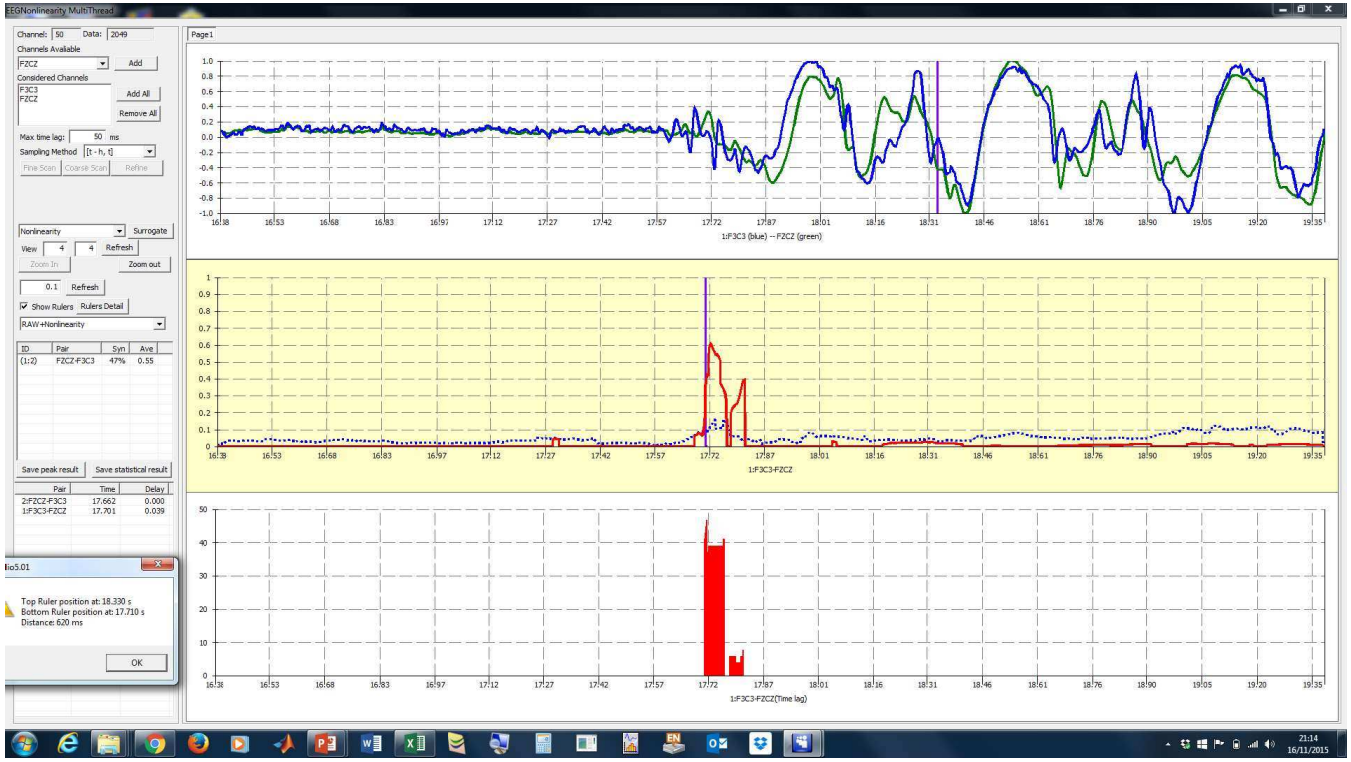

Case 13 absence 3

Linear and nonlinear bidirectional synchronisation

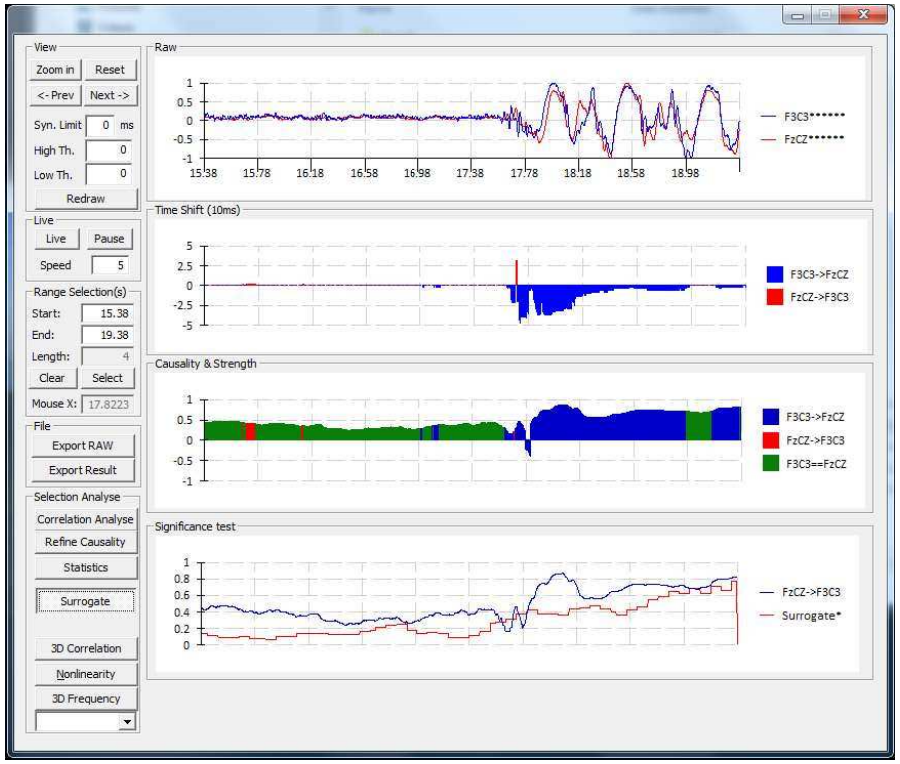

Case 14 absence 2

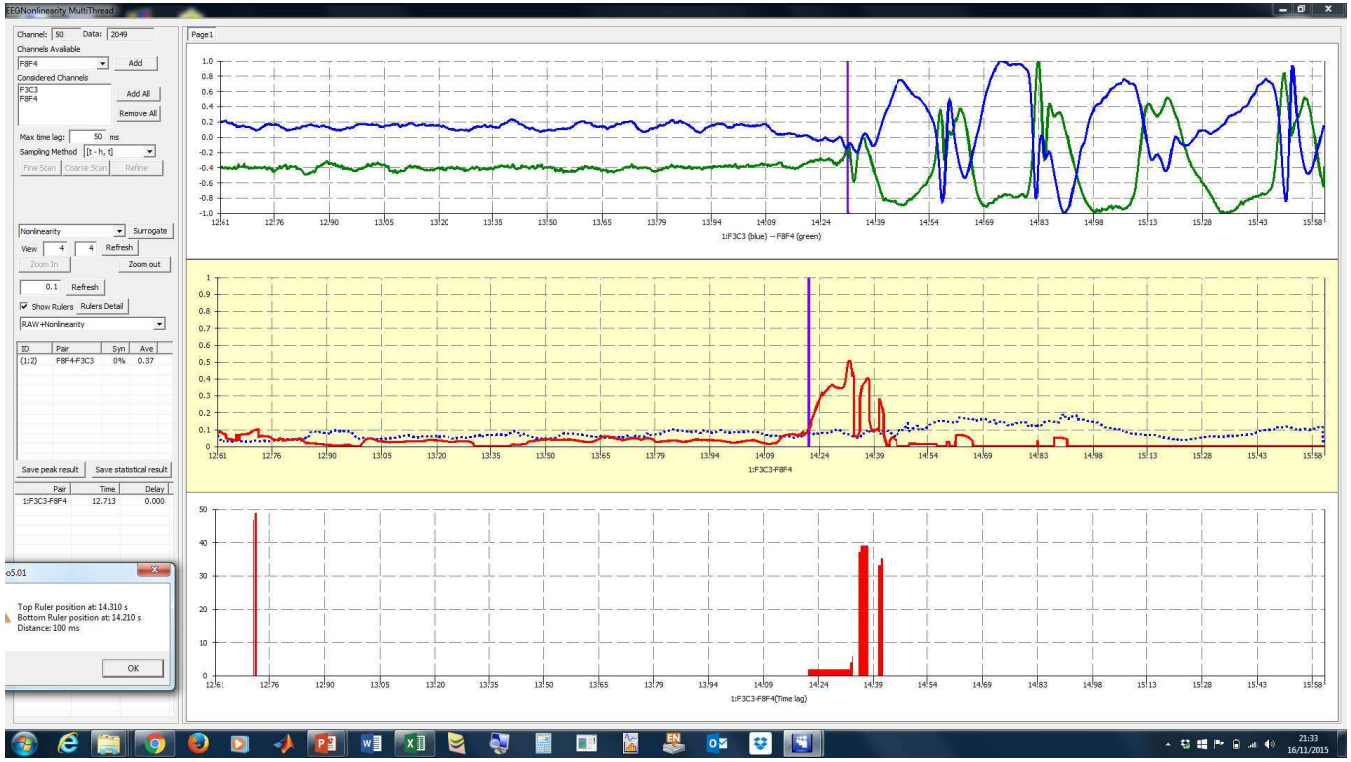

Case 15 absence 1

Case 16 absence 1

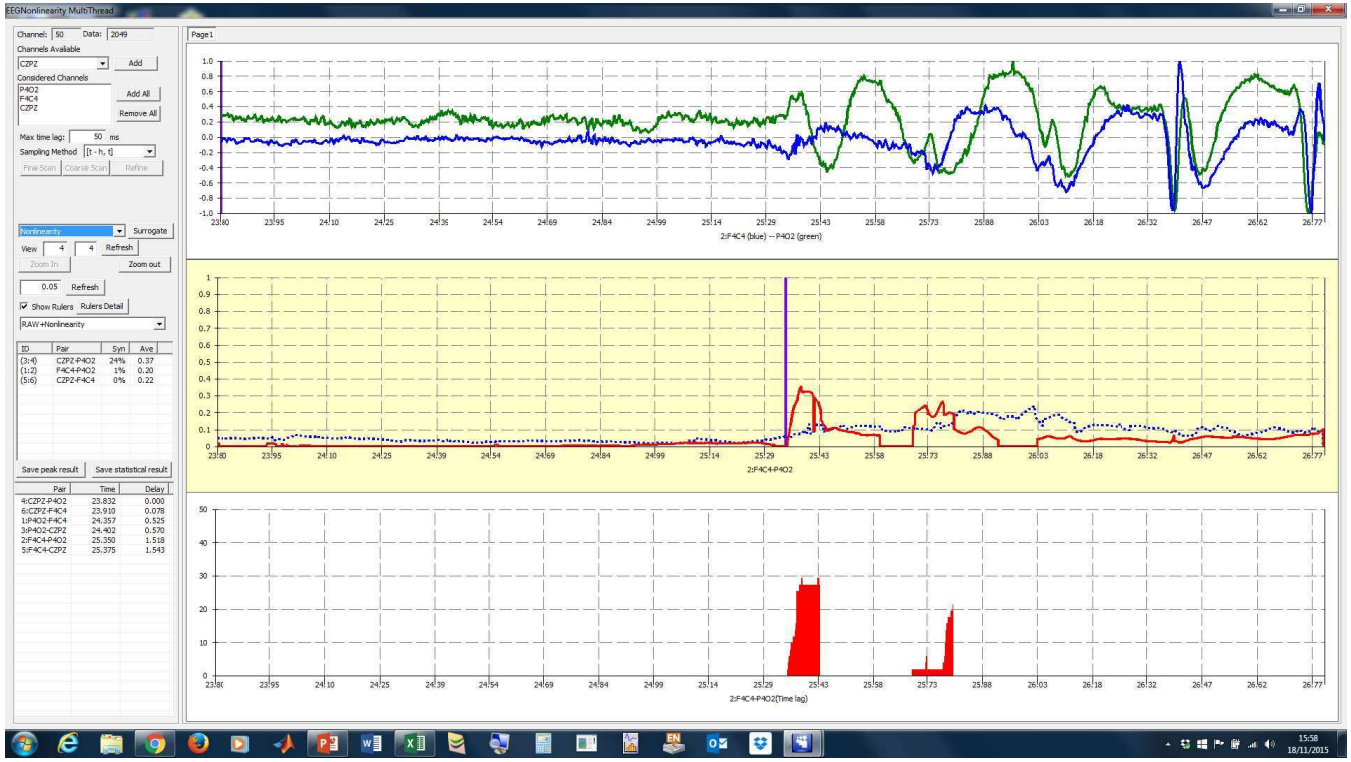

Case 17 absence 1

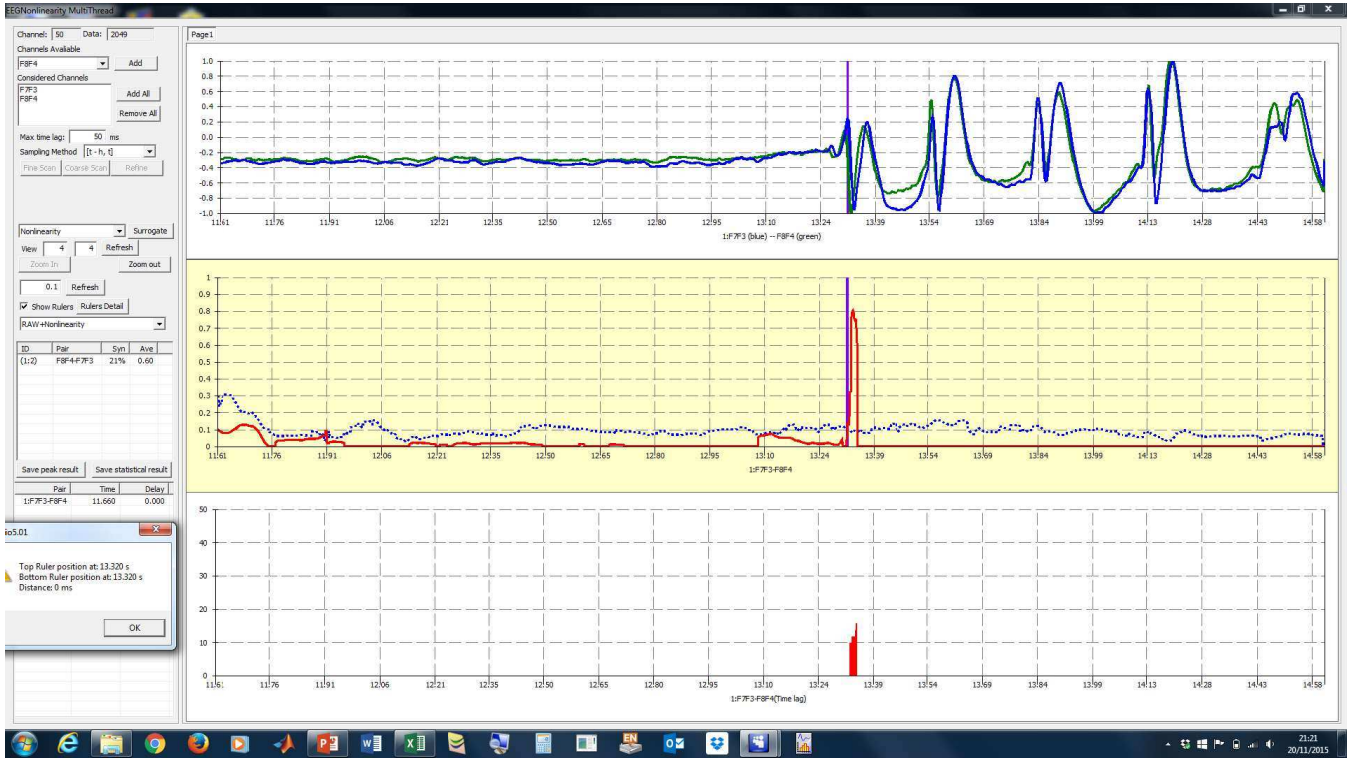

Case 17 absence 1
Linear synchronisation

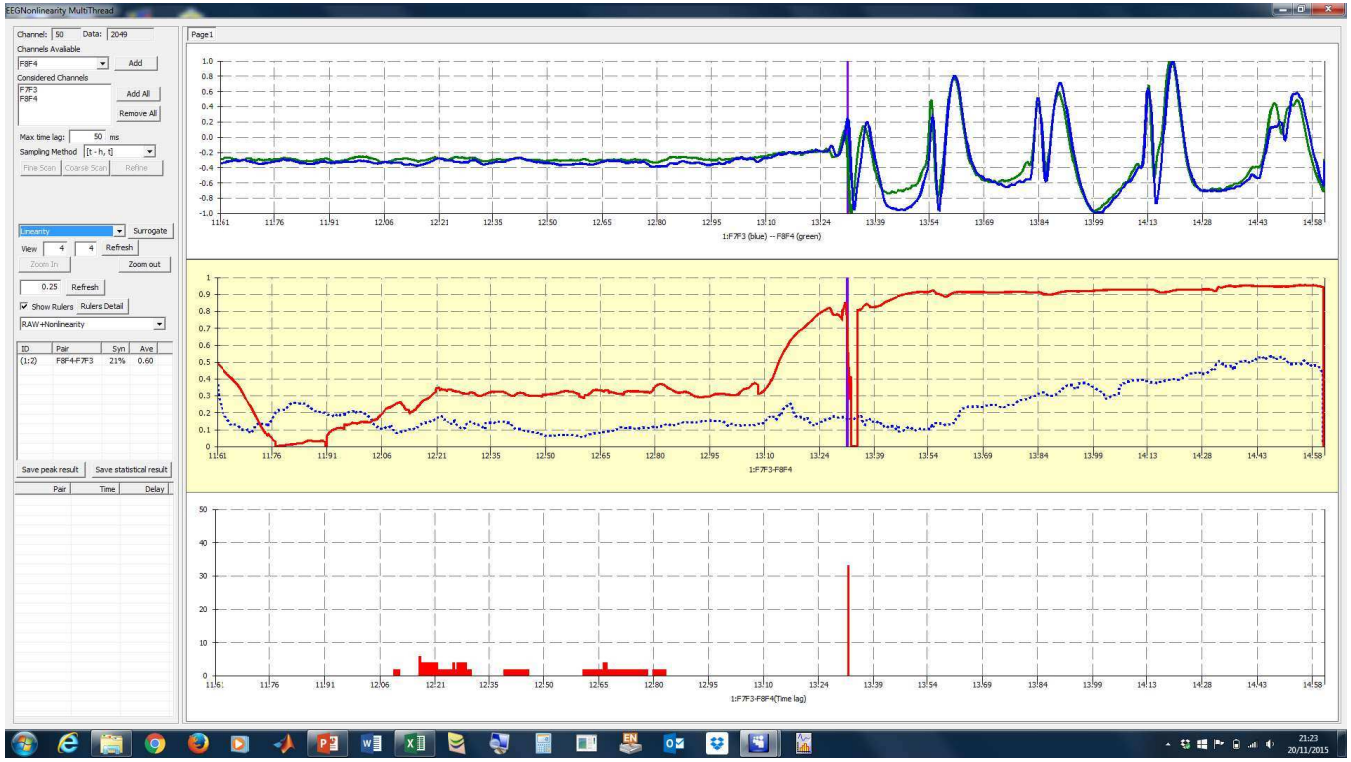

Nonlinear synchronisation throughout the absences
Case 1, case 3 and case 17, shown in fig. 4 and fig. 6 and case 1 in fig. 7

Case 1 F7F3-FzCz

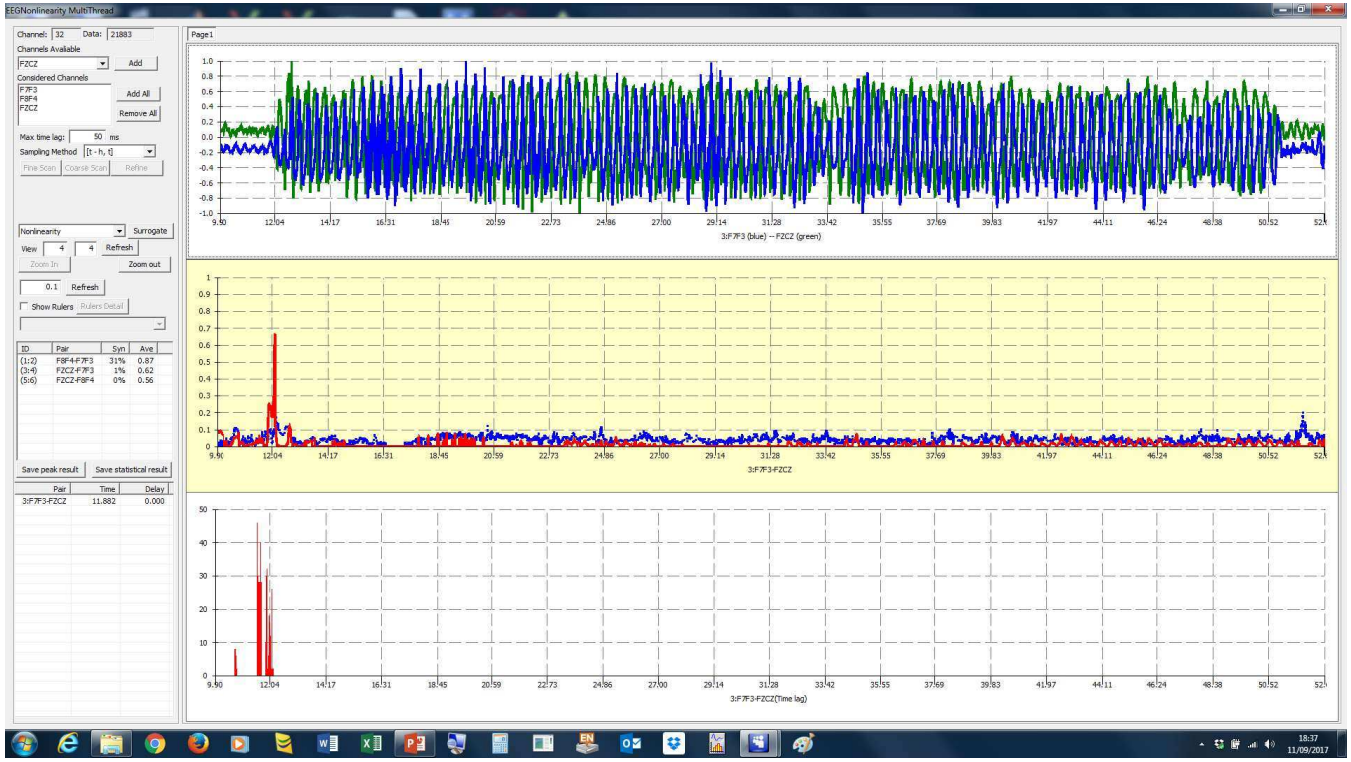

Cases 1 F7F3-F8F4

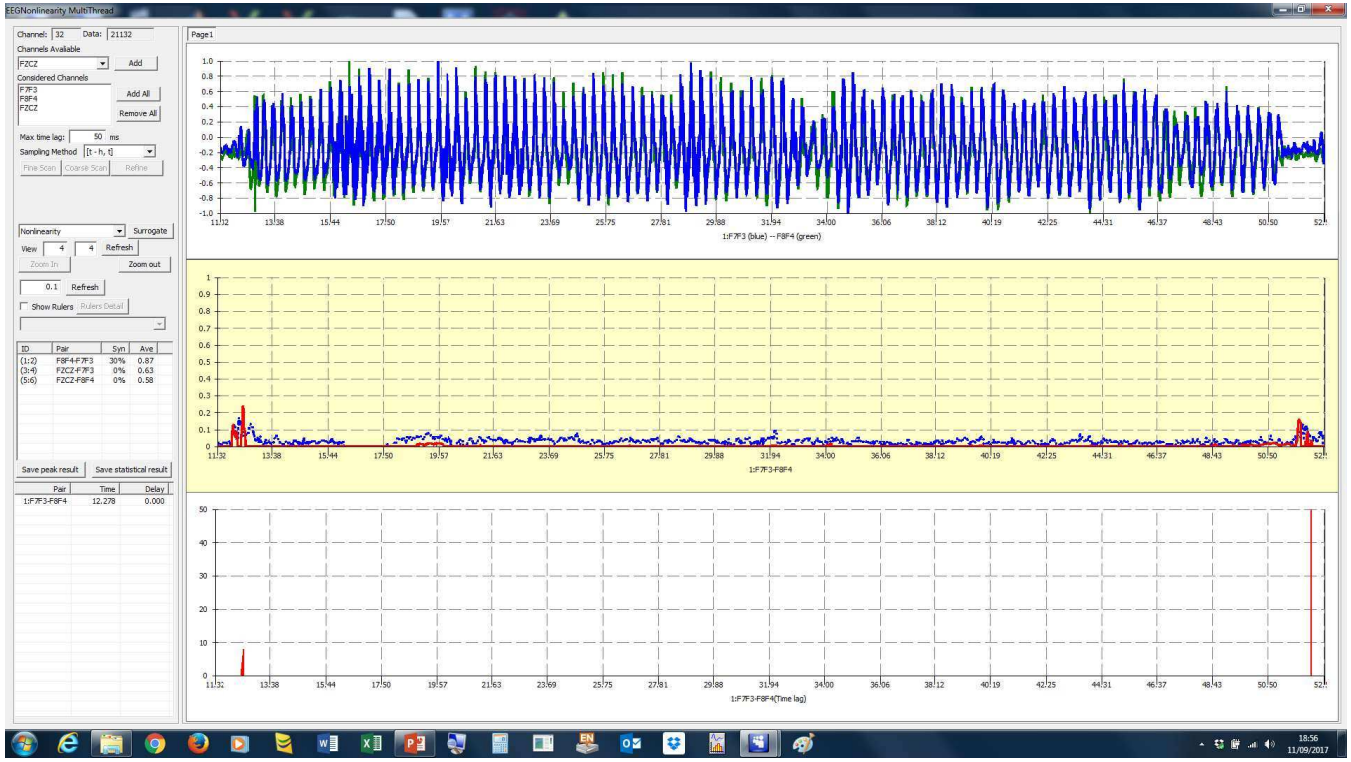

Case 3 F4C4-F7F3

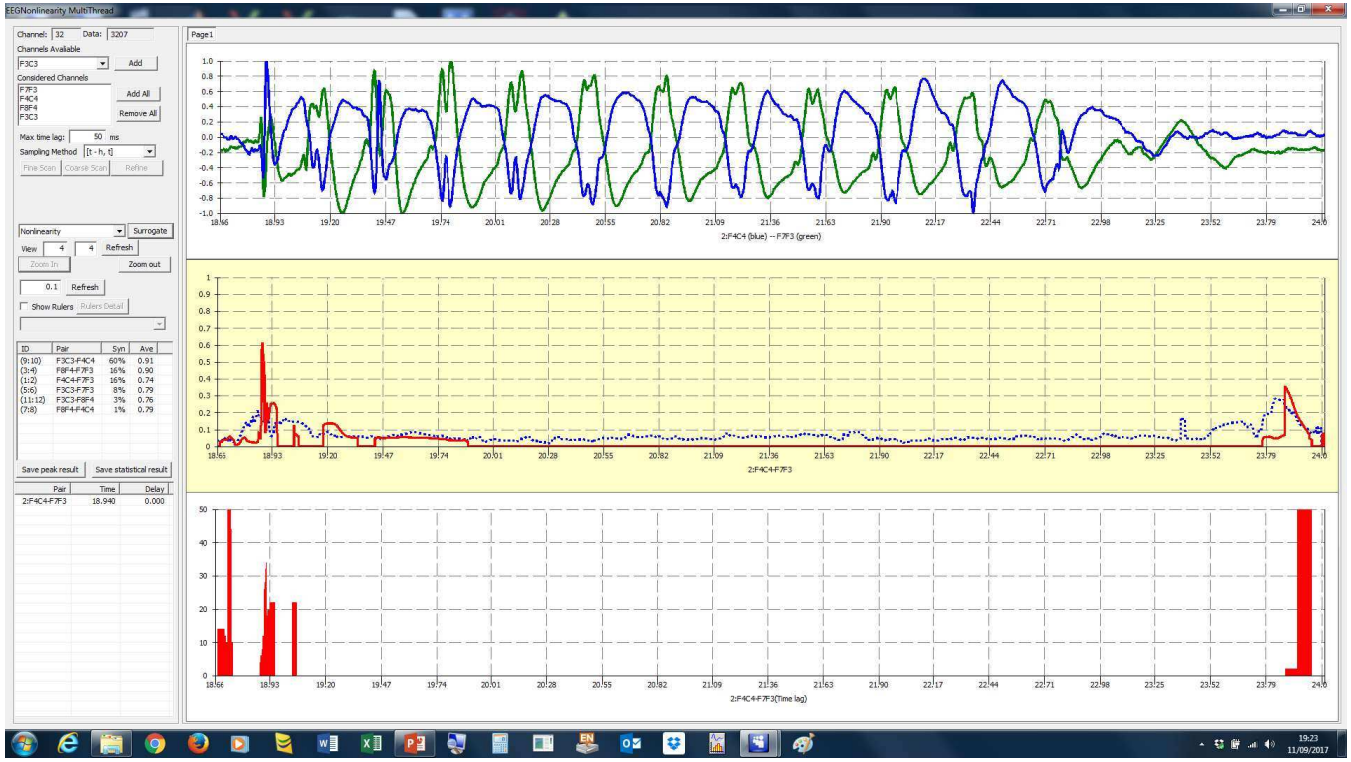

Case 17 F7F3-F8F4

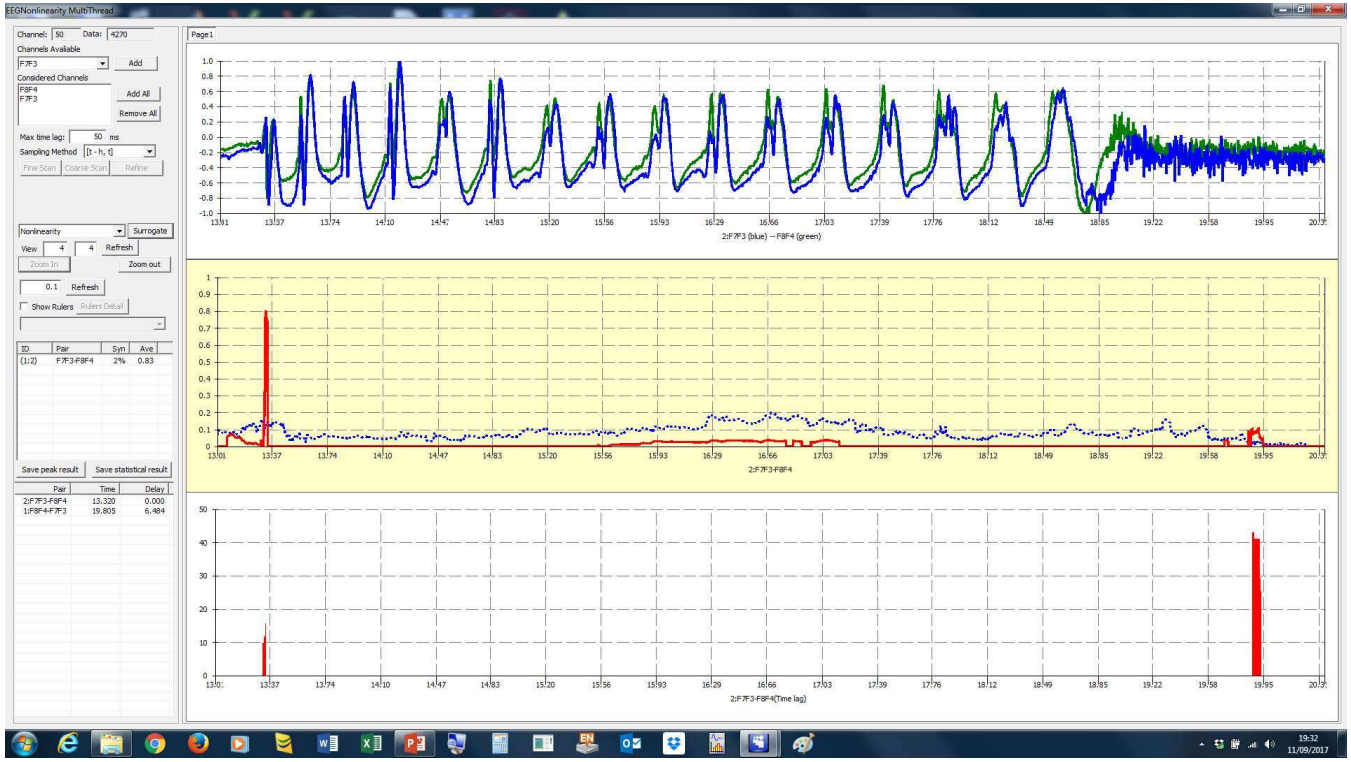

Supplementary PowerPoint 2

Total ERR synchronisation estimates for the channel pair (out of 91 different combinations) with highest scoring value for each absence (1absence/case)

Corresponding time lags (produced for synchronisation strength above surrogate)

and direction of synchronisation are shown.

The surrogate line demarcates the statistically significant levels of synchronisation

The sliding FFT shows the frequency content during the absences

Time Shift scale goes from -10 to +10ms(corresponding to 1 and -1)

Case 1 Absence 1

F8F4-F7F3

Top ranked

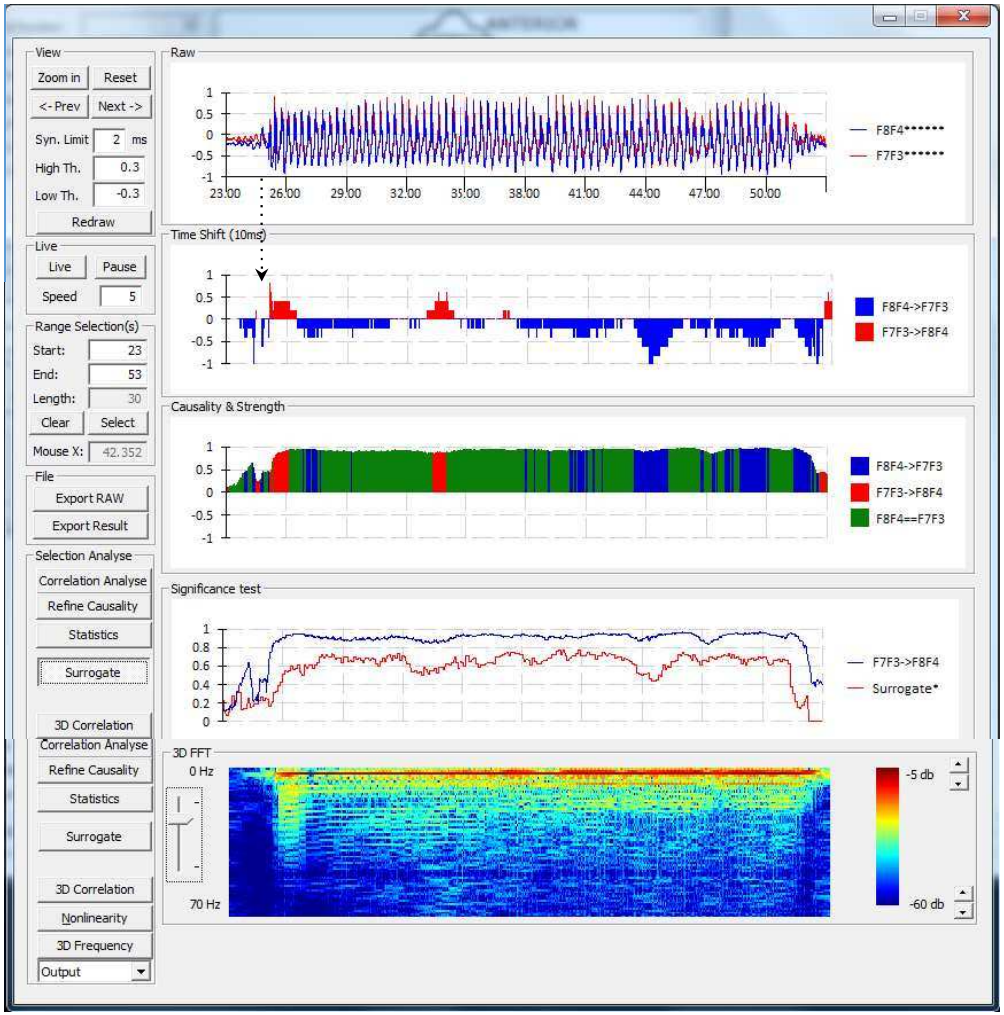

Case 2 absence 1

F8F4-F7F3

Ranked 2nd

Top ranked T5O1-T6O2

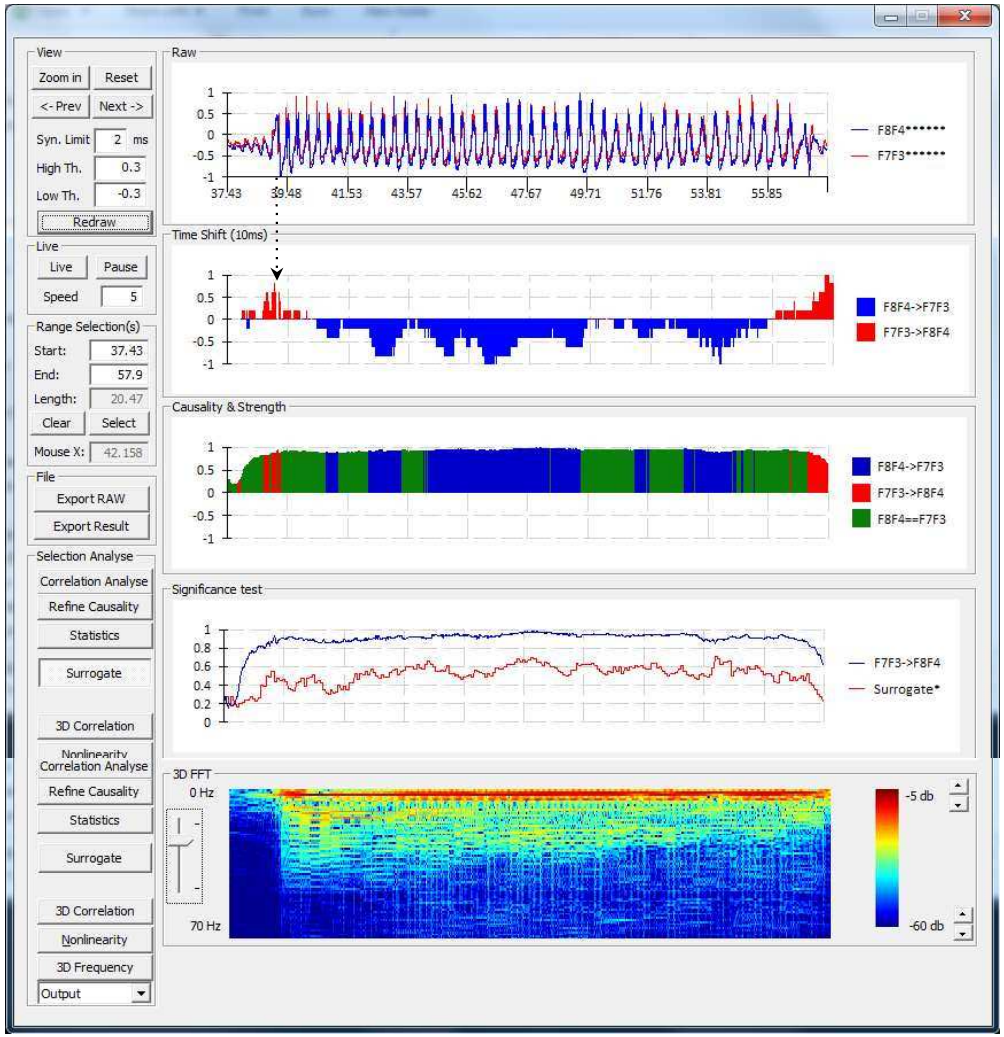

Case 2 absence 1

OIRDA +

First ranked T5O1-T6O2

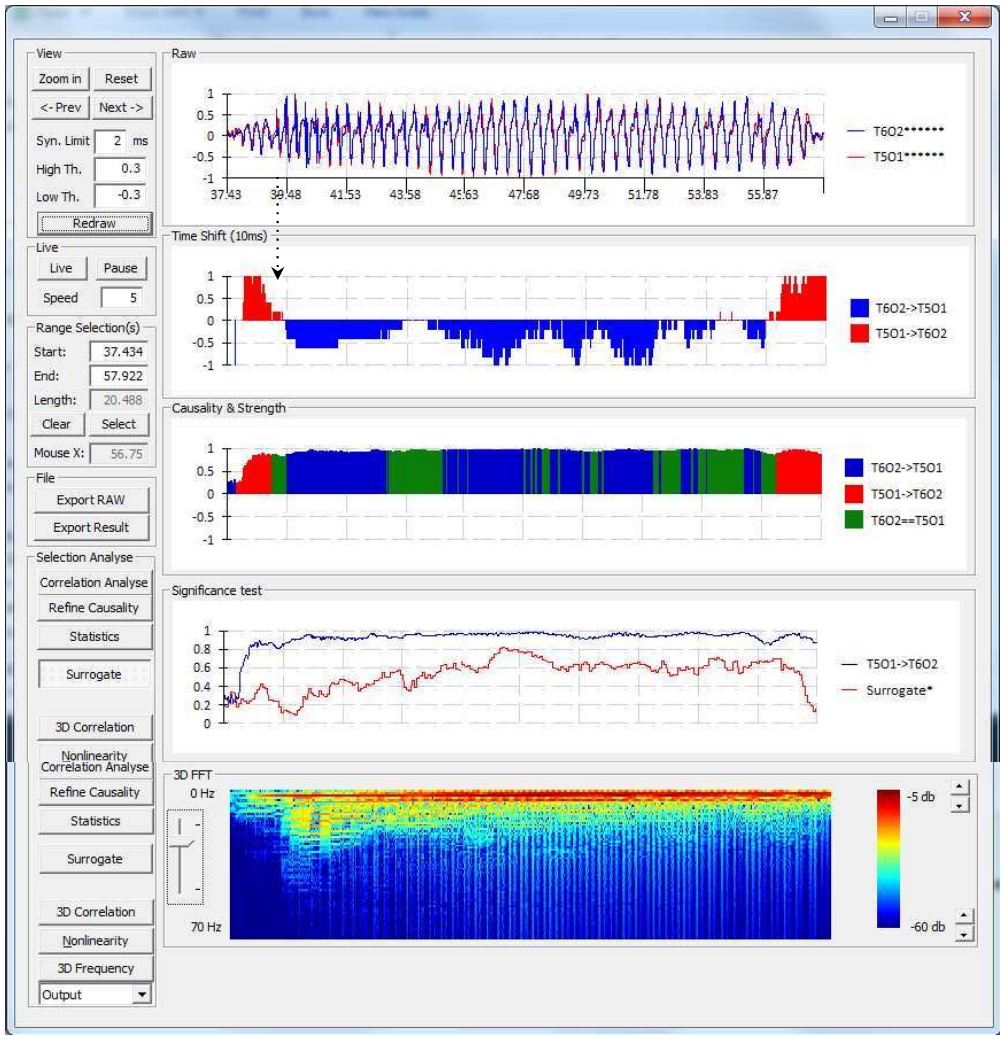

Case 3 absence 1

F8F4-F7F3

Top ranked

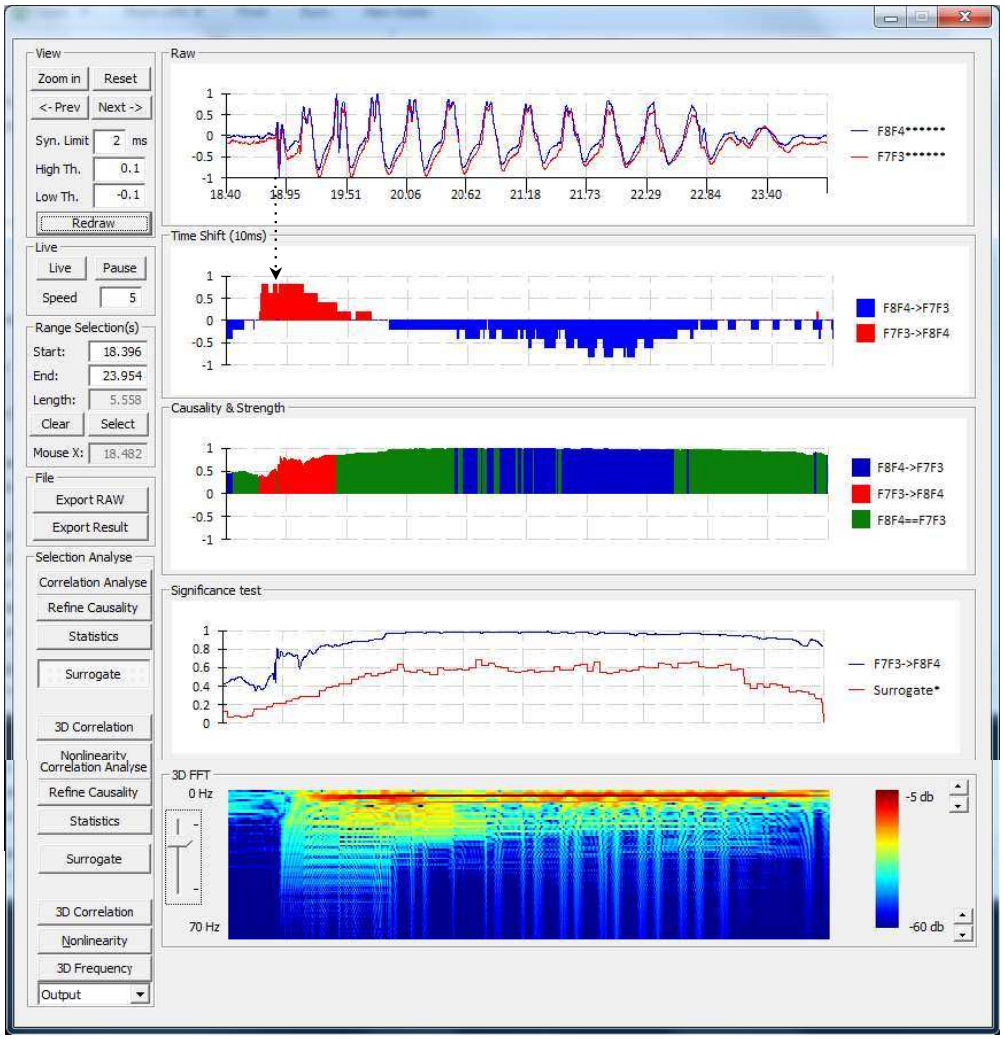

Case 4 Absence 1

F8F4-F7F3

Top ranked

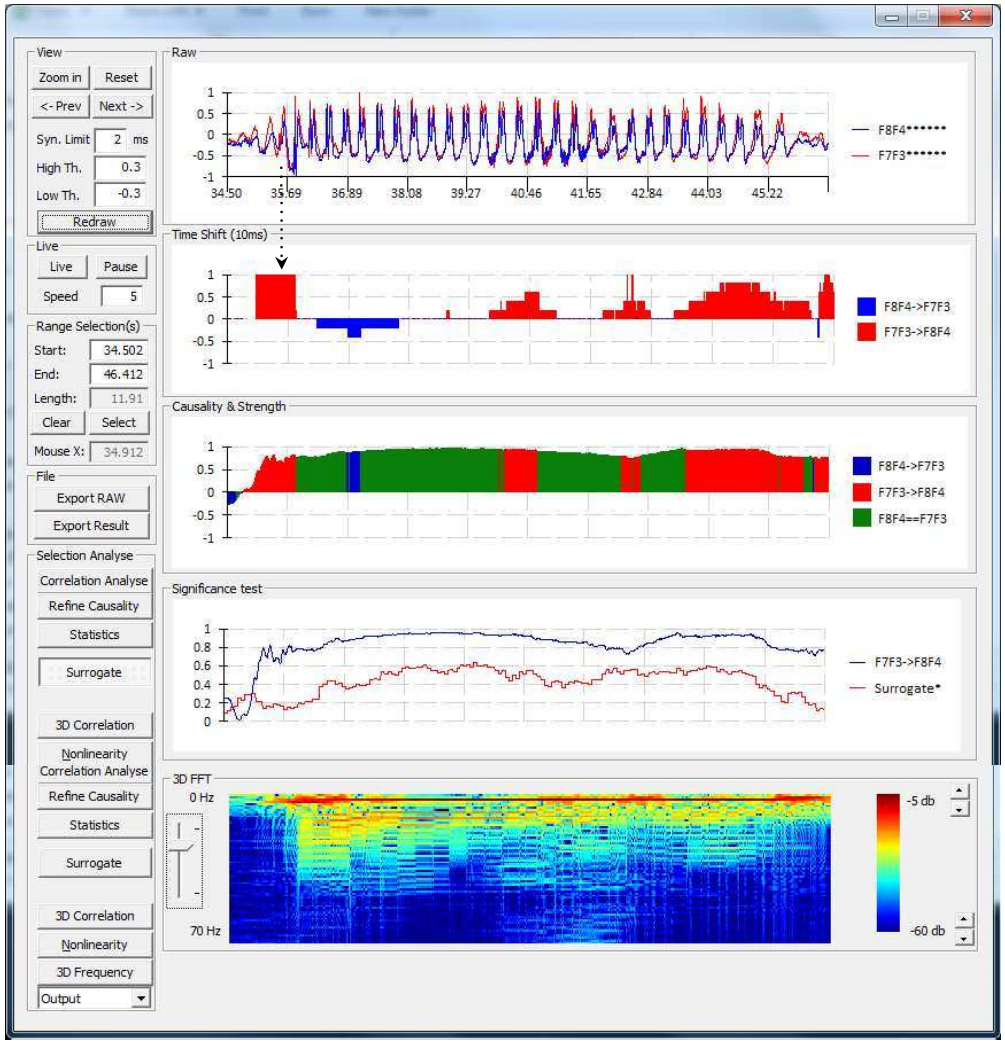

Case 5 absence 1

F8F4-F7F3

Ranked 1st

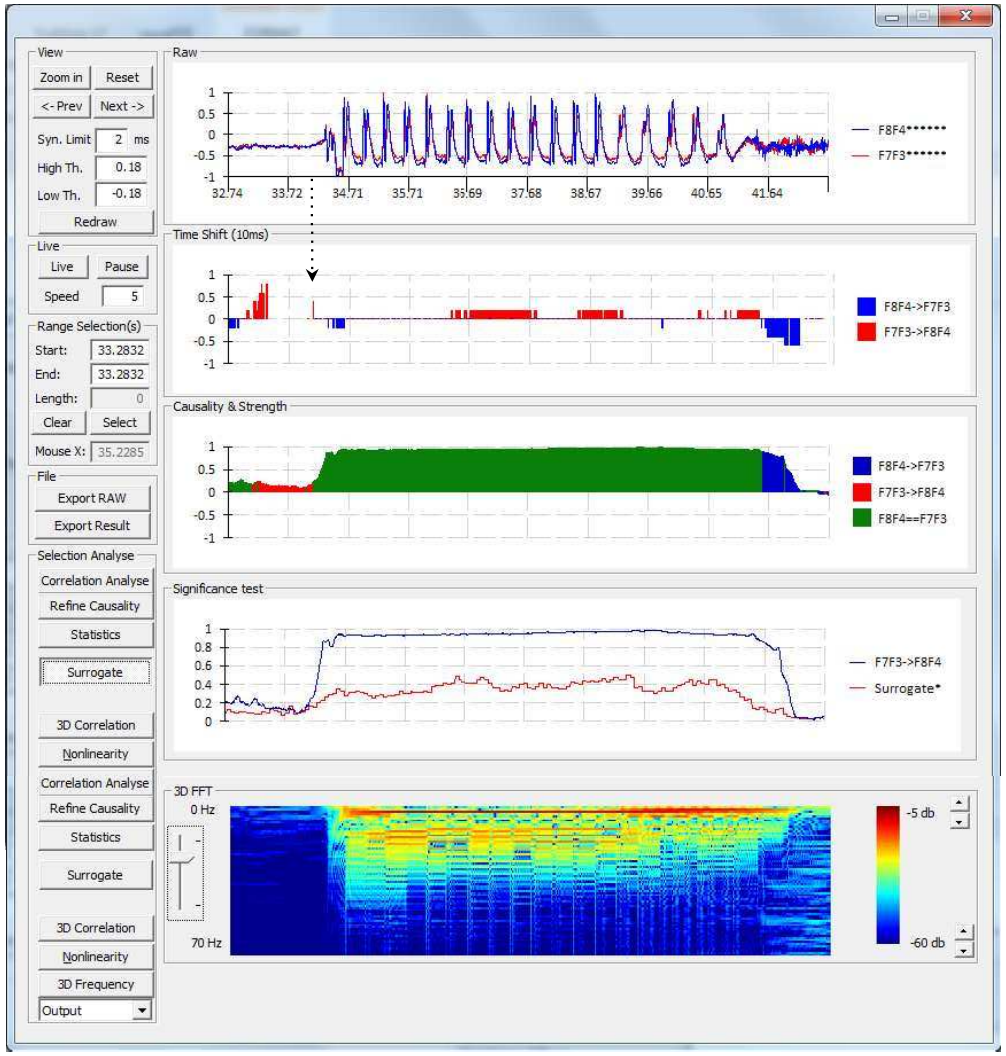

Case 5 absence 2

F8F4-F7F3

Ranked 1st

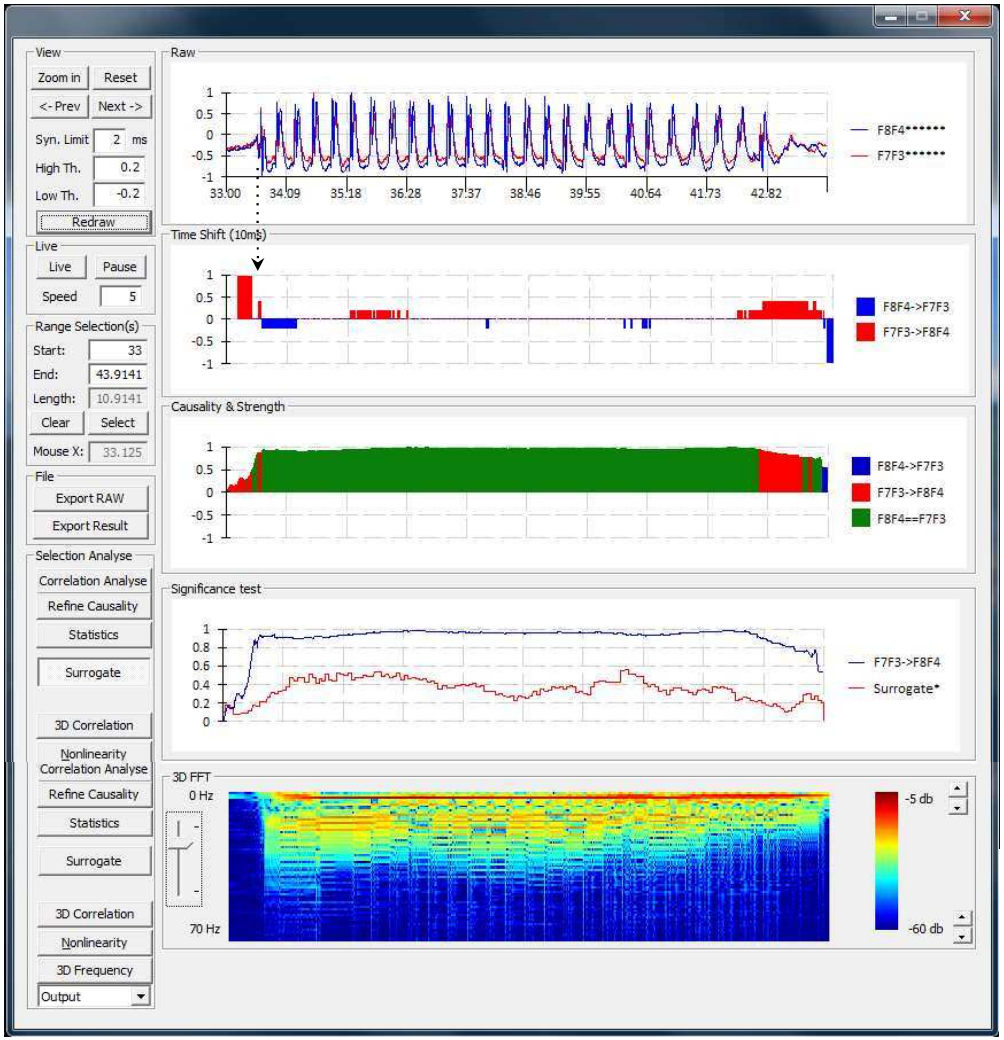

Case 6 absence 1

T4C4-T3C3

Ranked 4th, first homotopic, all above heterotopic

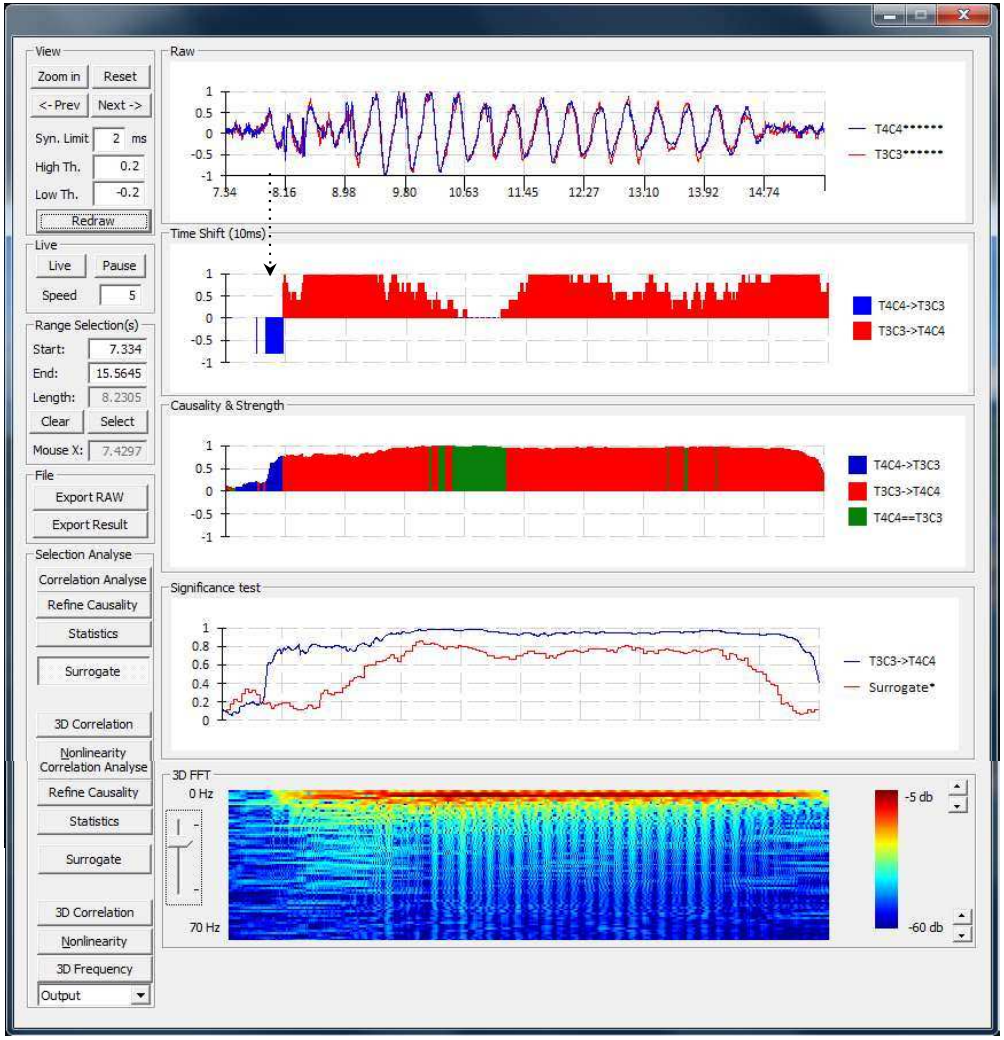

Case 6 absence 2

F8F4-F7F3

Ranked 2nd, 1st heterotopic

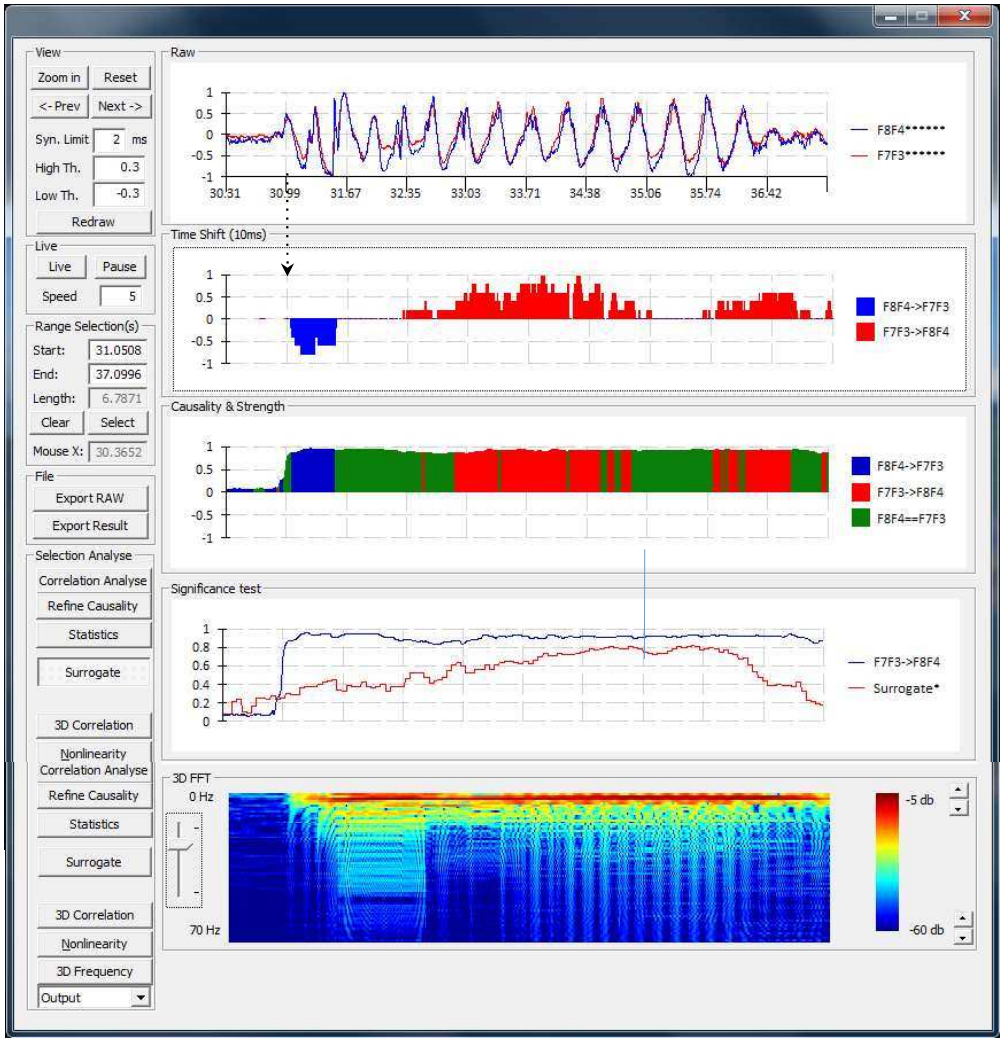

Case 7 absence 1

F4C4-F3C3

Ranked 1st

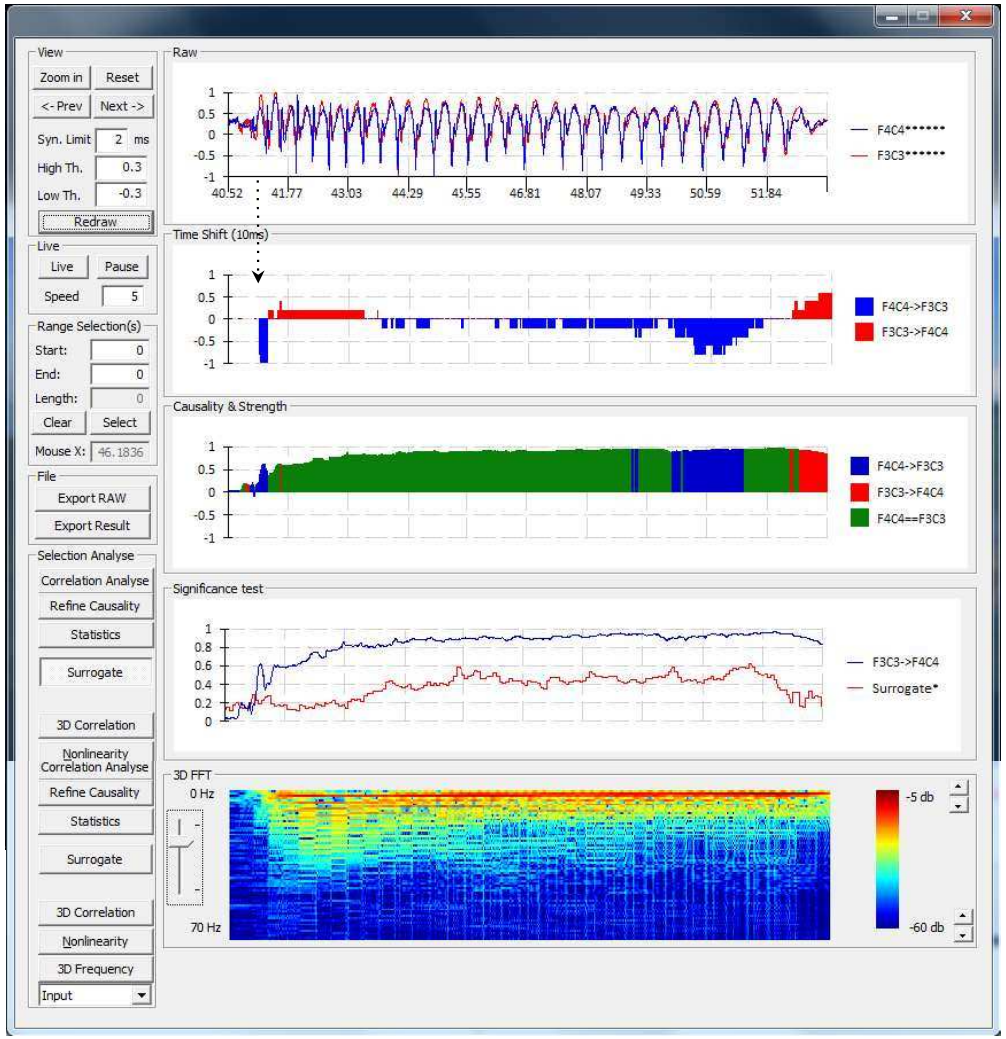

Case 8 absence 1

T4C4-T3C3

Ranked 1st

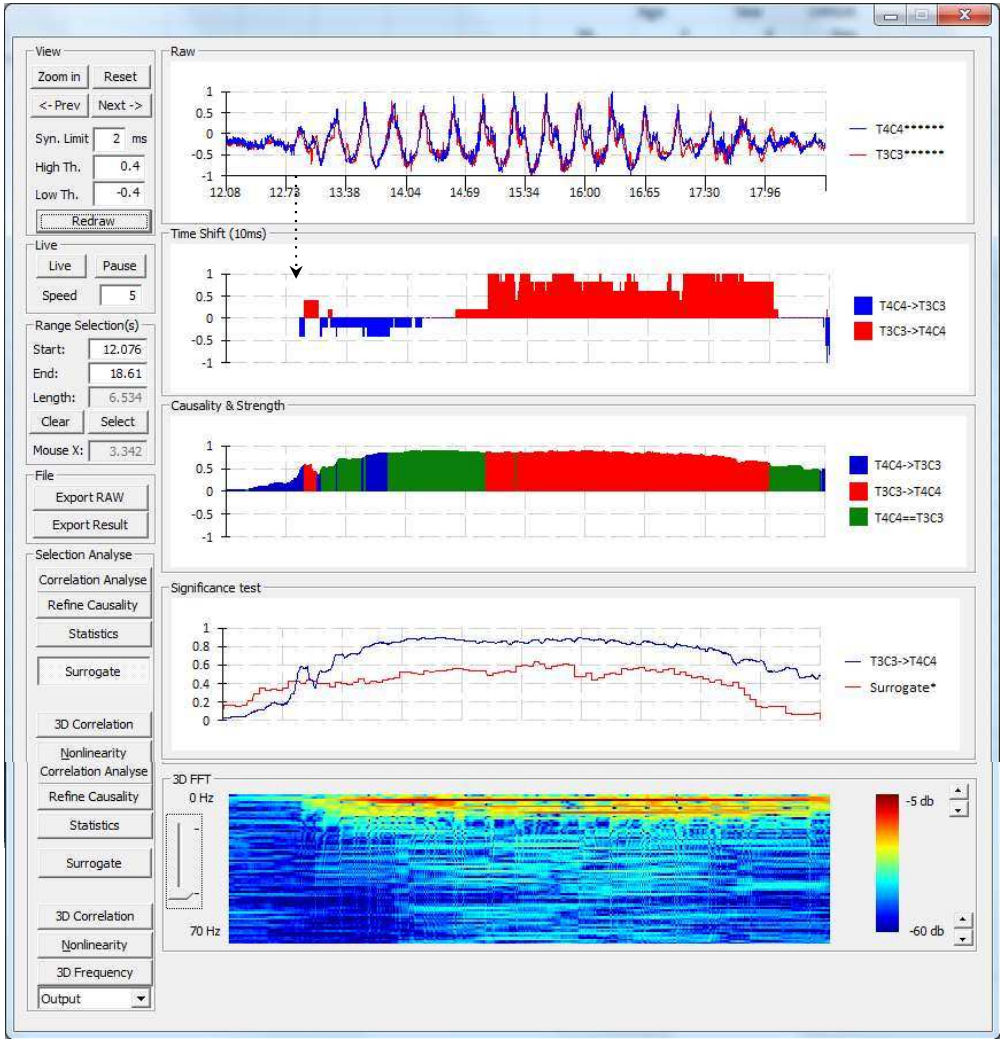

Case 9 absence 1

F8F4-F7F3

Ranked 2nd, First homotopic

(one above heterotopic)

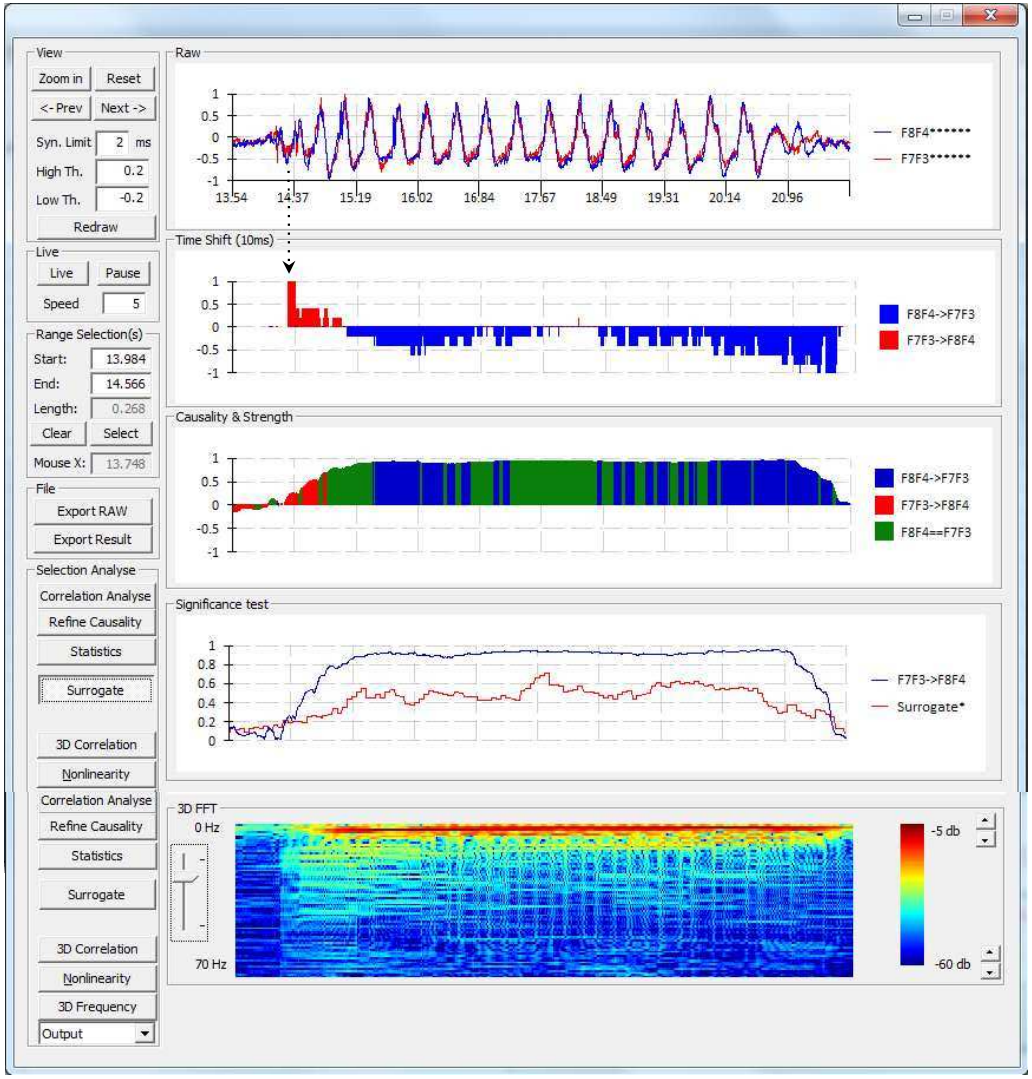

Case 10

F8F4-F7F3

Ranked 1st

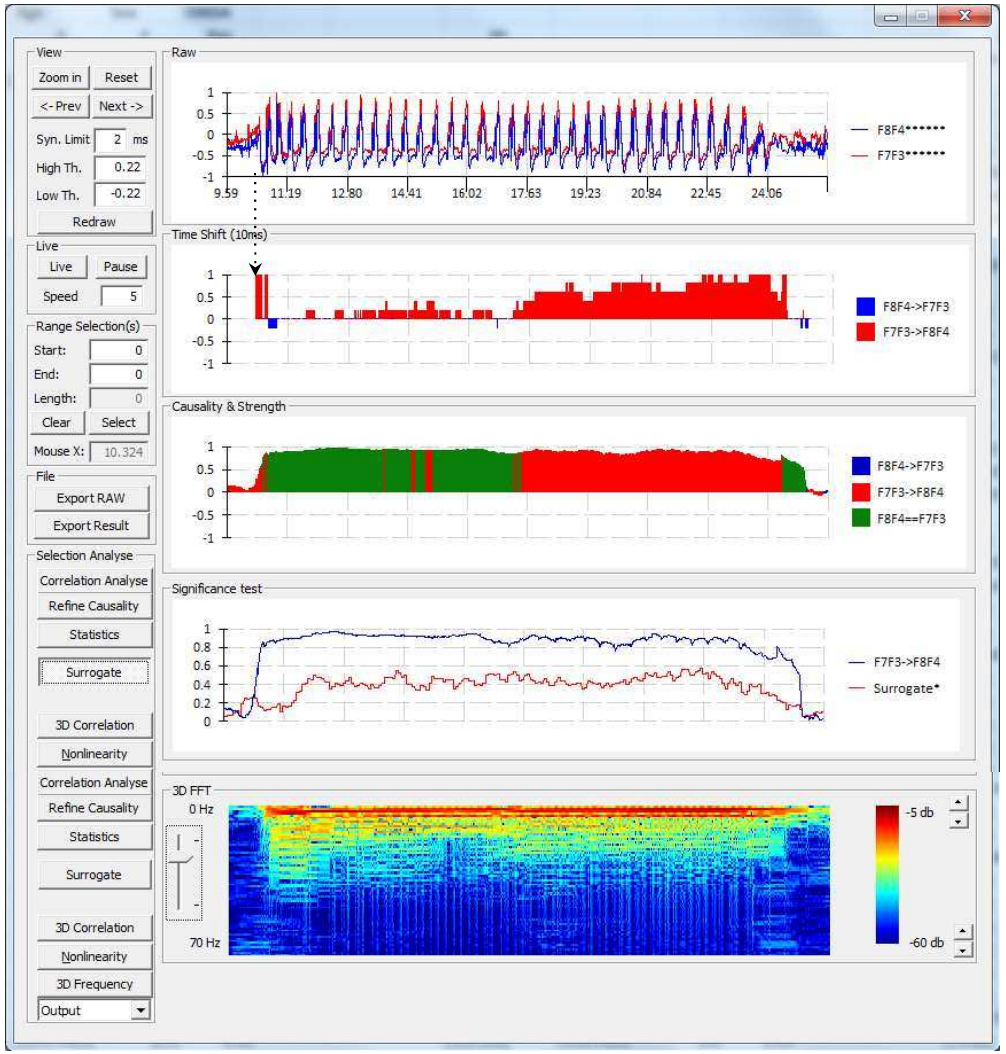

Case 11

F4C4-F3C3

Ranked 2nd, first homotopic

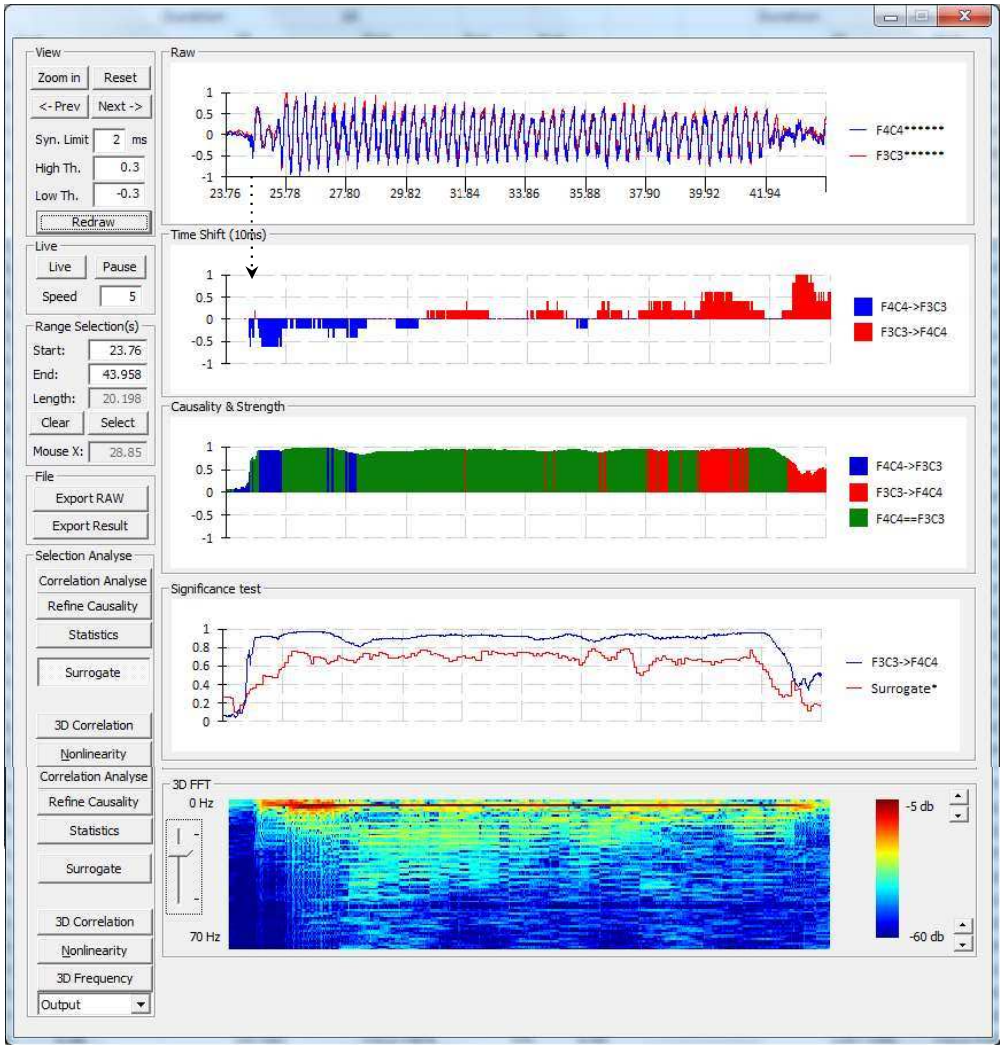

Case 12 absence 1

F8F4-F7F3

First ranked

Good example of high time lags in typical areas where lags are low in most other cases

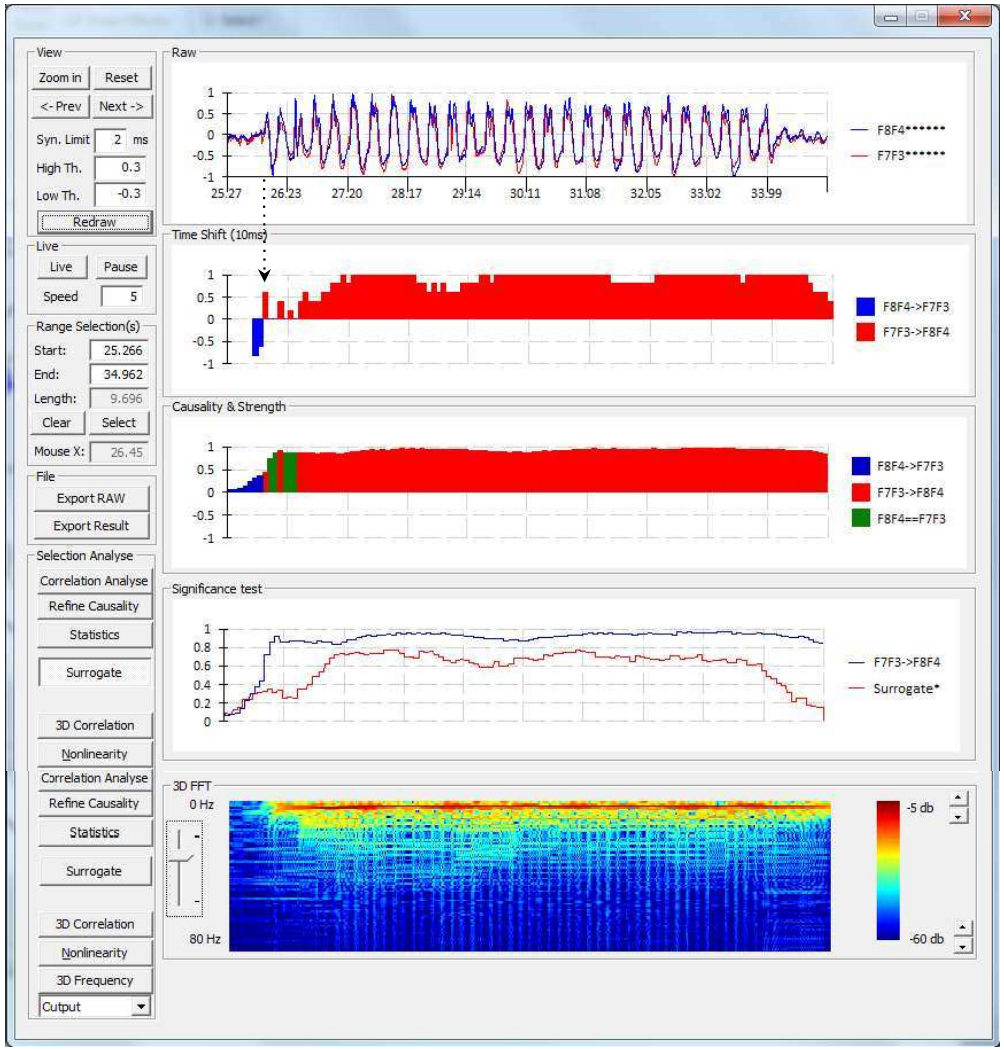

Case 12 abs 1

T4C4-T3C3

Highest ranked within first 5 with high 0Lag

Nice example showing highest synchronisation does not equate highest % 0Lag during an absence

The pathway connecting homotopic areas can be variable and high synchronisation can be achieved through different pathways

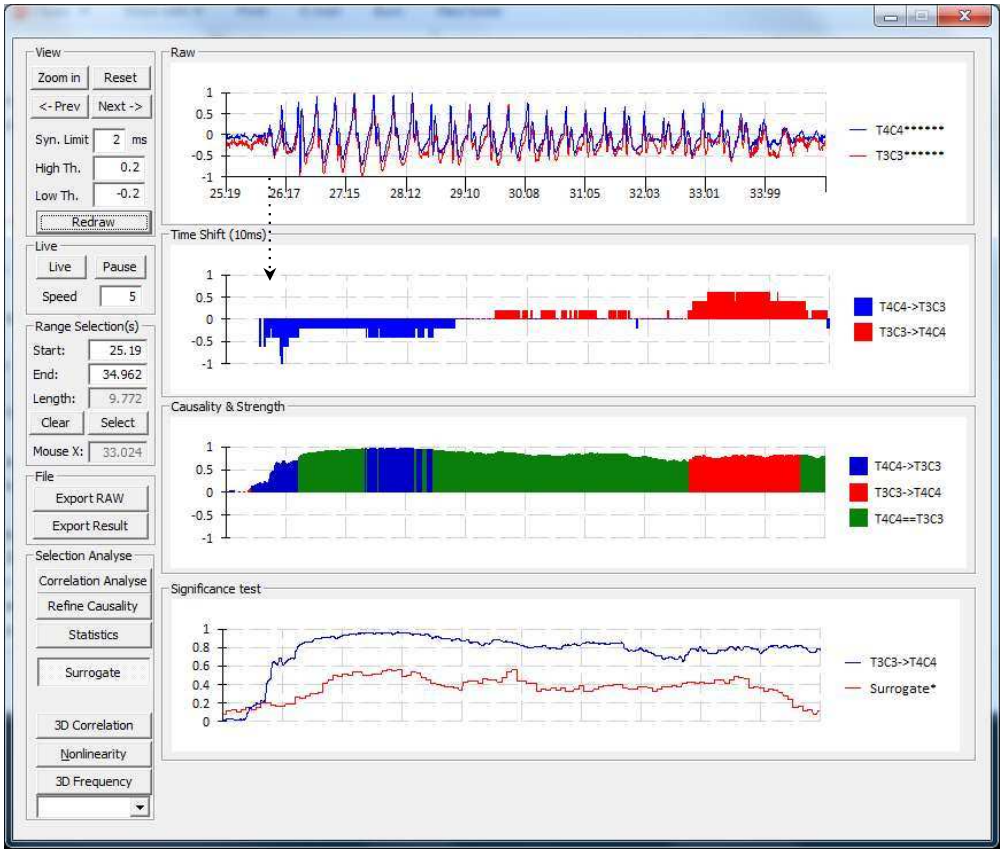

Case 13 absence 1

F8F4-F7F3

Top ranked

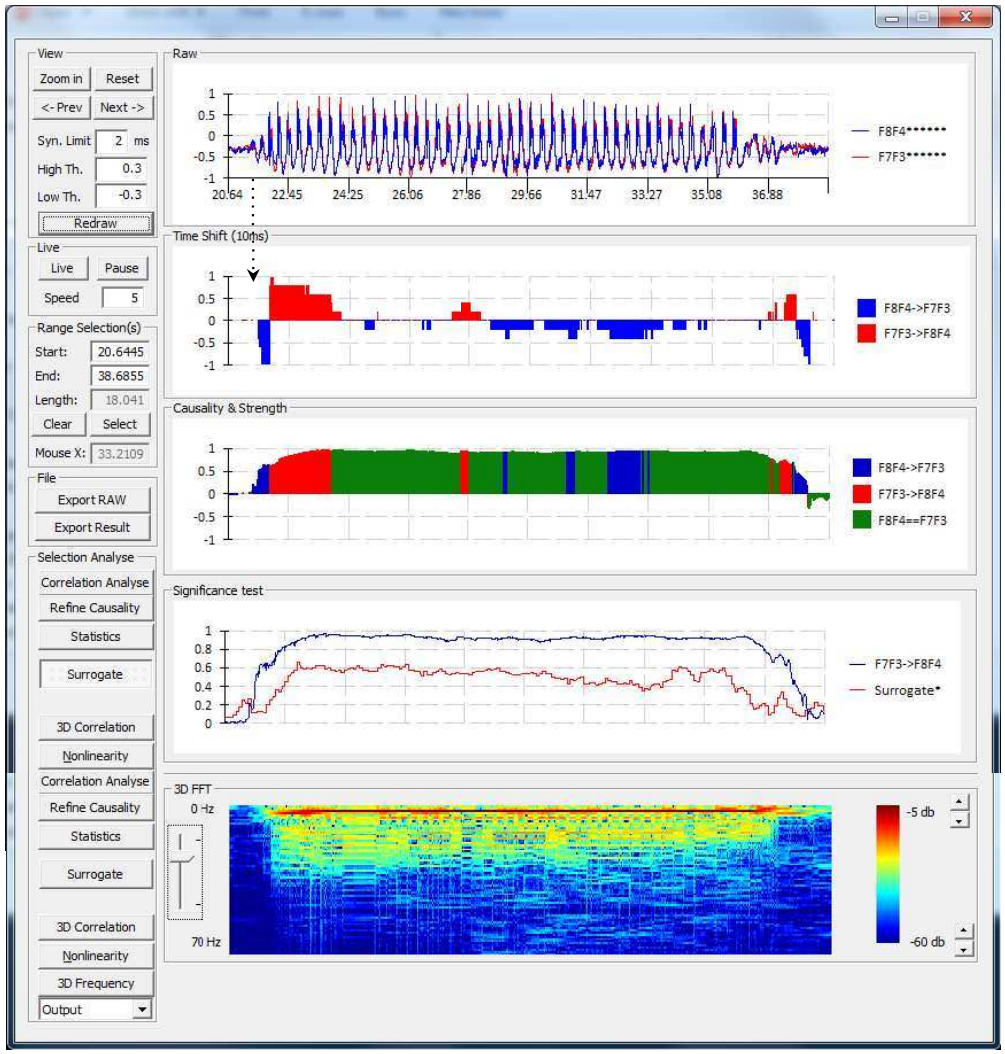

Case 13 abs 1

Zoom in

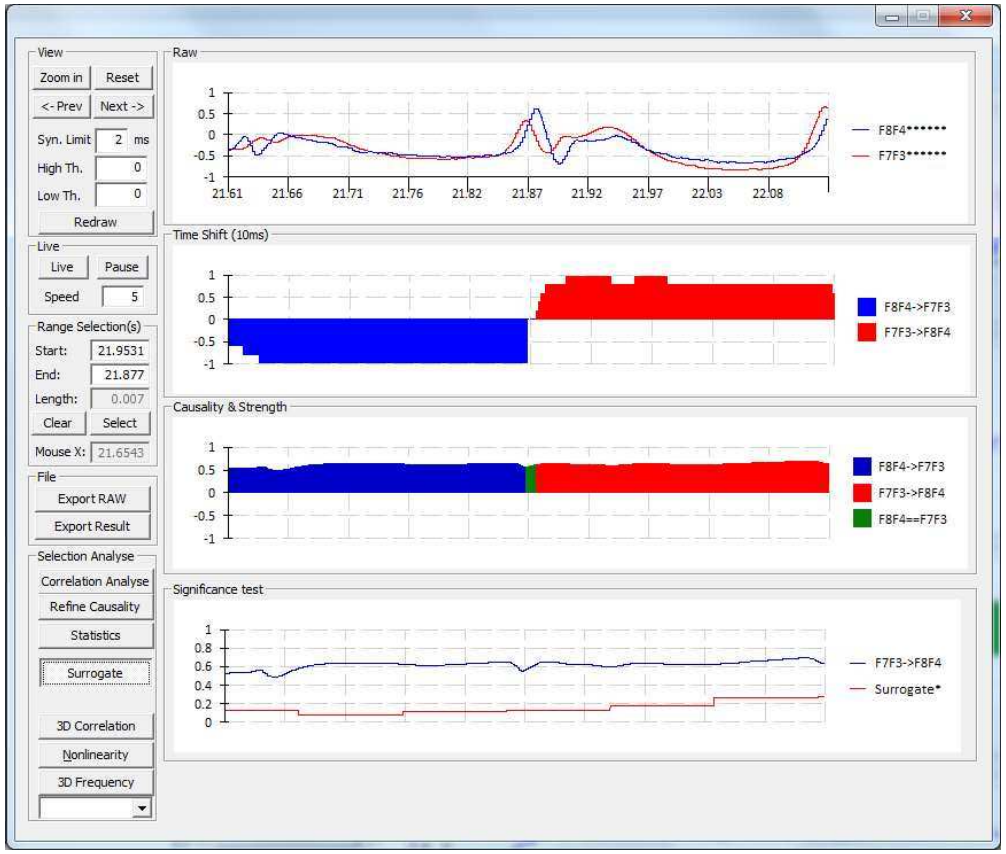

Case 14

F8F4-F7F3

Top ranked

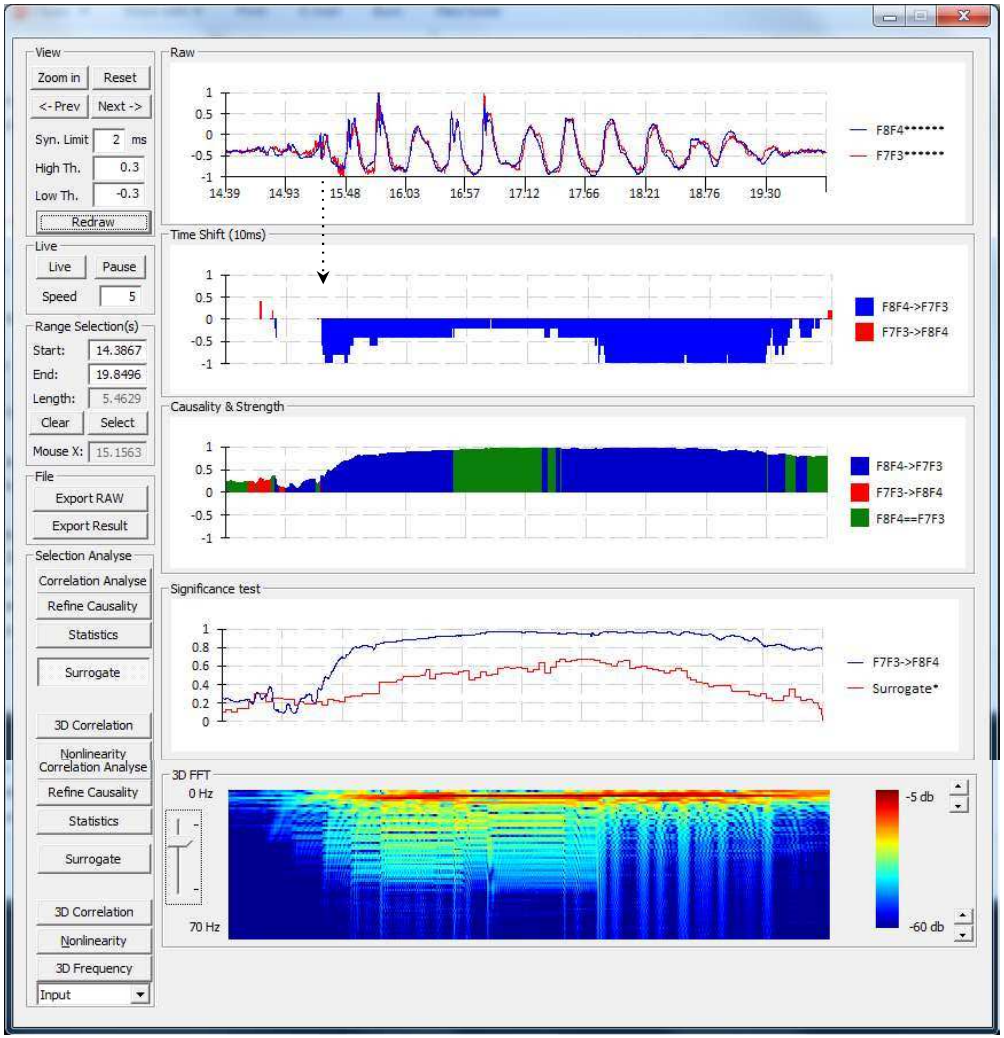

Case 15

F4C4-F3C3

2nd ranked for strength of synchronisation

Highest % of 0 lag synchronisation

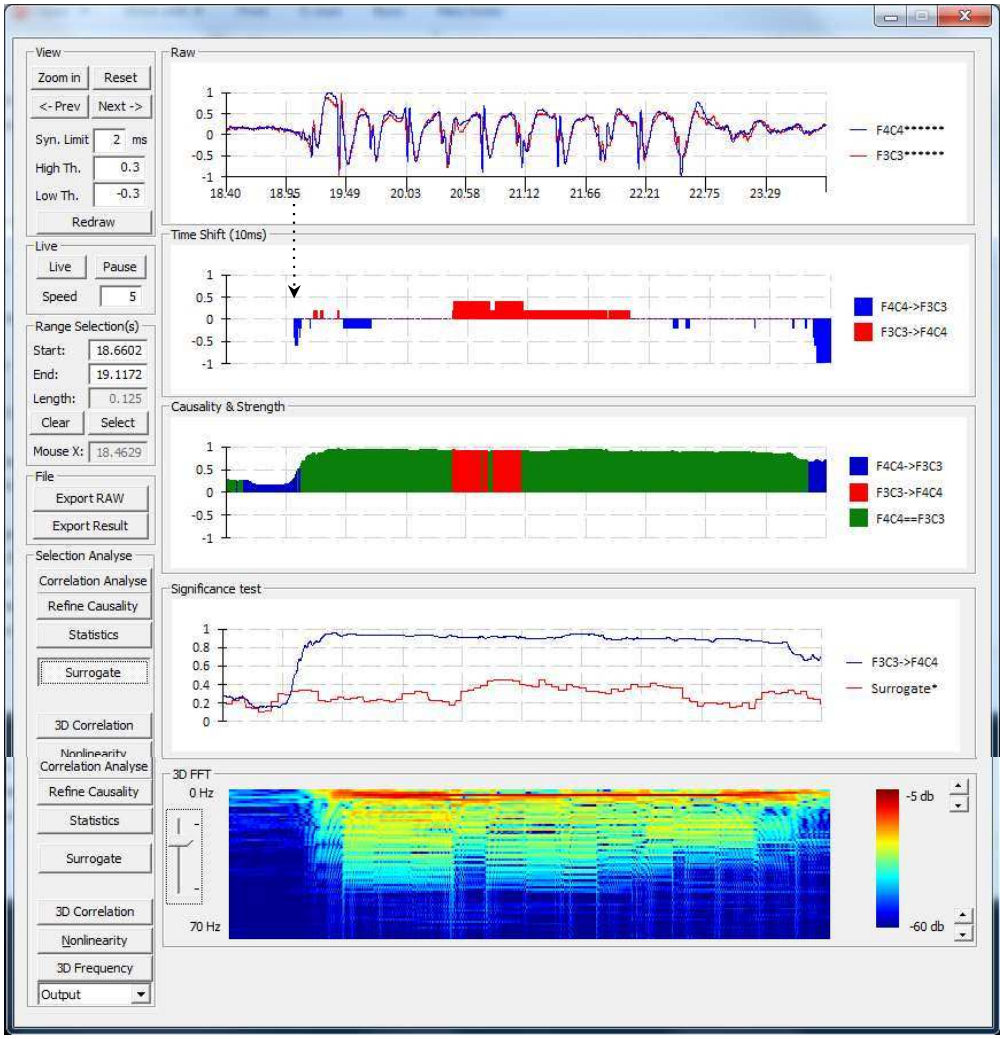

Case 15 absence 1

Fifth ranked channel

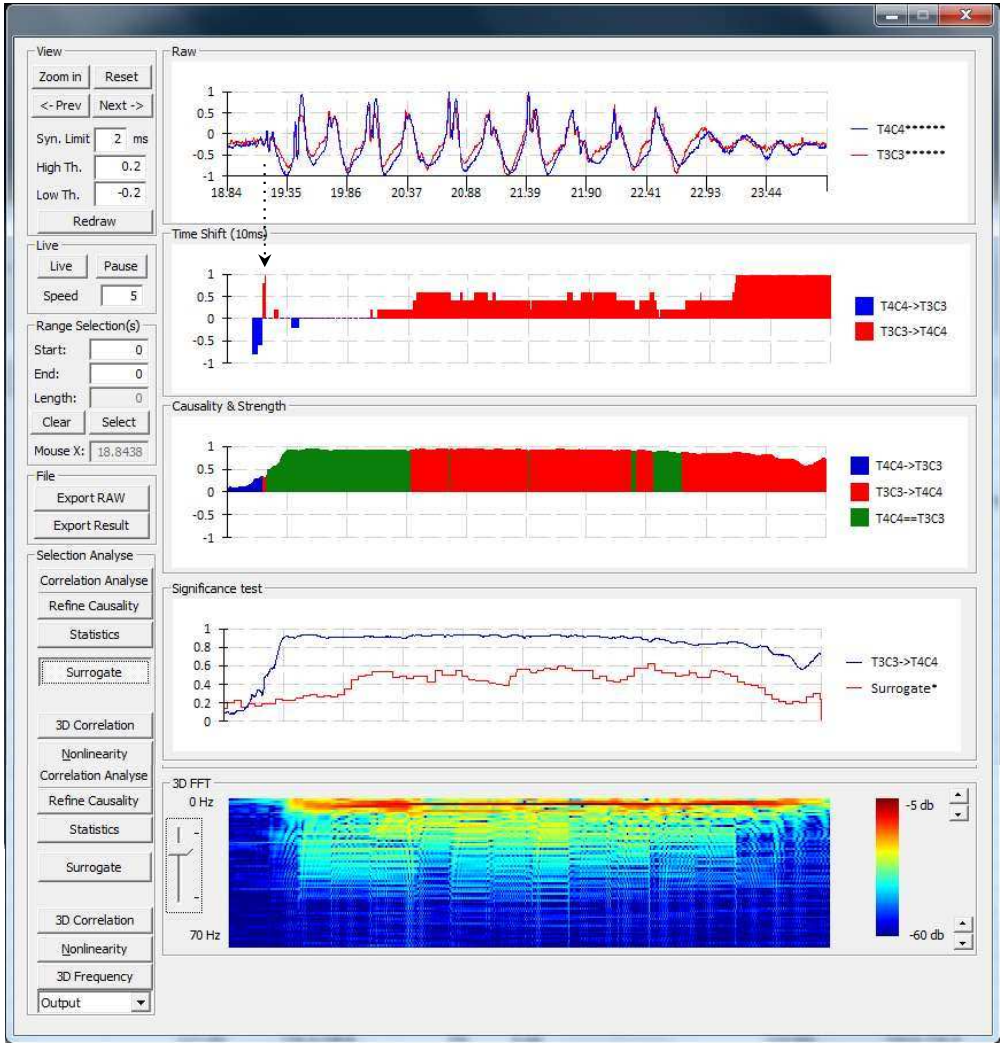

Case 16 absence 1

T4C4-T3C3

First ranked

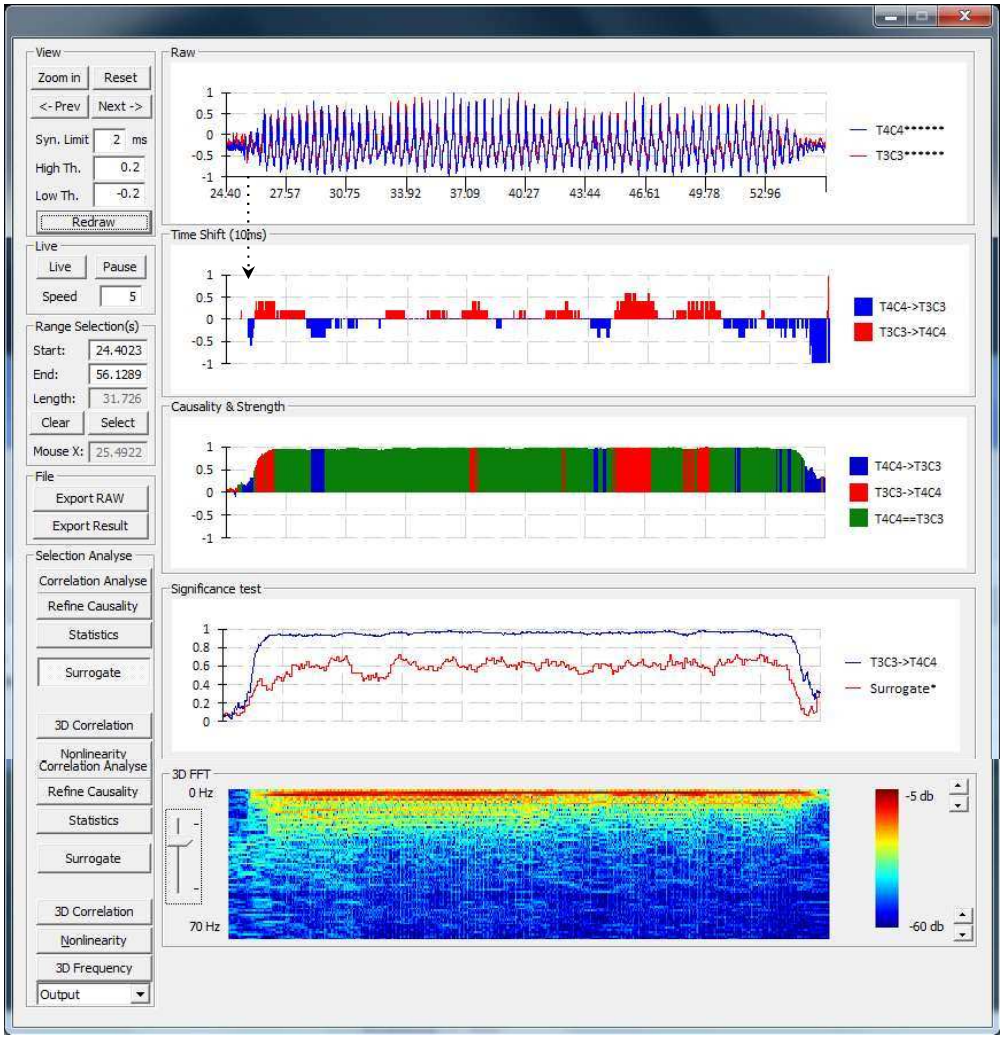

Case 17 absence 1

F8F4-F7F3

Top ranked

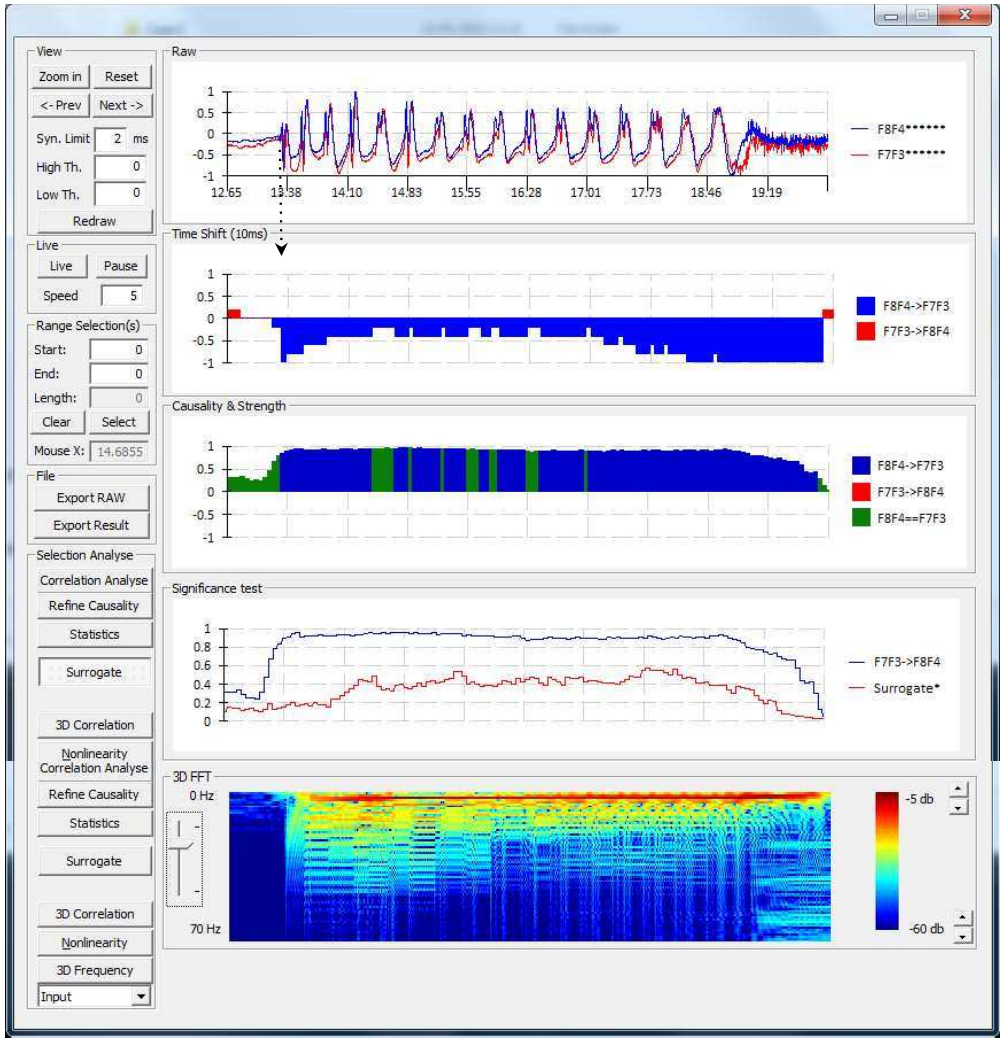

Case 17 abs 1

T4C4-T3C3

Second ranked

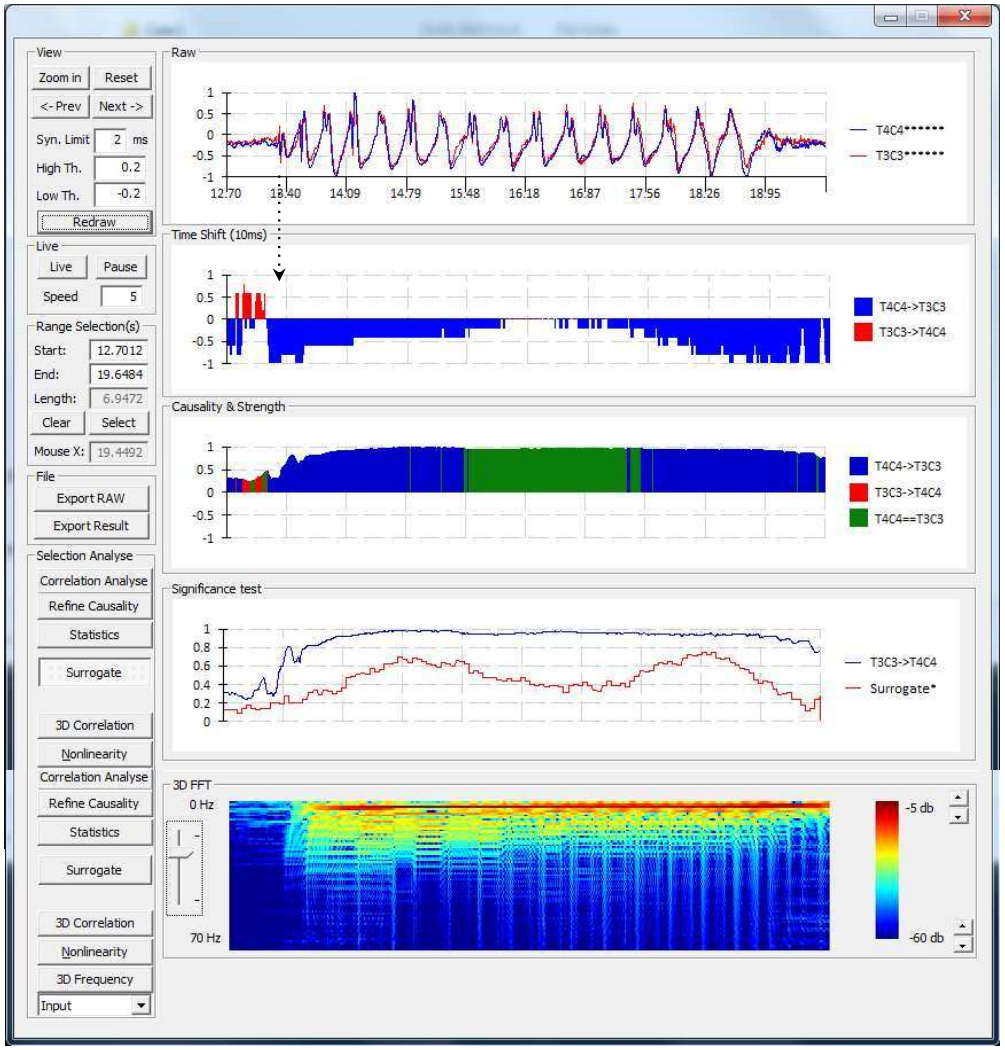

Supplementary XL

	No Abs	**Age**		**Sex**	**OIRDA**	
	1		**5**	**F**	**Yes**	
	Case 1 abs 1			**max synch**	**0.4**	
Duration /s	29					Duration
	ID	Pair		Time	Delay	
	1	CZPZ-F4C4		25.178	0	
	2	CZPZ-F7F3		25.194	0.016	
	3	CZPZ-F8F4		25.206	0.028	
	4	T6O2-F4C4		25.226	0.048	
	5	CZPZ-F3C3		25.244	0.066	
	5	**182:CZPZ-FZCZ**		**25.242**	**0.064**	

Supplementary PDF

Pair with earliest rise in nonlinear synchronisation	case	age	Gender	OIRDA	Duration	Synchronisation Level
F7F3-FZCZ	1	5	F	1	40	0.6
P4O2-T5O1	2	6	F	1	20	0.5
FZCZ-T4T6	3	9	M	0	5	0.6
FZCZ-F8F4	4	8	M	0	9	0.7
F4C4-F7F3	5	8	M	0	11	0.6
FZCZ-F7F3	6	7	M	0	6	0.7
P3O1-T4C4	7	5	F	0	13	0.6
P4O2-FZCZ	8	7	F	1	6	0.4
CZPZ-T3C3	9	6	F	1	8	0.7
FZCZ-P4O2	10	10	M	0	16	0.5
F8F4-FZCZ	11	9	F	0	22	0.6
F4C4-CZPZ	12	6	F	0	19	0.5
F3C3-FZCZ	13	7	F	1	14	0.6
F3C3-F8F4	14	9	F	1	6	0.5
FZCZ-F8F4	15	10	M	1	5	0.5
F4C4-P4O2	16	6	F	0	30	0.3
F7F3-F8F4	17	10	M	1	6	0.8

From anterior to posterior areas	EEG channel source for 17 abs absence with highest synchronisation/case	Count	Area
1	Frontal (2 electrode recording positions)	3	Anterior
2	Fronto-central (2 electrode recording positions)	5	
3	Fronto-central midline (1 electrode recording position)	5	
4	Centro-temporal (2 electrode recording positions)	0	-
5	Centro-parietal midline (1 electrode recording position)	1	Posterior
6	Temporal (2 electrode recording positions)	0	-
7	Temporo-occipital (2 electrode recording positions)	0	Posterior
8	Parieto-occipital (2 electrode recording positions)	3	Posterior